Titre: Title:	Optical Microcavities for Real-Time Detection of Bacteria
Auteur: Author:	Hala Ghali
Date:	2016
Type:	Mémoire ou thèse / Dissertation or Thesis
Référence: Citation:	Ghali, H. (2016). Optical Microcavities for Real-Time Detection of Bacteria [Thèse de doctorat, École Polytechnique de Montréal]. PolyPublie. https://publications.polymtl.ca/2267/

URL de PolyPublie: PolyPublie URL:	https://publications.polymtl.ca/2267/
Directeurs de recherche: Advisors:	Yves-Alain Peter, & Pablo Bianucci
Programme: Program:	Génie physique

UNIVERSITÉ DE MONTRÉAL

OPTICAL MICROCAVITIES FOR REAL-TIME DETECTION OF BACTERIA

HALA GHALI
DÉPARTEMENT DE GÉNIE PHYSIQUE
ÉCOLE POLYTECHNIQUE DE MONTRÉAL

THÈSE PRÉSENTÉE EN VUE DE L'OBTENTION
DU DIPLÔME DE PHILOSOPHIÆ DOCTOR
(GÉNIE PHYSIQUE)
JUIN 2016

UNIVERSITÉ DE MONTRÉAL

ÉCOLE POLYTECHNIQUE DE MONTRÉAL

Cette thèse intitulée :

OPTICAL MICROCAVITIES FOR REAL-TIME DETECTION OF BACTERIA

présentée par : GHALI Hala
en vue de l'obtention du diplôme de : Philosophiæ Doctor
a été dûment acceptée par le jury d'examen constitué de :

M. LEBLOND Frédéric, Ph. D., président
M. PETER Yves-Alain, D. Sc., membre et directeur de recherche
M. BIANUCCI Pablo, Ph. D., membre et codirecteur de recherche
M. GERVAIS Thomas, Ph. D., membre
M. PACKIRISAMY Muthukumaran, Ph. D., membre externe

DEDICATION

To my family and to Benoit, my husband. . .

ACKNOWLEDGEMENTS

RÉSUMÉ

Au cours de la dernière décennie, les microcavités à mode de gallerie ont fait le sujet de plusieurs études où elles sont utilisées comme biosenseurs sans marquage. Leur capacité à confiner la lumière pendant un certain temps leur confère des facteurs de qualité élevés, donc une très bonne sensibilité face aux molécules qui s'attachent à leur surface.

Ce projet de doctorat s'intéresse aux microdisques optiques pour la détection de bactéries, plus spécifiquement la bactérie Staphylococcus aureus (S. aureus). À notre connaissance, c'est la première fois que des bactéries sont détectées spécifiquement avec des microdisques optiques. Afin d'obtenir un biosenseur fiable et efficace, il est important qu'il présente une grande sélectivité face aux bactéries d'intérêt. Pour réaliser cette bonne sélectivité, la surface des microcavités doit être proprement fonctionnalisée. La fonctionnalisation consiste à choisir les anticorps qui sont spécifiques aux antigènes qui seront détectés. Dans ce cas, le choix des bactériophages spécifiques à la détection de la bactérie S. aureus a été fait après plusieurs séries d'expériences avec différents bactériophages. Puisque les étapes de préparation et de purification des bactériophages peuvent être longues et compliquées, l'isolation de protéines spécifiques des bactériophages s'est avérée plus appropriée. Le procédé de fonctionnalisation utilisé dans ce projet a été développé en collaboration avec le groupe de la professeure Jay L. Nadeau du département de génie biomédical à McGill. Des phages protéines LysK vont attacher les bactéries S. aureus lors des exprinces de détection en temps réel. Plusieurs expériences ont été réalisées en utilisant la bactérie E. coli afin de démontrer la spécificité du procédé de fonctionnalisation utilisé. Comme prévu, la LysK était spécifique à la S. aureus et n'a pas attaché de bactéries E. coli.

L'attachement des bactéries sur la surface du résonateur est observé grâce au déplacement des pics de résonance vers les plus longues longueurs d'onde, un mécanisme connu sous le nom de principe réactif de détection (reactive sensing principle). Ce déplacement permet d'en apprendre davantage sur le lien qui se forme entre les protéines et les bactéries. Pour une concentration de bactéries 5.10^9 cfu/ml, un déplacement de 0.22 nm a été observé. En diminuant cette concentration, le déplacement lui aussi décroît, car moins de bactéries s'attachent aux sites sensibles du microdisque. Une formulation théorique de ce principe, utilisant l'expression approximative du champ électrique dans un microdisque, a également été développée pour la première fois dans cette thèse afin de relier le déplacement de résonance avec le nombre de bactéries qui s'attachent à la surface ainsi que la cinétique de la liaison entre les bactéries et les protéines. Les résultats ont permis de déduire que l'attachement de bactéries

commence dès que ces dernières sont injectées sur la surface du disque fonctionnalisé. Il faut autour de 15 minutes pour attacher un nombre maximal de bactéries. Un nombre d'environ 46 bactéries est requis afin de générer un déplacement de longueur d'onde de 0.22 nm. Après ce temps, le pic de résonance commence à retourner à son état initial, car la protéine agit sur la bactérie et la détruit avec le temps.

Un avantage à utiliser les microdisques optiques comme biosenseurs est leur simplicité de fabrication. Étant fabriqués par les techniques de photolithographie, il est possible de les intégrer en grand nombre sur des puces afin de produire des biosenseurs portables capable de diagnostiquer des maladies et d'analyser des échantillons environnementaux, tels l'eau ou la nourriture. Les avancements dans le domaine de l'optique et la microfluidique permettent aussi d'intégrer des éléments comme les guides d'onde ou les canaux fluidiques sur la même puce afin d'obtenir un biosenseur complet et robuste prêt à être commercialisé.

ABSTRACT

Researchers showed a lot of interest in studying whispering gallery microcavities as a tool for biosensing in the last decade. Optical microcavities are structures that confine light at the microscale due to total internal reflection of light at the interface between the cavity and its surrounding medium. If a molecule binds to the surface of the microcavity, light can interact with it several times, making optical microcavities very sensitive tools for label-free sensing.

During this Ph.D. project, optical microdisks are used to detect the presence of Staphylococcus aureus (S. aureus) bacteria. To our knowledge, this is the first time optical microdisks are used to specifically detect bacteria. In order to have a reliable and efficient biosensor, it needs to be highly specific. Specificity is achieved by choosing an appropriate functionalization process. The functionalization process uses the antibody that is specific to the antigen of interest. In this case, the choice of a specific bacteriophage to bind S. aureus bacteria is crucial to obtain a specific sensor, and many experiences were done in order to identify the most appropriate. However, the purification of bacteriophages can be long and complex. An alternative to working with whole bacteriophages is the use of purified protein phages that can be easier to prepare. The functionalization process used in this thesis was developed in collaboration with professor Jay L. Nadeau's group from the biomedical engineering department at McGill university. LysK protein phage is added to the microdisk and will attach S. aureus bacteria during the real-time detection experiments. In order to demonstrate the specificity of the functionalization process, LysK was used with E. coli bacteria. As predicted, since LysK is only specific to S. aureus strains, it did not attach any E. coli.

The binding of bacteria to the microdisk surface is observed through the reactive sensing mechanism. When bacteria bind to the surface of the resonator, it increases the optical path length and changes the refractive index, which leads to a shift of the resonance peaks towards longer wavelengths. This shift can give practical information about the kinetics of the binding between the bacteria and the protein. For a concentration of 5.10^9 cfu/ml, a shift of 0.22 nm was observed. When the concentration was decreased, the value of the shift also decreased, meaning less bacteria bind to the surface of the resonator. Using the approximate expression of the electric field inside a microdisk, a theoretical formulation of the wavelength shift was developed for the first time. It helped give an approximation of the number of bacteria that attach to the surface. For the 0.22 nm shift, around 46 bacteria bound to the sensitive area of the microdisk and contributed to the shift. It takes about 15 minutes to attach a maximum number of bacteria. After that time, the shift starts to decrease and go

back to its original position. LysK has a high lysing efficiency over S. aureus strains, most of the bacteria bound to the surface will be dead after 30 minutes.

Since optical microdisks are fabricated using standard lithographic techniques, they can easily be integrated at large scale into lab-on-chips to make portable biosensors to be used for point-of-care testing. The advancements in the optics and microfluidics fields allow the integration of several elements like the waveguides and microfluidic channels. This will lead the way towards robust fully integrated optical biosensors that can be used for disease diagnostics and analysis of environmental samples like water and food in order to detect the presence of bacteria in a very short time.

TABLE OF CONTENTS

LIST OF TABLES

LIST OF FIGURES

LIST OF SYMBOLS AND ABBREVIATIONS

2D	Two dimensions
3D	Three dimensions
BOE	Buffer Oxide Etch
CW	Clockwise
CCW	Counterclockwise
CFU	Colony-forming unit
DI	Deionized
DNA	Deoxyribonucleic acid
DRIE	Deep Reactive Ion Etching
E. coli	Escherichia Coli
EDC	1-Ethyl-3-[3-dimethylaminopropyl]carbodiimide hydrochloride
ELISA	Enzyme-Linked Immunosorbent Assay
EtOH	Ethanol
FET	Field-Effect Transistor
FSR	Free spectral range
HCl	Hydrochloric acid
HF	Hydrofluoric acid
HMDS	Hexamethyldisilazane
ICP	Inductively Coupled Plasma
IR	Infrared
MEMS	Microelectromechanical systems
MRSA	Methicillin-Resistant Staphylococcus Aureus
NaCl	Sodium chloride
NH_4F	Ammonium fluoride
O_2	Oxygen
OD	Optical density
PBS	Phosphate-Buffered Saline
PCR	Polymerase Chain Reaction
PEG	Polyethylene Glycol
PSG	Phosphosilicate glass
Q	Quality Factor
RI	Refractive index
RIE	Reactive Ion Etching

RMS	Root mean square
RNA	Ribonucleic acid
S. aureus	Staphylococcus Aureus
SCREAM	Single Crystal Reactive Etching and Metallization
SD	Standard deviation
SEM	Scanning Electron Microscope
SF_6	Sulfur Hexafluoride
Si	Silicon
SiO_2	Silicon Dioxide
Si-PEG	Triethoxysilane-Polyethylene Glycol
SMF	Single mode fiber
SOI	Silicon-on-Insulator
SPR	Surface Plasmon Resonance
TE	Transverse Electric
TM	Transverse Magnetic
UV	Ultraviolet
WGM	Whispering Gallery Modes
WHO	World Health Organization
XeF_2	Xenon difluoride
XPS	X-Ray Photoelectron Spectroscopy

LIST OF APPENDICES

CHAPTER 1   INTRODUCTION

Pathogenic bacteria and virus particles present in food supplies, air conditioning and contaminated water can cause serious infections and are responsible of a high percentage of mortality around the world (around 32% of all deaths in 2012 according to WHO). In addition, the potential bioterrorism threat is increasing around the world. For these reasons, it becomes crucial to possess tools that can quickly, reliably and accurately detect the presence of these biomolecules in solution and in the atmosphere. The need for fast diagnostics and clinical testing, and the advances in the health care field lead to the development of biological sensors that can be highly efficient devices for those purposes.

Several biosensing techniques have been used over the years, ranging from label-based sensors like enzyme-linked immunosorbent assay (ELISA) and polymerase chain reaction (PCR), to label-free biosensors based on electrical, mechanical and optical transducers. One biosensor that has been studied intensively in the last decade and has been found to be a highly sensitive, very selective when properly functionalized, low-cost and easily fabricated sensor is based on whispering gallery mode (WGM) microcavities, also known as optical microcavities. Their name comes from the similitude between the propagation mode of the electromagnetic wave inside the microcavity and the propagation of the acoustic wave along the long conduit of the St-Paul's Cathedral in London, as explained by Lord Rayleigh in 1912.

Optical microcavities are structures that can efficiently confine light at the microscale due to total internal reflection of light at the interface between the cavity and its surrounding medium. They have a wide range of applications in telecommunications as filters and lasers, optomechanics and sensing. They come in a variety of shapes and sizes with different characteristics and Q-factors, such as spheres, disks, toroids or rings. They are made of a dielectric material, such as silica, and have high quality (Q) factors due to low intrinsic material loss of silica in visible and near-IR. This characteristic makes WGM cavities good candidates for biosensors. High-Q means that the photons have a longer cavity lifetime, and can thus interact many times with the target molecules.

The first main objective of this project is to obtain a specific and selective WGM biosensor for the detection of Staphylococcus aureus bacteria. The first step towards achieving a specific biosensor is surface functionalization. A highly specific and sensitive biosensor will allow to eliminate the risk of false positives in complex environments and will give accurate and reliable results. An appropriate functionalization using protein phage will help detect specifically the S. aureus bacteria.

Once a proper functionalization is achieved, fast, real-time detection of S. aureus bacteria becomes thus possible. This step accounts for the second main objective of the thesis. The experiments are done using an optical characterization setup and results of the bacterial binding to the surface of the microdisk are observed as a shift of the resonance frequency of the cavity.

The third objective of this thesis is to quantify the number or concentration of bacteria that bind to the surface of the microresonator and contribute to the spectral shift. The attachment of bacteria to the surface of the microdisk is observed via the reactive sensing principle. This binding will increase the optical path length, leading to the shift of the resonance frequency towards longer wavelengths. Knowledge of the microdisk's modes will help find a theoretical expression of the spectral shift induced by the bacterial binding to the resonator. It is also important to observe the kinetics of the binding between LysK protein phage and Staphylococcus bacteria.

Details of the functionalization process, results of the real-time detection and the theoretical formulation of the spectral shift are given in details in the subsequent chapters.

Chapter 2 gives an overview of the numerous biosensing techniques that have been developed and used so far. At first, a description of the label-based biosensing techniques such as ELISA and PCR is given, followed by the main label-free sensing techniques used, including WGM microcavities. The main applications of these techniques along with their advantages and limitations are also described.

Chapter 3 details the theory of WGM microcavities. The principle of light confinement inside the microcavity, light coupling using a tapered optical fiber, as well as the characteristics of the WGM cavities are explained. The second part of the chapter gives an overview of the different sensing mechanisms used to detect the binding of biomolecules to the surface of the cavity.

Microfabrication of optical microdisks is detailed in chapter 4, along with the suface functionalization process developed to detect S. aureus bacteria specifically and the optical characterization setup used to carry out the experiments.

In chapter 5, a synthesis of the work and the experimental results are stated, starting by demonstrating the specificity of the functionalization process, then describing the results of real-time binding of bacteria to the surface of a microdisk. The second part of the chapter is dedicated to a theoretical development of the reactive shift for a microdisk.

Finally, a general discussion about the difficulties faced during the project, including the environmental and experimental parameters that could influence the real-time detection of

bacteria are explained in chapter 6. The conclusion summarizes the work done during this Ph.D. and gives some recommendations in order to use biosensors based on optical microdisks as on-site lab-on-chips for point-of-care tests.

In this thesis, a specific and selective biosensor based on optical microdisks is developed. Specificity of the biosensor is ensured by a proper functionalization process. LysK protein phage is used to specifically bind Staphylococcus aureus bacteria. To our knowledge, this is the first time this functionalization process is used on an optical biosensor to detect the presence of bacteria in real-time. The limit of detection achieved with this technique for a microdisk with a Q factor of 10^4 is 5 pg/ml. This is also the first time optical microdisks are used for specific bacterial sensing.

A theoretical expression of the spectral shift is developed. It allows to find the approximate number of bacteria that bind to the surface of the microresonator and contribute to the reactive shift. It also allows to obtain the optimal parameters in order to achieve single-bacterium detection using whispering gallery optical microdisks.

CHAPTER 2   STATE OF THE ART

Virus particles and pathogenic bacteria are major causes of diseases and mortality around the world. They can be present in contaminated water, air conditioning and food supplies and cause serious infections. The overuse of antibiotics has given rise to antibiotic-resistant strains of bacteria, such as multi-drug resistant Gram-negative bacteria. According to the world health organisation (WHO), highly resistant bacteria such as Methicillin-Resistant Staphylococcus Aureus (MRSA), which is a common cause of severe infections, are responsible of high percentage of hospital-acquired infections, and people with MRSA are 64% more likely to die than those who have a non-resistant form of the infection. It becomes thus very important to use accurate detection techniques to achieve early detection of these viruses and pathogens in order to prevent the spread of disease and find appropriate treatments to these illnesses. In this chapter, a brief description of the methods used to detect the presence of infectious diseases caused by bacteria or viruses is given, starting with label-based biosensors, followed by a comparison of label-free biosensing techniques that are used, including sensors based on whispering gallery microcavities.

But first, it is important to appropriately define a biological sensor, or a biosensor. A biosensor is an analytical device designed to detect the presence of biological elements and convert the response into a signal that can be easily read and quantified. A biosensor is typically composed of two main elements : a biological recognition element that is able to interact specifically with a target, and a transducer that will convert the recognition event into an easily measured signal (Fig. 2.1) (Hurk and Evoy, 2015). This element needs to be highly specific and to have a high affinity with the measurand, their interaction needs to be stable and detectable by the transducer and their specificity should not be altered by their immobilization on the surface of the transducer (Hunt and Armani, 2010). A wide variety of bio-recognition elements have been used since the first biosensor was described in 1962 by Clark and Lyons, where they immobilized glucose oxidase on an amperiometric oxygen electrode in order to measure the concentration of glucose in the sample (Clark and Lyons, 1962). These bio-elements can range from tissues to enzymes, DNA, cells and antibodies. Classification of the biosensors rely mostly on their transducing elements, and can be classified as electrochemical, mechanical, piezoelectric, thermal and optical sensors (Koyun et al., 2012).

In order to obtain an accurate and reliable biosensor, some very important features need to be present. The sensor must be highly specific to the analyte of interest, meaning that the bio-recognition element must specifically detect the presence of only a certain biomolecule.
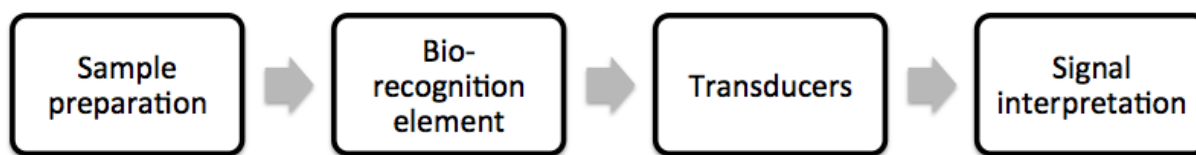
Figure 2.1 Schematic of the elements composing a biosensor

It also needs to be stable under normal storage conditions and produce accurate, precise and reproducible responses. If the biosensor is intended for point-of-care use, it needs to be biocompatible and not have any toxic products. Some added values to a successful biosensor are its low cost, small size, portability and being user-friendly.

2.1 Label-based biosensors

The first biosensors used required labeling of the target molecule in order to detect its presence. In this section, three different label-based techniques are presented. One of the first methods used was Enzyme-Linked Immunosorbent Assay (ELISA). It was developed in the early 1970s by (Engvall and Perlmann, 1971) and (Van Weemen and Schuurs, 1971), independently. It has been used to detect the presence of bacteria such as E. coli and salmonella (Basta et al., 1989; Janyapoon et al., 2000) and other viruses and antibodies (Lee et al., 2013; Suzuki et al., 2003).

ELISA is a plate-based assay technique that uses antibodies and color change to detect the presence of either antigens such as peptides, proteins and hormones or antibodies in a sample. It also allows to measure the concentration of an analyte in solution (Leng et al., 2008).

ELISA is performed in a 96-well plate. Each plate is coated with an antigen that will bind to an enzyme-labeled antibody to be measured. Finally, a substance containing the enzyme's substrate is added to the wells, which yields a visible color change indicating the presence of antigens. Once the enzyme reaction is completed, the optical density (OD) of each well is measured in order to determine the concentration of antigens present. The change in color is proportional to the amount of primary antibodies that bound to the antigens. Non-specific binding events are eliminated by washing the plate between each step. Fig. 2.2 shows the steps to detect the presence of an antigen using ELISA.

There exist three main types of ELISA (Gan and Patel, 2013) : direct ELISA where the antigen is detected by an antibody that is directly conjugated to an enzyme, indirect ELISA

where the antigen is detected in two stages; first, an unlabeled primary antibody specific to the antigen is immobilized, which in turn is bound to an enzyme-labeled secondary antibody. The third type is sandwich ELISA where the analyte to be measured is bound between two primary antibodies, the capture and detection antibodies. This last technique is the most robust and sensitive of all three.

ELISA is a highly specific, very sensitive technique to be used in complex samples such as blood. However, the need to label the antibodies can be time consuming ($\sim$ 4 hours) and expensive, and the labeling could adversely affect the immunoreactivity of the antibody. Table 2.1 summarizes the advantages and limitations of each of the three ELISA techniques described above.
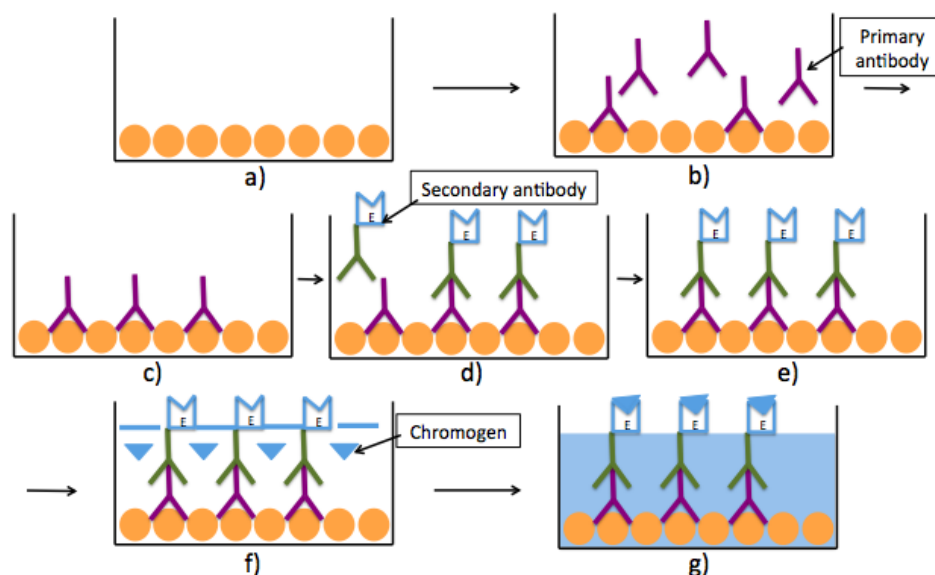
Figure 2.2 Enzyme-linked Immunosorbent Assay (ELISA) protocol : a) Antigens coated onto the ELISA plate - b) Sample containing primary antibodies is added - c) Non-antigen binding antibodies are washed off the plate - d) Secondary antibody-conjugated with an enzyme is added - e) Excess secondary antibody is washed off the plate - f) Substrate for the enzyme (Chromogen) is added - g) Enzyme reacts with the substrate producing color. Intensity of the color correlates with the level of antigen (Image is reproduced from Gan and Patel (2013)).

Another label-based technique that is widely used is Polymerase Chain Reaction (PCR). PCR was developed by Kary Mullis in 1983 (Saiki et al., 1985). It has since been used in numerous studies to diagnose diseases and identify the presence of different strains of bacteria, viruses and DNA (Senda et al., 1996; Wang et al., 1996; Garcia et al., 2001; Cai et al., 2014).

PCR is used in molecular biology to amplify a single copy of a particular DNA sequence and generate billions of copies in few hours ($\sim$ 2 to 4 hours) (Olerup and Zetterquist, 1992). The

Table 2.1 Advantages and limitations of the ELISA techniques

	Advantages	**Limitations**
Direct ELISA	- Quick, few steps - Less prone to error	- Time consuming (can take up to 4 hours) and expensive - Labeling affects adversely the immunoreactivity of primary antibody - Minimal signal amplification
Indirect ELISA	- Wide variety of secondary antibody is commercially available - The presence of two labeled primary antibodies increases its sensitivity - Immunoreactivity of the primary antibody is not altered because it is not labeled - Cost-saving since it requires fewer labeled antibodies	- The presence of a secondary antibody may create a cross-reactivity with the primary, leading to non-specific signal - Extra incubation step is required - A known antigen or antibody must be generated in order to detect a given antibody or antigen
Sandwich ELISA	- The use of two antibodies increases its specificity - Antigen does not require prior purification, making it suitable to use in complex environments	- Not all antibodies can be used, so no flexibility in the choice of primary antibody - Microwells must be read quickly since the reaction between the enzyme and the substrate is quick - Expensive

technique is achieved through three thermal cycles. The first step is the denaturation of the DNA that will separate into two pieces of single strand DNA called primers. The original DNA is called the template. This step is done at a temperature between 94 and 98 °C for 20-30 sec. The next step is the annealing and occurs at temperatures varying between 50 and 60 °C for 20-40 sec. The two primers are used in this step and they will bind to the beginning of the sequence that will be copied, generating two separate strands of DNA. The last step is the extension, where the temperature is increased to about 72 °C. Nucleotides in solution are added to the annealed primers by the DNA polymerase to create a new strand of DNA. DNA polymerase is a complex of proteins that naturally occurs and its function is to copy a cell's DNA before it divides it in two. By the end of the process, two identical copies of the original DNA will be made. This cycle is repeated between 30 to 40 times, generating billions of copies of the original DNA segment (Garibyan and Avashia, 2013). A schematic of the polymerase chain reaction process is shown in Fig. 2.3. PCR is a very sensitive technique that can allow early diagnosis of diseases, and specific detection of infections caused by bacteria or viruses.

However, the use of DNA polymerase makes it prone to error and can lead to mutations in the generated fragment. Non-specific binding of the primers to other similar sequences on the template DNA can alter the specificity of the technique. And since it is label-based, a prior sequence information is necessary in order to design the primers. The advantages and limitations of the technique are summarized in Table 2.2.
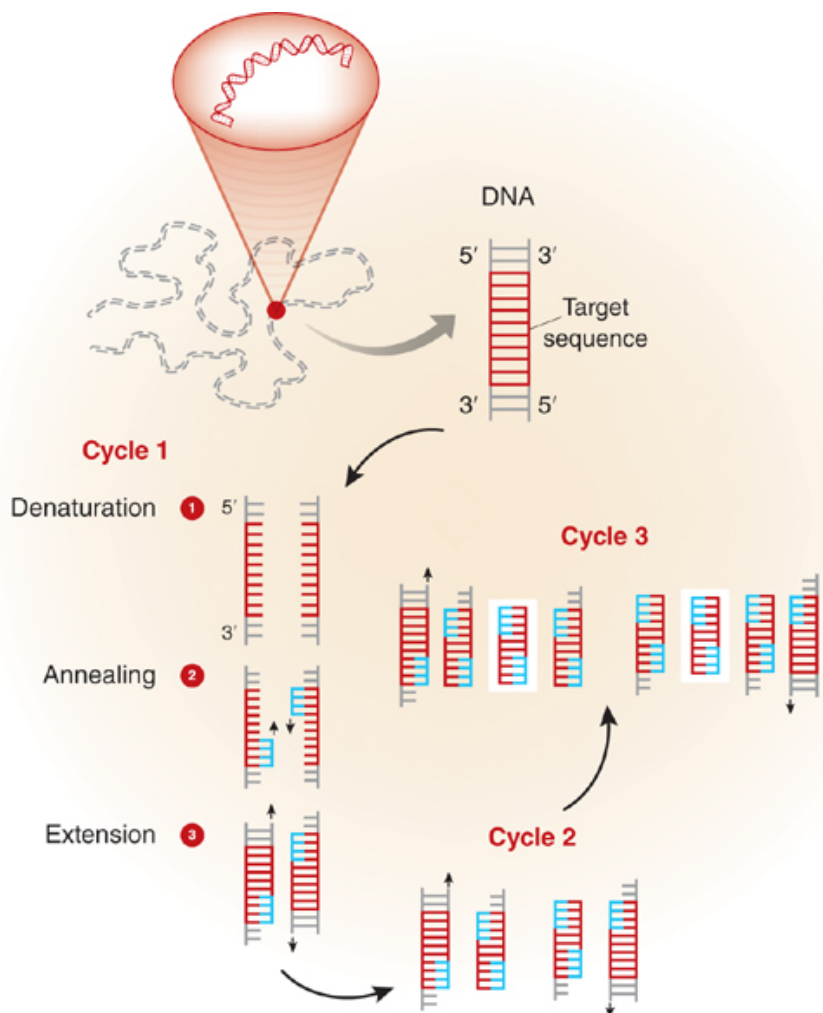
Figure 2.3 Polymerase chain reaction (PCR) process (Garibyan and Avashia, 2013)

Many label-based biosensors use fluorescent tags such as dyes to label either the bio-recognition element or the target molecule. The presence of the target molecule and the interaction between the molecule and the bio-recognition element are demonstrated by the intensity of the fluorescence (Fan et al., 2008). These techniques can be highly sensitive, with detection limits down to a single molecule (Moerner, 2007), and the dual confirmation of the presence of the analyte reduces the number of false-positive responses (Mehrabani et al., 2014). Nonetheless, the labeling process can be laborious and time-consuming, making the resulting sensor

Table 2.2 Advantages and limitations of PCR technique

Advantages	Limitations
- It is a very sensitive technique that allows early and specific diagnosis of infectious diseases - It makes billions of copies of DNA strands which allows detection and identification based on size - Modified versions of PRC, called Real-time PCR, allow quantitative measurements of gene expression	- It takes between 1 to 4 hours to amplify a specific segment of DNA - A prior knowledge of the sequence is necessary in order to generate the primers for PCR - Non-specific bindings of the primers to the template DNA may alter the specificity of the PCR product - DNA polymerase is prone to errors which can cause mutations in the fragment generated

complicated to use and pricey, not to mention that labels could interfere with the function of the antibodies or proteins (Pires et al., 2014). Results need to be analyzed fast since the fluorescent dyes tend to photobleach, meaning they become permanently unable to fluoresce when exposed to light.

2.2   Label-free biosensors

Since label-based biosensors have many flaws, it becomes crucial to find new techniques that don't require any labeling. In addition to being label-free, these new techniques need to be sensitive and specific to the target molecule and be able to achieve fast response real-time detection in aqueous environments since most of the biological and clinical samples are water-based (Wu and Vollmer, 2014). Numerous label-free detection techniques have been employed so far. They can be mainly divided into three categories : electrical, mechanical and optical methods. In what follows, a brief description of the electrical and mechanical biosensors is given, followed by a more detailed explanation of the optical biosensors, more specifically whispering gallery mode resonators. A brief summary of the different techniques is given in Table 2.3.

Table 2.3 Label-free biosensors and detection modalities

Detection technique	Devices / Detection mechanisms	Detection response	Example of detections	References
Electrical	Nanowires	Changes in electrical signal such as current, resistance, voltage or conductance	Single virus	(Patolsky et al., 2006)
	Field-effect transistors	Changes of inherent biomolecular charge	Protein	(Ishikawa et al., 2009)
Mechanical	Cantilevers	Mechanical resonant frequency due to mass change or bending of cantilever due to stress/strain deflection	Single cell	(Fritz et al., 2000; Burg et al., 2007)
Optical	Surface plasmon resonance	Shift in plasmon resonance	Proteins, DNA, bacteria	(Kuo et al., 2003; Yao et al., 2006; Taylor et al., 2005)
	Optical microcavity resonator	Shift in resonance wavelength	Single virus, proteins	(Vollmer et al., 2008; Arnold et al., 2010)

2.2.1 Electrical biosensors

Electrical biosensors are one of the most widely used label-free biosensing techniques. When a chemical or a biomolecule binds to the surface of an electrical biosensor, it interacts with its electrodes or probes, creating a change in the output electric signal and the response is observed as a variation in one or more of the following characteristics : potential, current, resistance or impedance (Pires et al., 2014; Hurk and Evoy, 2015). Since electrical sensors are fabricated using standard lithographic techniques, they can be easily integrated into lab-on-chips platforms (Hunt and Armani, 2010). Several applications have been reported in the literature using electrical platforms or biosensing. One study reported the use of nanowires based on field-effect transistors (FET) to detect the nucleocapsid protein, a specific biomarker for the severe acute respiratory syndrome (SARS) (Ishikawa et al., 2009). Another study used antibodies immobilized on the sensor's surface to bind E. coli bacteria (Radke and Alocilja, 2005). Despite electrical-based biosensors being highly sensitive, cost effective, easy to integrate into microfluidic chips, providing good precision and consuming low power (Sassa et al., 2008; Pires et al., 2011), the fact that they are highly influenced by variations of temperature, pH and ionic concentrations limit their shelf life, and hence, limit their use in point-of-care in complex environments (Pires et al., 2014).

2.2.2 Mechanical biosensors

Mechanical biosensors have been studied for decades for biosensing applications. The most common type of these sensors is based on cantilevers, which are typically made of sili-

con/silicon dioxide (Gupta et al., 2004), silicon nitride (Berger et al., 1997) or polymers (Nordström et al., 2008). Microcantilevers have been widely used to detect different types of analytes, such as DNA and bacteria (Huber et al., 2006; Weeks et al., 2003). They have been demonstrated to measure single-cell binding events (Burg et al., 2007), and to detect ultra-low concentrations of prostate specific antigen, which is a biomarker for prostate cancer in complex media (Wu et al., 2001a). The detection mechanism of a cantilever can be divided into two operating modes. The first one is a static deflection. When biomolecules bind on one side of the cantilever, they cause an imbalance to the surface stress, and hence, a deflection of the cantilever. This deflection is the detection response measured due to biomolecule binding to the sensor (Fritz et al., 2000). Eq. 2.1 shows the relation that governs this response.

$$\Delta h = 3 \ \sigma \ (1 - \nu)/E \ \text{x} \ (L/d)^2 \tag{2.1}$$

where σ is the change in the surface stress, ν the Poisson ratio, E Young's modulus of the cantilever, L its length and d its thickness.

The second detection mechanism is a dynamic one. When biomolecules bind to the surface of the cantilever, they cause a change in its mass. The resonant frequency will thus shift consequently. This dependence is shown in Eq. 2.2 (Datar et al., 2009).

$$f = \frac{1}{2 \ \pi} \sqrt{\frac{k}{m^* + \alpha \Delta m}} \tag{2.2}$$

where k is the spring constant of the cantilever, m^* the effective mass, α the numerical constant that describes where the biomolecule binds on the surface, and Δm is the change in mass due to bound molecules.

Similar to electrical sensors, mechanical sensors are also fabricated using surface micromachining and MEMS lithographic techniques, which allow easy integration to lab-on-chips and microfluidic systems. However, their sensitivity is limited by the mechanical losses that are due to the viscous damping, thus limiting their use in liquid samples (Pires et al., 2014). The detection time can also be relatively long, around 30 minutes, making mechanical sensors not suited for real-time detection (Ferrari, 2005). A summary of both electrical and mechanical biosensors is given in Table 2.4 describing the advantages and drawbacks of each technique.

The limitations in both electrical and mechanical biosensing techniques drew the researchers toward the use of optical devices such as Surface Plasmon Resonance (SPR) and optical microcavities for biodetection applications. The next section presents an overview of the prior art of label-free detection with optical devices.

Table 2.4 Summary of the electrical and mechanical biodetection techniques

Biodetection technique	Advantages	Drawbacks	References
Electrical	-Rapid, real-time detection -Low-cost fabrication -Widely employed point-of-care	-Short shelf life -Control of ionic concentrations before detection	(Wongkaew et al., 2013)
Mechanical	-Monolithic sensor integration	-Detection needs ~ 30 min -Damping effects in liquid samples -Complex fabrication	(Ferrari, 2005)

2.2.3 Optical biosensors

Surface Plasmon Resonance

Surface plasmon resonance was first demonstrated for biosensing by Liedberg et al. (1983). It has been since extensively studied and became a powerful tool for label-free detection of several biomolecules, such as cells (Krupin et al., 2013), proteins (Kuo et al., 2003), DNA (Yao et al., 2006) and bacteria (Taylor et al., 2005).

The most convenient SPR method that yields the best sensing detection limit (DL) is based on prism coupling, as shown in Fig. 2.4 . The incident light is totally reflected on the interface between the prism and the metal (gold) and an evanescent field excites a propagating surface plasmon at the surface of the gold layer. The propagation constant of the evanescent field matches that of the surface plasmon at resonant wavelength, the photon will then be coupled inside the surface plasmon, as described in Eq. 2.3.

$$\frac{2\pi}{\lambda} \, n_p \, sin\theta = \beta_{sp} \tag{2.3}$$

where λ is the incident wavelength, n_p the prism refractive index, θ the incidence angle and β_{sp} the surface plasmon propagation constant.

Biosensors using SPR are highly sensitive to multiple analytes and can provide fast responses and detection limits ranging from picomolar to nanomolar (Tombelli et al., 2005; Chinowsky et al., 2007). However, they are bulky and the instrumentation used for SPR measurements is complex, making it very hard and expensive to integrate them into a lab-on-chip with microfluidics for point-of-care use. In addition, SPR sensors require the use of gold surfaces or
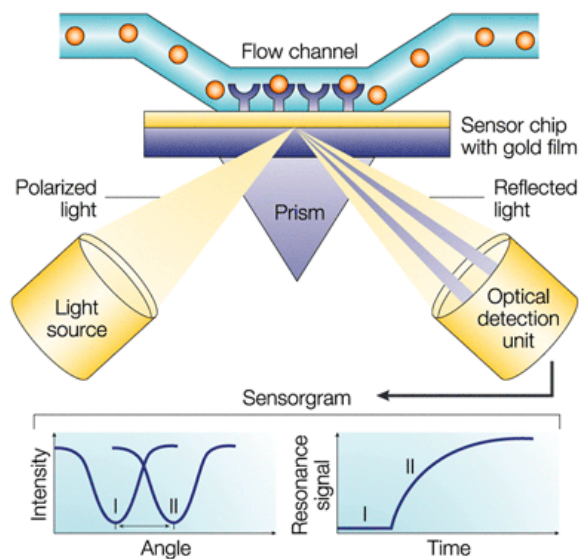
Figure 2.4 Schematic of a prism-coupled SPR biosensor (Cooper, 2002)

nanoparticles, and they are strongly influenced by the temperature, making the fabrication of portable, point-of-care devices near impossible. The advancements in optoelectronics, integrated optics and microfluidics techniques are leading the way towards integrated platforms, such as fiber, waveguide-SPR or SPR on silicon. However, these improvements are decreasing the sensitivity of the biosensor (Hoa et al., 2007). Since it is difficult to have a robust, low-cost sensor with integrated microfluidics, the use of SPR sensors will still be limited to the laboratory.

A new family of biosensors has emerged in the last decade that possesses all of the desired capabilities, from being label-free, cost-effective, highly sensitive, to the possibility of being integrated on lab-on-chips and used in complex environments; whispering gallery optical microcavities.

Whispering Gallery Mode Microcavities

Whispering gallery microcavities (WGM) gained a strong popularity in the past decade as new techniques for label-free biosensing applications. WGM are structures that can efficiently confine light at the microscale due to total internal reflection of light at the interface between the microcavity and its surrounding medium. The long photon lifetime inside the microcavity yields to high quality factors, thus increasing the sensitivity of the biosensor since the light can interact several times with the binding molecule. A detailed explanation of this process along with the theory of WGMs are given in Chapter 3.

WGM microcavities come in different geometries : spheres, toroids, rings, disks and cylinders, just to name a few, and can be fabricated using different materials, such as silica (Bergeron et al., 2009), silicon (Borselli et al., 2005) and polymers (Chao and Guo, 2003). Different biological molecules have been detected using these geometries, including proteins, viruses and DNA. An overview of some of these geometries along with some biodetection demonstrations are given in Table 2.5.

Table 2.5 Overview of WGM cavity geometries and their biodetection demonstration

Geometry	Material	Q-factor (air)	Q-factor (water)	Biodetection examples	Multiplexing possibility	References
Microsphere	Silica	$>10^9$	$>10^6$	Single virus, protein, DNA	Difficult	(Gorodetsky et al., 1996; Vollmer et al., 2002, 2008)
Microtoroid	Silica	$>10^8$	$>10^8$	Single molecule in buffer and in serum, fluorophore	Difficult	(Armani et al., 2007)
Microring	Silicon, SiN, polymers	$\sim 10^3$ - 10^5	$\sim 10^3$ - 10^5	Bacteria, glucose	Demonstrated	(Chao and Guo, 2002; Ramachandran et al., 2008)
Microdisk	Silica	$\sim 10^4$ - 10^6	$\sim 10^4$ - 10^6	Virus, protein, DNA	Straightforward once waveguides are integrated (Demonstrated)	(Boyd and Heebner, 2001)

Microspheres

Silica microspheres, shown in Fig. 2.5, were the first microcavity structures used in biosensing (Vollmer et al., 2002). They are easily fabricated by melting the tip of an optical fiber using a CO_2 laser beam and have very high Q-factors in air ($\sim 10^9$) and in water ($\sim 10^6$). Microspheres were demonstrated to detect the presence of a single virus (Vollmer et al., 2008), protein (Vollmer et al., 2002), and DNA with detection limits of few pg/mm^2 (Vollmer et al., 2003). Despite being highly sensitive and easy to fabricate, microspheres remain very difficult to integrate with microfluidics or for multiplexed sensing because of their bulky structure.

Microtoroids

Microtoroids are made of silica and are fabricated using lithographic techniques (Fig. 2.6). Photolithography is used to transfer the patterns of microdisks onto a silica wafer. Hydrofluoric acid is then used to etch the silica to form the disks. Silicon pedestals are formed using a xenon difluoride (XeF_2) plasma etch. The last step is the reflow of the disks to form toroids using a CO_2 laser. Microtoroids have high Q-factors ($\sim 10^8$) and are able to achieve a single molecule detection. Because the reflow process cannot be controlled, the dimensions of the
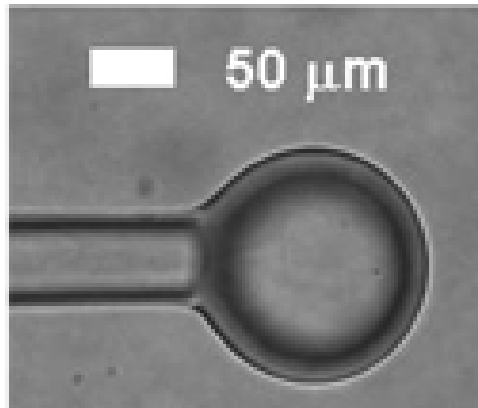
Figure 2.5 Silica optical microsphere (Vollmer et al., 2002)

microtoroids can vary of several micrometers, making the integration with microfluidics quite difficult. A monolithically integrated silica microtoroid with a bent waveguide have been demonstrated (Zhang and Armani, 2013). The resulting microtoroid has a 70 μm diameter and a Q-factor of 3.2x10^6 at 1550 nm. However, the fabrication process is quite laborious and is complicated to integrate with microfluidics.
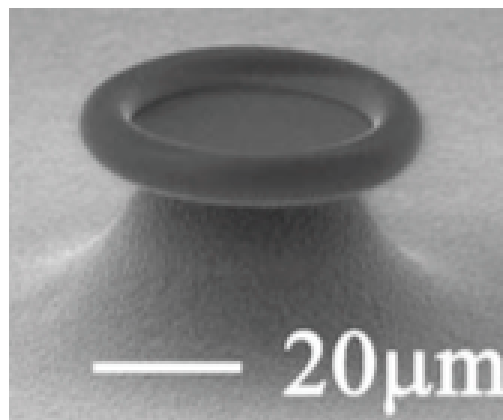
Figure 2.6 Scanning electron micrograph of an optical microtoroid (Zhang et al., 2010)

Microrings

Microring biosensors, shown in Fig. 2.7, are the only WGM sensors to be commercialized. They are fabricated on-chip using photolithographic techniques, and can be made of silicon, silica and organic polymers. They are ideal for integration into portable electronic devices and for multiplexed detection. Commercial silicon microrings have been used to detect the

presence of a cancer biomarker antigen in an undiluted serum (Washburn et al., 2009). However, they have relatively low Q-factors ($\sim 10^3$), which makes them less sensitive than other optical resonators, limiting their ability to detect ultra low concentrations of analytes or a single molecule binding.
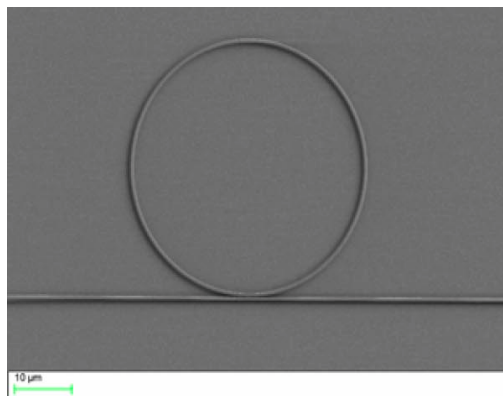
Figure 2.7 Scanning electron micrograph of a silicon microring (Li et al., 2008)

Microdisks

Optical microdisks are fabricated the same way as microtoroids but without the reflow step at the end, as can be seen in Fig. 2.8. Their quality factors can range between 10^4 to 10^6. They can easily be integrated once the waveguides are integrated (Grutter et al., 2012), and used for multiplexed sensing. Optical microdisks have been demonstrated to detect the presence of virus particles, proteins and DNA (Boyd and Heebner, 2001) .

2.3   Conclusion

Several biosensing techniques have been developed over the years to diagnose illnesses and detect the presence of infectious diseases caused by viruses and bacteria. Biosensors requiring labeling of the target analyte were the first to be studied and used. However, they can be very expensive, time-consuming, and the labeling process can interfere with the immunoreactivity of the antibodies. Label-free biosensors were then developed to overcome these problems. They can be divided into three main categories : electrochemical, mechanical and optical. Despite being very sensitive and widely employed in point-of-care, the limitations of both electrochemical and mechanical techniques lead the researchers to turn towards a new family of biosensors, optical biosensors, and more specifically whispering gallery microcavities. WGM

Mag	HV	Det	VacMode	WD	01/20/15	Tilt	———50 µm———
1300x	5.0 kV	Etd	Highvacuum	7.54 mm	22:05:27	75.9 °	
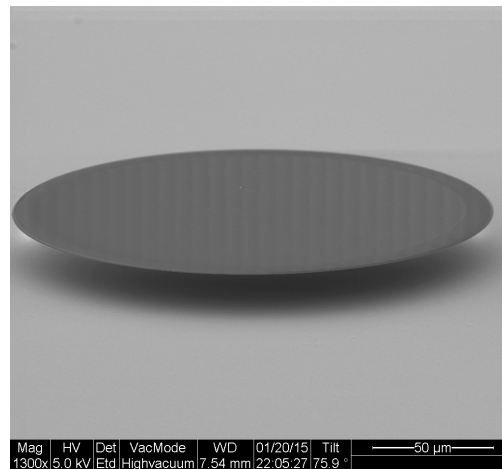
Figure 2.8 Scanning electron micrograph of an optical microdisk

resonators have been studied for the last decade and have many applications as biosensors. Each geometry of microcavities has its advantages and limitations for use as a biosensor. One geometry that can be a good compromise is optical microdisks. Optical microdisks have relatively high Q-factors, are easy to fabricate, to integrate with microfluidics and to use for multiplexed sensing. All of these characteristics make them ideal for biosensing applications.

In this thesis, detection of bacteria will be performed for the first time on the surface of optical microdisks that will be properly functionalized to obtain a specific binding. The binding event will be observed as a shift in the resonance wavelength of the disk, also known as the reactive sensing mechanism, described in more details in the following chapter.

CHAPTER 3   THEORY OF WHISPERING GALLERY MICROCAVITIES

In this chapter, the theory of whispering gallery microcavities is explained. First, an overview of the phenomena of light confinement and propagation of the electromagnetic waves inside the cavity is presented. This is followed by the main characteristics of the optical microresonators. The second part of this chapter focuses on the different biosensing mechanisms that govern the use of WGM microcavities as biosensors.

3.1   Theory of WGM

3.1.1   Light confinement and eigenmodes

Whispering gallery mode microcavities are structures that can efficiently confine light at the microscale. They are named after Lord Rayleigh's explanation of the "whispering gallery" of St. Paul's Cathedral in London, where acoustic waves are reflected along the curved walls of the gallery, making it possible to hear a word whispered at the front end of the gallery at its far end (Vahala, 2004). In a similar way, the optical wave is confined inside the microcavity due to total internal reflection of light at the interface between the microcavity and its surrounding medium.

The refraction of light at the interface between two media is pictured in Fig. 3.1 as described by the Snell-Descartes law, also called the refraction law, presented in Eq. 3.1.

$$n_1 \; sin \; \theta_i = n_2 \; sin \; \theta_t \tag{3.1}$$

Total internal reflection occurs when the angle of incidence (θ_i) of light is larger than a critical angle (θ_c) that is measured with respect to the normal to the surface. The critical angle is found according to Eq. 3.2, with $n_1 > n_2$,

$$sin \; \theta_c = \frac{n_2}{n_1} \tag{3.2}$$

Considering a microcavity made of silica and surrounded by air, the critical angle would be equal to 43.6°. The total internal reflection of light inside an optical microdisk is shown in Fig. 3.2.

In the following, a description of the eigenmodes of a microcavity as well as the methods to calculate them are presented, starting by finding the spatial distribution of the electric
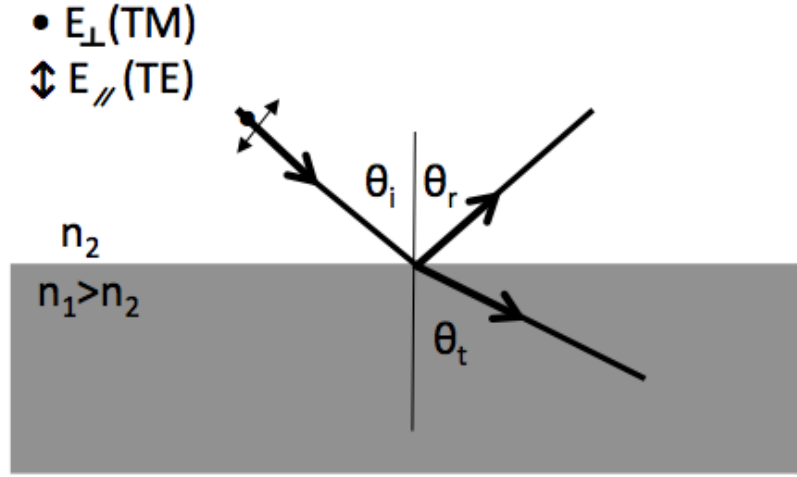
Figure 3.1 Refraction and reflection of light at the interface between the optical microcavity and its surrounding medium
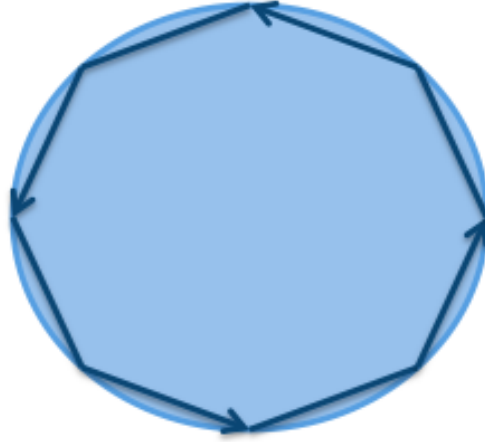
Figure 3.2 Total internal reflection of light inside a microdisk

and magnetic fields confined inside the cavity. Detailed explanations of the microresonators theory can be found in the following references : Vahala (2004), Heebner et al. (2008), Bures (2009) and Bergeron (2010). Although the microdisk is a three dimensional structure, the wave equation is solved in two dimensions (2D) using the effective refractive index (n_{eff}) approximation. In this case, the 2D problem is appropriate to apply on thin disks, and it gives a good qualitative understanding of the nature of the modes.

The electric and magnetic fields inside a resonator each have three components, each of these

components being the projection of the field on a coordinates system's axis. There exists two eigen-states of polarization where the magnetic (or electric) field is perpendicular to the incidence yz and are called Transverse Magnetic wave [TM] where $H_y = H_z = 0$ (or Transverse Electric wave [TE] where $E_y = E_z = 0$) (Bures, 2009). Since both of these modes can be resolved similarly from the Maxwell's equations, the following will detail the calculation of the electric field $E_z(r, \phi, z)$. The other components can be easily found accordingly.
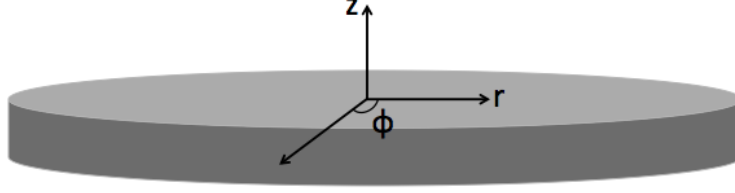
Figure 3.3 Schematic of a silica microdisk and the coordinates system used to find the modes and the electric field inside the cavity

In cylindrical coordinates (Fig. 3.3), the electric and magnetic fields of a monochromatic stationary wave, assuming non-dispersive non-absorptive medium, can be expressed as follows :

$$\mathbf{E}(\mathbf{r}, t) = \mathbf{E}(r, \phi) \exp(-i\omega t) \tag{3.3}$$

$$\mathbf{H}(\mathbf{r}, t) = \mathbf{H}(r, \phi) \exp(-i\omega t) \tag{3.4}$$

$$\begin{cases} \nabla \wedge \mathbf{E} = -\mu_0 \frac{\partial \mathbf{H}}{\partial t} & \text{and} \quad \nabla.(\epsilon_0 n^2 \mathbf{E}) = 0 \\ \nabla \wedge \mathbf{H} = \epsilon_0 n^2 \frac{\partial \mathbf{E}}{\partial t} & \text{and} \quad \nabla.(\mu_0 \mathbf{H}) = 0 \end{cases} \tag{3.5}$$

with $\vec{E}$ being the electric field, $\vec{H}$ the magnetic field, ϵ_0 the vacuum permittivity, μ_0 the vacuum permeability and n the medium refractive index.

By deriving Eq. (3.3) and (3.4) according to Maxwell's equations (Eq. 3.5), they can be rewritten as a scalar equation, known as Helmholtz wave equation with two variables, as described in Eq. 3.6 :

$$\frac{1}{r} \frac{\partial}{\partial r} \left(r \frac{\partial E_z(r, \phi)}{\partial r} \right) + \frac{1}{r_2} \frac{\partial^2 E_z(r, \phi)}{\partial \phi^2} + k^2[1 - n^2(r)]E_z(r, \phi) = k^2 E_z(r, \phi) \tag{3.6}$$

where k is the wave number or propagation constant (rad m^{-1}).

The circular symmetry will facilitate the resolution of the problem, and the electric field can hence be written as a product of a radial and azimuthal functions, i.e. $E_z(r, \phi) = R(r)\Phi(\phi)$. Using the variable separation to resolve this equation, Eq. 3.6 can be rewritten as :

$$\frac{\partial^2 R(r)}{\partial r^2} + \frac{1}{r}\frac{\partial R(r)}{\partial r} + \left(k^2 n^2 - \frac{m^2}{r^2}\right)R(r) = 0 \tag{3.7}$$

$$\frac{\partial^2 \Phi}{\partial \phi^2} = -m^2\Phi \tag{3.8}$$

where m is the constant resulting from variable separation, and $k^2 n^2 = \beta^2$ is the mode propagation constant.

Resolution of the Eq. 3.8 is straight forward, and the azimuthal function can be expressed as a complex exponential equation, as demonstrated in Eq. 3.9, where A and B are the integration constants.

$$\Phi_m(\phi) = A \exp(im\phi) + B \exp(-im\phi) \tag{3.9}$$

The radial equation (Eq. 3.7) can be reduced to the well-known Bessel equation. It can thus be written as a linear combination of Bessel functions of order m. Due to the boundary conditions, the radial equation can be written as a linear combination of a first-kind Bessel function of order m ($J_m(n_{eff}kr)$) inside of the cavity (r<ρ), and a first-kind Hankel function of order m ($H_m(kr)$) outside of the cavity (r>ρ), as shown in Eq. 3.10 and Eq. 3.11, with A_m and S_m their integration constants respectively and ρ being the radius of the cavity.

$$R^m_{r<\rho}(r) = A_m J_m(n_{eff}kr) \tag{3.10}$$

$$R^m_{r>\rho}(r) = S_m H_m(kr) \tag{3.11}$$

The general equations of the electric field for the TM mode have been established, the next step is to determine an exact solution to these equations. The integration constants will be calculated using the continuity of the electric field and its derivative at the interface between the cavity and its surrounding medium (air), as can be shown in Eq. 3.12 and Eq. 3.13.

$$A_m J_m(n_{eff}k\rho) = S_m H_m(k\rho) \tag{3.12}$$

$$A_m \frac{dJ_m(n_{eff}kr)}{dr}\bigg|_\rho = S_m \frac{dH_m(kr)}{dr}\bigg|_\rho \qquad (3.13)$$

For a given value of m, it will be possible to determine the constants A_m and S_m and the eigenvalues of the wavenumber $k = \omega/c$. Each of these eigenvalues will correspond to a certain radial mode number l. Each mode will thus be defined by two mode numbers, the radial mode number l (= 0, 1, 2, ...) and the azimuthal mode number m (= -l, -l+1, ..., 0, l-1, l). Fig. 3.4 shows the simulations for a 10 μm-diameter microdisk at a 5 μm wavelength, done using COMSOL Multiphysics Modeling Software (Bergeron, 2010). These parameters were used to easily visualize m=10 modes, compared to greater disk diameters characterized at telecommunication wavelengths (1.5 μm) where m would be of the order of few hundreds.
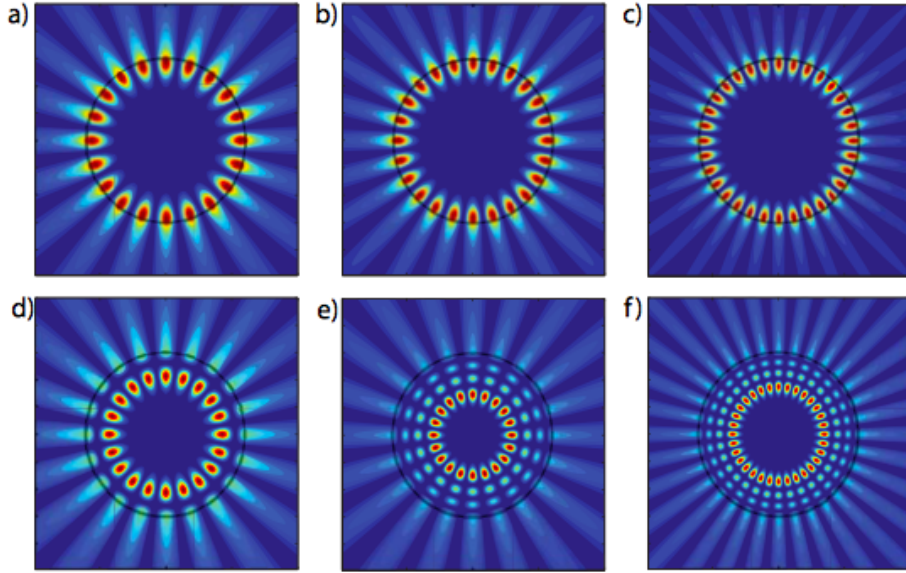
Figure 3.4 TM modes inside a 10 μm-diameter circular cavity at a 5 μm wavelength. a) m =10, l = 1 b) m = 12, l = 1 c) m = 16, l = 1, d) m = 10, l = 2, e) m = 10, l = 4 f) m = 16, l = 4 (Bergeron, 2010)

3.1.2   Light coupling using tapered optical fiber

Once the eigenmodes of a silica microdisk are well known, the next step would be to examine the method used to excite these modes.

There exist several techniques to couple light inside optical microcavities, ranging from free-space illumination to evanescent coupling techniques (Vahala, 2004). For biosensing applications, it is important to have high efficient coupling and low losses of power, which is why

evanescent coupling is the most appropriate technique for this specific application, especially since the fundamental whispering gallery modes are confined near the surface of a micro-cavity. Evanescent coupling is achieved using a tapered optical fiber, as shown in Fig. 3.5. Tapered fibers are fabricated using standard optical fibers (SMF-28) that are stretched using a torch and highly precise motorized stages in order to obtain 2 μm-diameter tapered fibers.
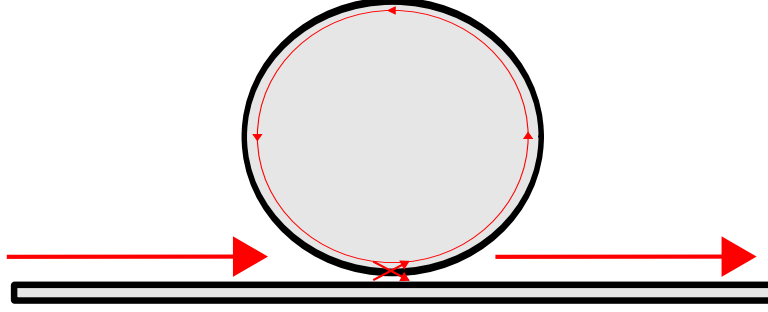
Figure 3.5 Coupling of light inside an optical microdisk using a tapered optical fiber

The evanescent field of the tapered fiber is part of its leakage losses. Stretching the fiber to obtain a 2 μm diameter contributes to the propagation of the evanescent field outside the fiber. The overlap of this evanescent wave with the microcavity modes will allow to quantify the energy transfer between the fiber and the microcavity. Considering that the coupling is weak, and using the theory of coupled modes (Little et al., 1997), it becomes possible to find the coupling coefficient (κ) between the microcavity's modes and the fundamental mode of the fiber. The fundamental mode of the electric field inside a microcavity ($\vec{e}_2$(x,y,z)) was found in the previous section for TM polarization. The same procedure can be used to find the electric field of the fundamental mode ($\vec{e}_1(x, y, z)$) inside the tapered fiber. The electric field of the fiber is a first kind Bessel function inside the core, and a modified second kind Bessel function on the outside (Bures, 2009).

Both fields are calculated using the same coordinates system, with the z axis being the propagation direction of the electric field inside the fiber, and the y axis being perpendicular to the plane of both structures. The instant coupling coefficient (κ_{12}(z)) describes the energy transfer from the guide 1 (tapered fiber) to the guide 2 (microcavity) and can be calculated using the overlap integral shown in Eq. 3.14, with k being the wave vector, β_1 the propagation constant of the mode in the fiber and β_2 that in the cavity, $\overline{n}$ the refractive index (RI) of the undisrupted mode of the fiber and n the RI of its disrupted mode. The total energy is given by integrating the coupling coefficient over the length of the fiber, in the direction of the z axis, as calculated in Eq. 3.15.

$$\kappa_{12}(z) = \kappa_{21}^*(z) = \frac{k^2}{2\sqrt{|\beta_1\beta_2|}} \int_{A_\infty} (n^2 - \overline{n}^2)\vec{e}_1^*(x,y,z)\vec{e}_2(x,y,z)dA \qquad (3.14)$$

$$\kappa_{12}(z) = \kappa_{21}^*(z) = \int_{-\infty}^{\infty} \kappa_{12}(z)\exp(-i\Delta\beta z)dz \qquad (3.15)$$

3.1.3 Optical microcavities characteristics

In this section, the main characteristics of optical microcavities are described, including the resonance, the free spectral range and the quality (Q-)factor. These features will help compare the different shapes and sizes of optical microcavities and choose the most suited for the desired application.

Resonances

Light remains confined inside an optical microcavity and recirculates for a long time since absorption loss in silica glass is less than 7 dB/km (Wu and Vollmer, 2014). As described earlier, the propagated light is reflected at the interface silica/air consecutively until it circumnavigates the entire cavity, and reaches its starting point. This interaction could be constructive, meaning that the wave is in phase with itself, and optical power can accumulate at that wavelength. If the interaction is destructive, the wave will be out of phase and accumulation of optical power is limited at this wavelength. It becomes thus possible to define a resonance wavelength as shown in Eq. 3.16 :

$$\lambda = \frac{2\pi R n_{eff}}{m} \qquad (3.16)$$

where R is the radius of the microcavity, n_{eff} is the effective refractive index of the mode and m its azimuthal order. The effective refractive index of the microcavity is the index seen by the guided mode, and it varies with the surrounding refractive index.

Free spectral range (FSR)

The free spectral range of a microcavity is the wavelength difference between two consecutive resonances, *m* and *m+1*. Using the expression found in Eq. 3.16, the FSR can be calculated as follows :

$$\lambda_m = \frac{2\pi R n_{eff}}{m} \qquad (3.17)$$

$$\lambda_{m+1} = \frac{2\pi R n_{eff}}{m+1} \tag{3.18}$$

$$FSR(\lambda) = \Delta(\lambda) = 2\pi R n_{eff} \left(\frac{1}{m} - \frac{1}{m+1}\right) \simeq \frac{\lambda^2}{2\pi R n_{eff}} \tag{3.19}$$

Given that $\lambda = c/\nu$ and $\Delta\lambda = c\,\Delta\nu/\nu^2$, the FSR can be rewritten as :

$$FSR(\nu) = \frac{c}{2\pi R n_{eff}} \tag{3.20}$$

Quality factor

The microcavity quality factor helps to quantify the efficiency of light confinement inside a microcavity. It is an expression of the time spent by light inside the microcavity (Eq. 3.21) (Vahala, 2004). The longer the light stays confined inside the cavity, the higher its quality factor will be. The photon lifetime can be measured by introducing a light wave at the resonant frequency of the microcavity then cutting off the excitation signal. The power acquisition right after stopping of laser allows to determine the half-life of the photon.

$$Q = \omega\tau = 2\pi\nu\tau \tag{3.21}$$

with ω being the frequency and τ the photon lifetime.

It can also be calculated by finding the resonance at full width at half maximum (FWHM) from the transmission spectrum (Eq. 3.22).

$$Q = \frac{\lambda}{\Delta\lambda} \tag{3.22}$$

Fig. 3.6 shows a typical transmission spectrum of a 200 μm-diameter microdisk coupled to a tapered optical fiber. The free spectral range and the FWHM are shown on the graph. For a Q-factor around 10^6, the photon lifetime inside the disk is about 1 ns.

The quality factor is also an expression of the losses, intrinsic and extrinsic, in the optical microcavity (Armani, 2010). The total or intrinsic Q-factor can be written as :

$$\frac{1}{Q_{total}} = \frac{1}{Q_{ss}} + \frac{1}{Q_{rad}} + \frac{1}{Q_{mat}} + \frac{1}{Q_{coup}} + \frac{1}{Q_{cont}} \tag{3.23}$$

where Q_{ss} is the surface scattering loss, Q_{rad} the radiation loss, Q_{mat} the material or absorp-
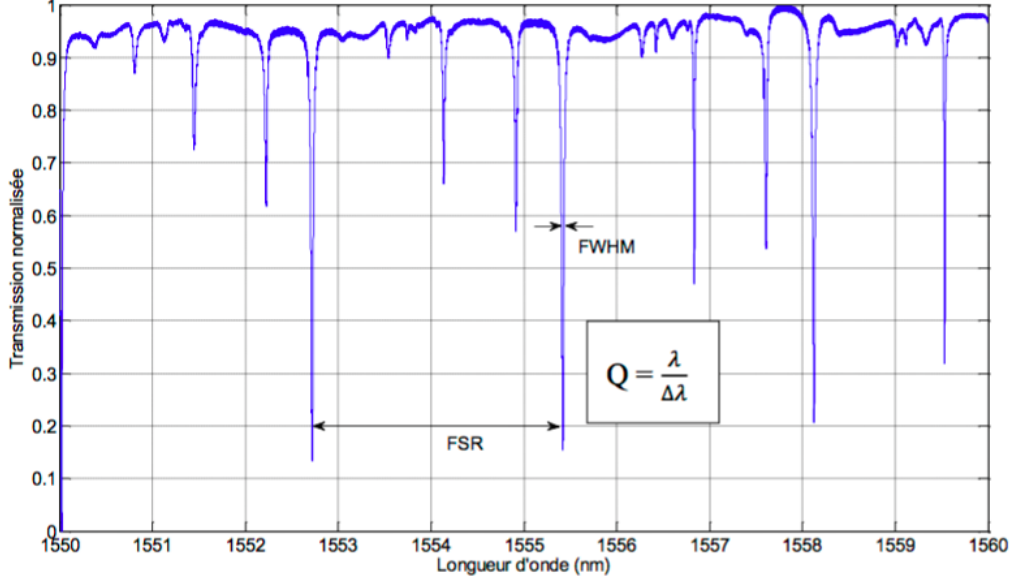
Figure 3.6 Typical resonance spectrum of a 200 μm-diameter microdisk coupled to a tapered optical fiber (Amrane, 2012)

tion loss, Q_{coup} the coupling loss, and Q_{cont} the contamination loss.

In order to maximize the quality factor and the sensitivity of a microcavity, it is important to minimize the loss mechanisms. The surface scattering (Q_{ss}) and radiation losses (Q_{rad}) rely on the quality and the resolution of the microfabrication process. The radiation loss increases when the radius of the microcavity is reduced. The absorption loss (Q_{mat}) is insignificant for silica microcavities because of low absorption of silica at telecommunications wavelength (around 1550 nm). Q_{mat} also depends on the effective refractive index of the cavity and can be expressed as follows :

$$Q_{mat} = \frac{2\pi n_{eff}}{\alpha_{eff}\lambda} \tag{3.24}$$

where n_{eff} is the effective RI, α_{eff} the effective material or absorption loss and λ the resonant wavelength. The absorption loss plays a crucial role when the microcavity is coupled in an aqueous environment, due to the high absorption coefficient of water in near-infrared (11.8 cm^{-1}). It becomes thus important to choose an appropriate wavelength to reduce the impact of absorption loss. For example, at 625 nm, the absorption coefficient of water is about 0.003 cm^{-1}.

It is also possible to decrease the impact of contamination on the quality factor (Q_{cont}) by

fabricating the microcavities in a sufficiently clean environment.

3.1.4 Biosensing mechanisms

There exist several methods of detecting biomolecules using optical microcavities, as shown in Fig. 3.7. The first one (Fig. 3.7 a)) is through a shift of a resonant frequency due to the reactive mechanism which occurs when a binding molecule changes the refractive index of the microresonator. The second technique (Fig. 3.7 b)) is a change of the quality factor of the cavity, mainly due to a change in the material absorption, also called line broadening. And lastly, a change in the transmission (Fig. 3.7 c)) which results from a change of the optical coupling.
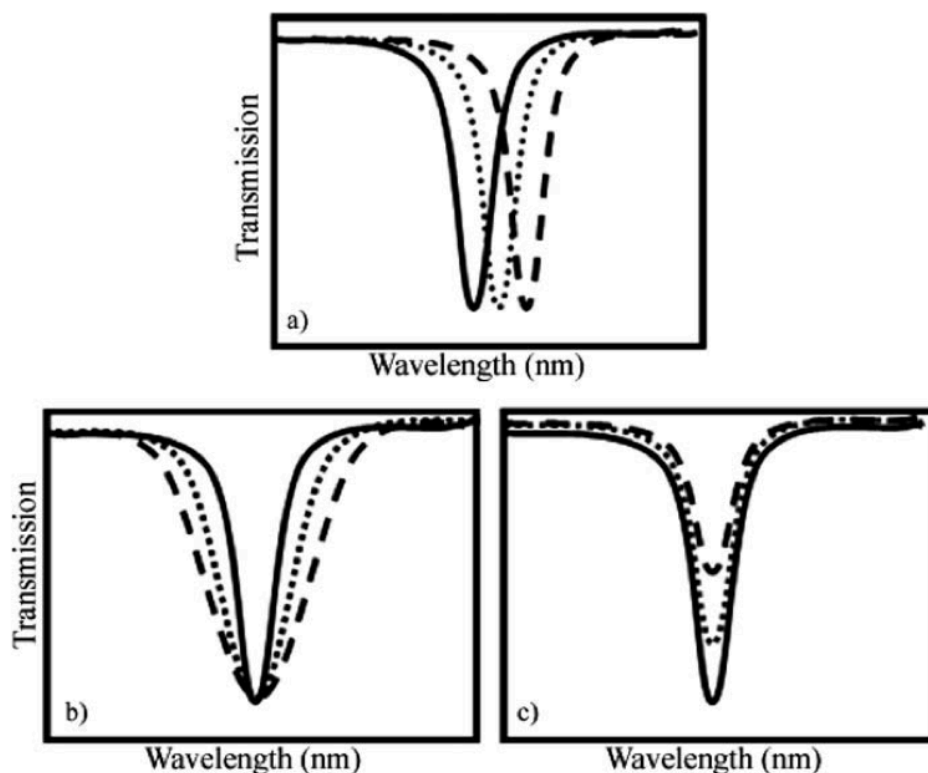
Figure 3.7 Detection techniques using optical microcavities : a) spectral shift due to the refractive index change, b) line broadening due to material absorption and c) peak transmission change resulting from the variation of the optical coupling (Armani, 2010)

Reactive sensing principle

When particles bind to the surface of the microresonator, they will interact with its evanescent field, hence increasing the optical path length. This will lead to a shift towards lower

frequencies, i.e. longer wavelengths, as shown in the relation of Eq. 3.25 and Fig. 3.7(a). This is known as the reactive mechanism for biosensing (Vollmer et al., 2008). The wavelength shift is given by :

$$\frac{\Delta\lambda}{\lambda} = \frac{\Delta R}{R} + \frac{\Delta n}{n} \tag{3.25}$$

where R is the radius and n the refractive index of the resonator.

The resonance condition described in section 3.1.3 yields the following equation :

$$\lambda_r = \frac{2\pi R n_{eff}}{m} \tag{3.26}$$

According to Eq. 3.26, the resonant wavelength can be varied by either changing the radius of the microcavity or changing the refractive index of the surrounding medium.

The resonance frequency is then expressed as :

$$\omega = 2\pi f = 2\pi \frac{c}{\lambda_r} = \frac{c}{n}\frac{m}{R} \tag{3.27}$$

The binding of a biomolecule to the surface of a microresonator (Fig. 3.8) will increase its path length by $2\pi\Delta l$, leading to a shift in the resonance frequency as following :

$$\frac{\Delta\omega}{\omega} = -\frac{2\pi\Delta l}{2\pi R} = \frac{\Delta l}{R} \tag{3.28}$$
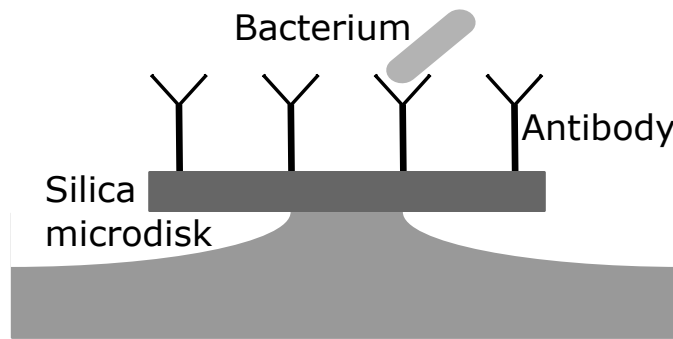
Figure 3.8 Biodetection of a bacterium on a functionalized microdisk

For more complex cases where the protein or biomolecules are not uniformly distributed across the resonator surface, the analysis becomes less straightforward. The polarizability of the particles as well as the surface density will have an effect on the resonant frequency shift. This relation has been established for a single protein binding to the equator of a microsphere,

and is shown in Eq. 3.33. The steps leading to this expression are briefly described below (Vollmer et al., 2002).

The resonant frequency shift in an optical microcavity can be described as follows :

$$\left(\frac{\delta\omega}{\omega}\right)_i \cong \frac{-\alpha_{ex}|\vec{E}_0(\vec{r_i})^2|}{2\int \epsilon_s|\vec{E}_0(\vec{r})|^2 dV} \tag{3.29}$$

The electric field can be written as :

$$\sum_i^N |E_0(\vec{r_i})|^2 \cong \sigma_p \int |E_0(\vec{r})|^2 dA \tag{3.30}$$

with the surface density of the molecules binding to the surface of the microsphere being

$$\sigma_s = \frac{N}{4\pi R^2} \tag{3.31}$$

and the excess polarizability of the molecules expressed as :

$$\alpha_{ex} = 4\pi\epsilon_0 \left(\frac{n_m}{2\pi}\right)\left(\frac{dn}{dc}\right)m \tag{3.32}$$

with n_m the medium refractive index, $\frac{dn}{dc}$ the differential refractive index of molecules in solvent, c the solvent concentration and m the mass of a single particle.

The resonant wavelength shift can thus be expressed as :

$$\frac{\delta\lambda}{\lambda} \cong \frac{\alpha_{ex}\sigma_s}{\epsilon_0(n_s^2 - n_m^2)R} \tag{3.33}$$

where α_{ex} is the excess polarizability of the bound protein, σ_s the surface density, ϵ_0 the vacuum permittivity, n_s and n_m the refractive indices of the sphere and the medium respectively, and R the orbital radius of the sphere.

Line broadening

Changes in the linewidth of the resonance can also be a consequence of a binding event on the surface of the cavity. This is due to the increase of the absorption or scattering losses generated by the interaction of the WGM with the biomolecule. The change in linewidth of the resonant mode (Fig. 3.7(b)) due to the molecular absorption is defined as :

$$\frac{\delta\gamma_{abs}}{\omega_0} \approx Im[\alpha]\frac{|\vec{E}(\vec{r_p})|^2}{\int_V \epsilon(\vec{r})|\vec{E}(\vec{r})|^2 d\vec{r}} \tag{3.34}$$

Mode broadening has been used to determine the concentration of an analyte (Ilchenko and Maleki, 2001) and for sensing individual polystyrene nanoparticles of 70 nm radius (Shao et al., 2013).

Transmission change

The intrinsic Q-factor of an optical microcavity is the result of several sources of losses as described in Eq. 3.23. Any binding event that occurs on the surface of the resonator can influence one or more of these Q-factors. Since most biosensing experiences are held in aqueous media, the absorption losses in water will increase. When coupling light via a tapered optical fiber, the addition or evaporation of the sample solution can interfere with the coupling efficiency between the fiber and the cavity. All these changes result in a variation of the optical coupling, which yields to a change in the transmission peak, as shown in Fig. 3.7(c).

The mode splitting principle

Another biosensing principle used is the mode splitting (Vollmer and Yang, 2012). This happens when one resonant mode splits into two resonances when light interacts with nanoscale objects, such as a nanoparticle. Since light propagates clockwise (CW) and counterclockwise (CCW) inside a WG microcavity, the optical mode has a two-fold degeneracy. Both modes propagate at the same resonant wavelength but in opposite directions. When the WGM field interacts with a nano-molecule, the light is scattered from the molecule. A part of the scattered light is lost to the environment, while the rest is scattered back into the mode volume, coupling between the CW and CCW modes, thus lifting the degeneracy of the two modes. This yields to a split of the resonance into two resonances in the transmission spectrum (Fig. 3.9). Several reasons can lead to the observation of the mode splitting. The presence of surface defects, inhomogeneities and nanoparticles are some of them.

3.2 Conclusion

In this chapter, the theory of the whispering gallery mode microcavities along with their characteristics were given. Since this project is based on the use of the WGM microdisks as biosensors, the different biosensing principles were explained. This gives a clear idea of the mechanisms that take place when a binding event occurs on the surface of the resonator.
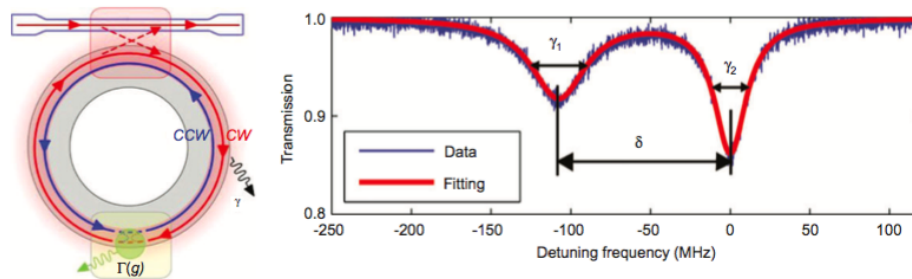
Figure 3.9 Mode splitting in a whispering gallery microcavity (Vollmer and Yang, 2012)

In the following chapter, the fabrication of silica microdisks is presented, along with the surface functionalization process that allows to obtain a specific biosensor, and the optical characterization setup used to conduct the biosensing experiments.

CHAPTER 4   WGM MICRODISKS : MICROFABRICATION, SURFACE FUNCTIONALIZATION AND OPTICAL CHARACTERIZATION SETUP

In this chapter, the microfabrication process of the whispering gallery microdisks as well as the experimental setup are presented.

This chapter starts by detailing the microfabrication process of WGM microdisks. Then, the surface functionalization process allowing specific sensing is described. Finally, the optical characterization setup is presented.

4.1   Microdisks fabrication

Optical microdisks are fabricated using standard microfabrication techniques. The fabrication is carried out in a clean room where contaminating particles as well as environmental parameters such as temperature and humidity are controlled. Since the resonators are in the order of the micrometer, the presence of even one dust particle or high humidity environment can affect the photolithography process, and hence, damage the fabricated resonator.

4.1.1   Photolithography

The substrates used for fabrication are purchased from Addison Engineering Inc., and are made of Silicon (Si) with an 800 nm layer of thermal silicon dioxide layer on top (Bergeron et al., 2009). The substrate is dehydrated in a vacuum oven and a thin layer of HMDS is deposited to allow a better adhesion of the photoresist to the surface of the wafer (Madou, 2002). The process starts by performing UV photolithography to generate photoresist patterns of the 200 μm-diameter microdisks with AZ5214-EIR photoresist (Fig. 4.1 a)). The photoresist is spread out on the substrate using a spinner at 4000 rpm for 30 sec. This is followed by a soft bake of the sample at 110°C for 1 min before exposing it using the UV lamp at a wavelength $\lambda = 365nm$ of the Karl Suss MA-4 aligner. The wafer is then submerged in a AZ-726-MIF solvent solution for 40 sec to be developed. The last step of photolithography is a hard bake at 120°C for 20 min. The thickness of the photoresist deposited is about 1.5 μm.

4.1.2   Silicon dioxide etch

The second microfabrication step is the isotropic etch of silicon dioxide using a Buffer Oxide Etch (BOE) solution (Fig. 4.1 b)). BOE is a mixture of Ammonium fluoride (NH_4F) and

Hydrofluoric acid (HF), with a volume ratio of 7 :1 NH_4F (40%) : HF (49%). It takes about 13 minutes to etch isotropically the 800 nm-thick Silicon dioxide (SiO_2).

The reaction for etching SiO_2 with BOE is :

$$SiO_2 + 4HF \rightarrow SiF_4 + 2H_2O \tag{4.1}$$

A downside for this etching technique is its isotropic nature that yields angled borders of the disks instead of vertical ones, which can reduce the quality factor of the resonator. For the purposed application of the disks in this thesis, the effect of this decrease did not influence the experimental results, and thus could be overlooked.

4.1.3 Reactive ion etching

The last step of the microfabrication process is Reactive Ion Etching (RIE) to obtain a silica microdisk on a silicon pedestal (Fig. 4.1 c)). The silicon is etched chemically using Sulfur Hexafluoride (SF_6) gas. The plasma is generated using an Inductively Coupled Plasma (ICP). It takes around 5 minutes to etch 10 μm of Si. Finally, the remaining photoresist is removed using an Oxygen (O_2) plasma. A process flow of the whole microfabrication process is shown in Fig. 4.1, and a Scanning Electron Microscope (SEM) image is shown in Fig. 4.2.
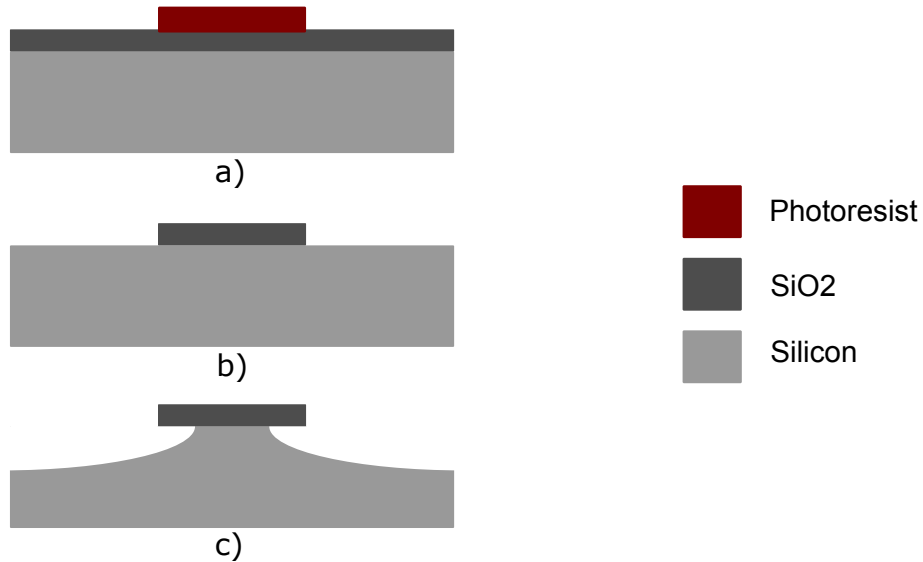
Figure 4.1 Microfabrication process flow of a silica microdisk. a) UV photolithography generating 200 μm-diameter disks patterns, b) Isotropic etch of silica using buffered oxide etch (B.O.E.) and c) Reactive ion etching of silicon pedestals using SF_6 plasma.
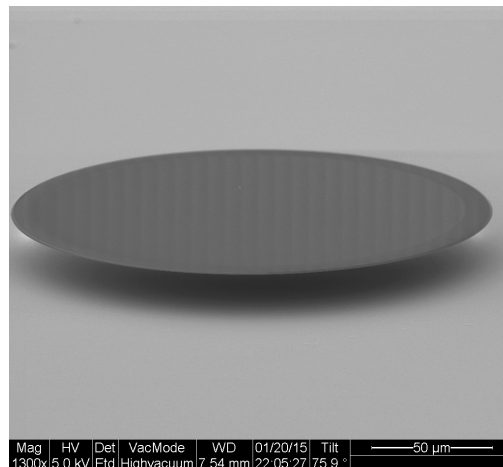
Figure 4.2 Scanning electron micrograph of an optical microdisk

4.2 Surface functionalization

One critical characteristic of a reliable biosensor is its specificity. It is a very important feature of the biosensor that will allow to eliminate the risk of false positives in complex environments. A proper surface functionalization becomes thus very important in order to have a specific and selective optical biosensor, while making sure not to alter the latter's optical properties nor sensing efficiency.

Whole bacteriophages have long been used as microbial agents and recognition elements for a wide variety of biosensors. However, purification of whole phages from host bacteria is difficult. They also show enzymatic activity that might cause some instabilities to the signal, and because of their large structure, they can decrease the signal strength, especially in sensing systems that depend upon distance like optical microcavities. For these reasons, isolating specific proteins from the whole bacteriophages will help overcome these problems. The functionalization process performed on the optical microdisks uses LysK phage protein.

The LysK phage protein is an endolysin from the staphylococcal phage K that acts strongly on S. aureus strains. It contains three domains : an N-terminal cystein, a histidine-dependent amidohydrolase/peptidase (CHAP) domain, a midprotein amidase-2 domain, and a C-terminal SH3b cell wall-binding domain (Becker et al., 2008).

The functionalization process starts by cleaning the samples in a piranha solution or with oxygen plasma to remove organic residues and free the hydroxyl radical (-OH) that will bind to the silane in the following step. The wafers are then submerged in an ethanol : water (95 :

5) solution that contains 2.5 % Triethoxysilane-Polyethylene Glycol (Si-PEG) (Nanocs, MW = 3400) for 2 hours, then thoroughly washed with ethanol and Deionized (DI) water. PEG is used to prevent non-specific binding to the surface of the microresonator. The wafers are then placed in a vacuum oven for annealing at 110°C for 2 hours. The next step is to add the LysK protein phage that is specific to the bacteria of interest, which is Staphylococcus Aureus (S. aureus) in this case. LysK will attach to the -NH$_2$ terminals of the Si-PEG using carbodiimide coupling.

1-Ethyl-3-[3-dimethylaminopropyl]carbodiimide hydrochloride (EDC) is a crosslinking agent used to couple carboxyl groups to primary amines. It is added to the LysK protein in a volume ratio of (1000 : 1) (EDC : protein). The PEGylated wafers are immersed in the protein : EDC solution that is added to a buffer (10 mM Tris.HCl pH 7.5, 150 mM NaCl, 1% glycerol) and stored at 4°C overnight, then thoroughly washed with Phosphate-Buffered Saline (PBS) and water.

A schematic of the functionalization process is shown in Fig. 4.3. Further details about this functionalization process can be found in reference (Chibli et al., 2014). Details of the protein purification process and bacterial culture are given in Appendix D.
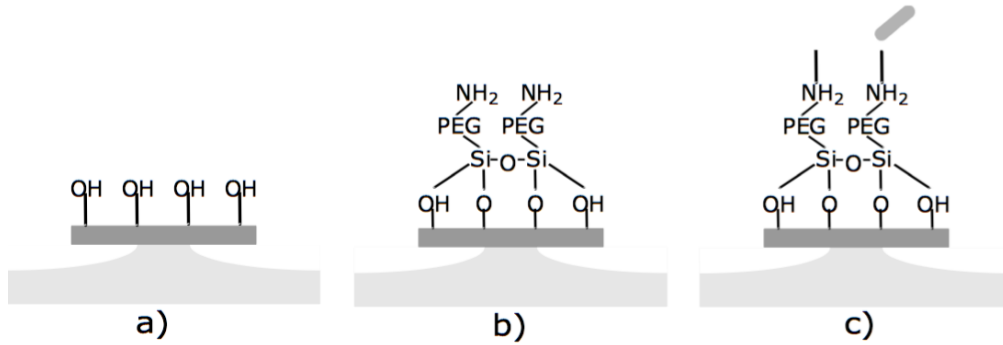
Figure 4.3 Functionalization process of silica microdisks. (a) The silicon dioxide surface is hydroxylated with oxygen plasma. (b) The disk is immersed in triethoxysilane-PEG-NH$_2$. (c) The free amines of the PEG-silane are covalently coupled to LysK using carbodiimide coupling.

4.3   Optical characterization setup

Evanescent coupling techniques are the most widely used techniques for whispering gallery mode resonators (Cai et al., 2000; Vahala, 2004). More specifically, the use of tapered optical

fibers can provide very efficient excitation of whispering gallery modes, and allows extraction of the optical power from the same fiber (Kippenberg et al., 2003).

In the following section, a description of the optical characterization setup is provided, as well as a description of all the optical and electrical components used to carry out the biosensing experiments.

The light from a tunable laser emitting in the red wavelengths is evanescently coupled inside the microdisk through a tapered optical fiber. A photodetector then conveys the output signal to an oscilloscope where the transmission spectrum of the microcavity is observed. The solution containing the S. aureus bacteria is deposited on the microdisk using a micropipette. The optical characterization setup is shown in Fig. 4.4, and it includes :

— Tunable laser (New focus TLB-6300-LN) : An external cavity tunable diode laser scanning between 632.5 and 637.5 nm at a 1 mW power. The choice of a red laser instead of one operating in the telecommunication wavelengths is due to the fact that the characterization is done in liquid environment. The absorption coefficient of water in the near-infrared to infrared is greater than that in visible light. The loss is about 11.8 cm^{-1} (Hale and Querry, 1973) at 1540 nm, which limits the sensitivity of the resonator. At shorter wavelengths, the losses are significantly smaller and are around 0.003 cm^{-1} at 625 nm, which makes the use of a red laser more suited to achieve highly sensitive biosensors using optical microcavities.

— Function generator (Agilent 33220A) : It feeds a trigger signal to the piezo input of the laser. The signal is set to pulse with a 10 ms width, 3.5 V amplitude and 1.75 V offset. These parameters can be adjusted to optimize the transmission spectrum.

— Polarization controller : It consists of a single mode fiber in red (Newport F-SV) that can be moved to change the polarization of the wave inside of it to optimize the coupling inside the microdisk. However, the exact polarization cannot be known since it is impossible to precisely control it with this device.

— Tapered optical fiber : Tapered fibers are fabricated in the optical fiber laboratory at Ecole Polytechnique. The SM fiber is stretched gently while it is heated over a flame, so the fiber and its core become thinner over a certain length. The length and the speed of the stretching are calculated in order to obtain an adiabatic taper, i.e. no coupling would occur between the fundamental mode and the other modes of the fiber (Bures, 2009). In the characterization setup described, a tapered single mode fiber in red (Newport F-SV) of 2 μm-diameter is used. The taper is mounted on a fork-shaped

holder and can be moved to optimize the coupling with the microdisk.

— Photodetector (Newport 818-SL/CM) : It is a silicon detector (400 - 1100 nm) that conveys the light from the red laser and transforms it into an electric signal that can be viewed on the oscilloscope.

— Oscilloscope (Agilent DSO6302A) : The sweep speed and the time unit are defined so the entire transmission spectrum can be viewed on the oscilloscope.

The use of all of these equipments allows to view the resonance peaks in real-time, making it a suitable setup to view real-time binding of bacteria on the surface of the micoresonator.
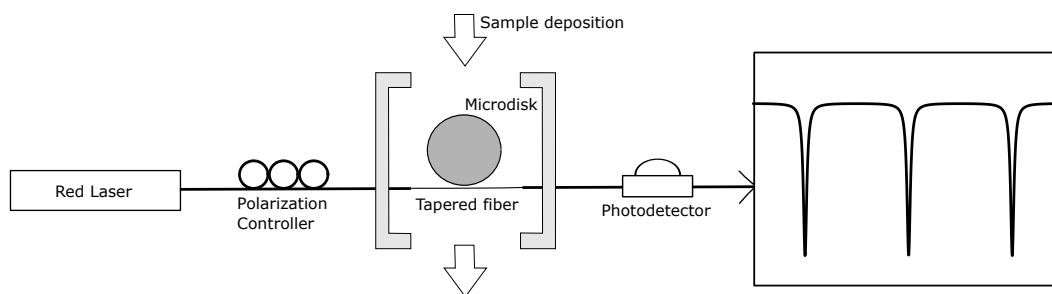
Figure 4.4 Optical characterization setup

An image of a 200 μm-diameter microdisk coupled to a tapered optical fiber is shown in Fig. 4.5.
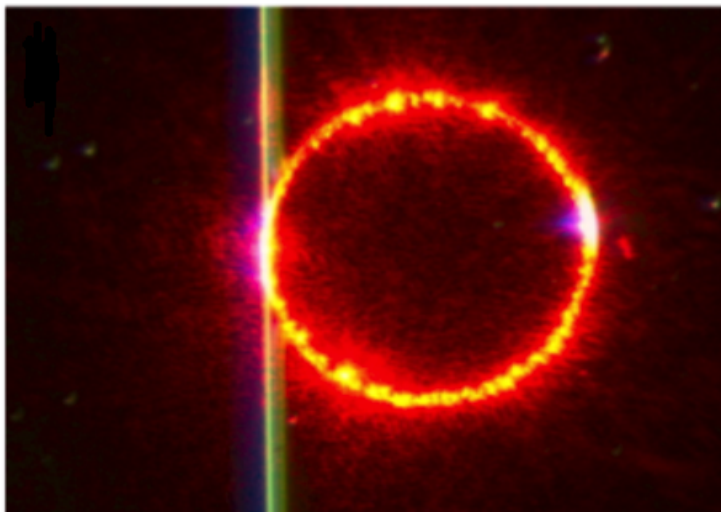
Figure 4.5 A tapered fiber coupling the light from the red laser inside a microdisk

Typical transmission spectra of a coupled silica microdisk in air and in buffer are shown in Fig. 4.6 and Fig. 4.7 respectively.
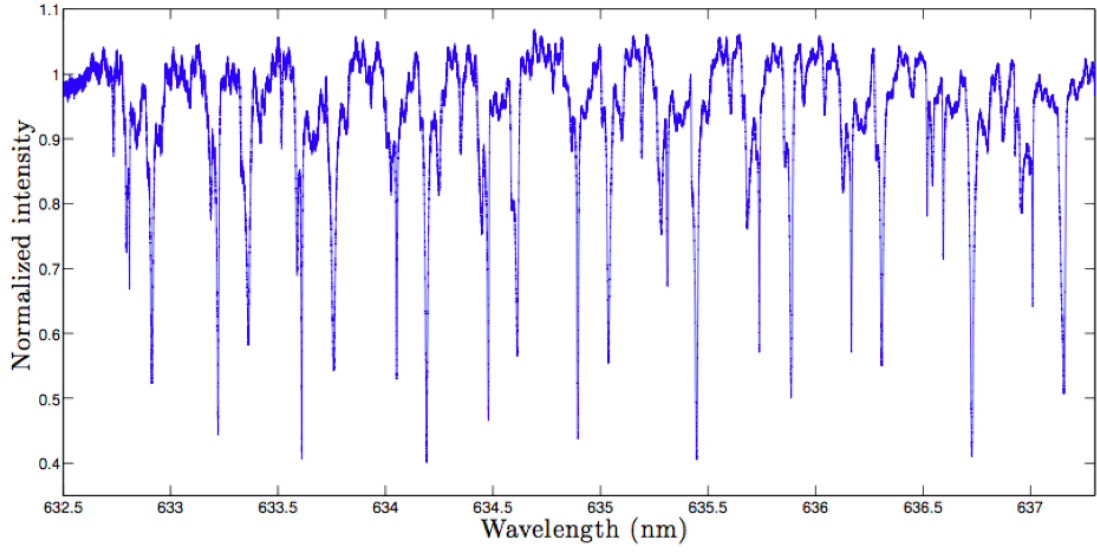
Figure 4.6 Transmission spectrum of a 200 μm-diameter silica microdisk in air ($Q \simeq 10^5$). Coupling was achieved using a 1.2 μm waist diameter taper made of single mode fiber in red.
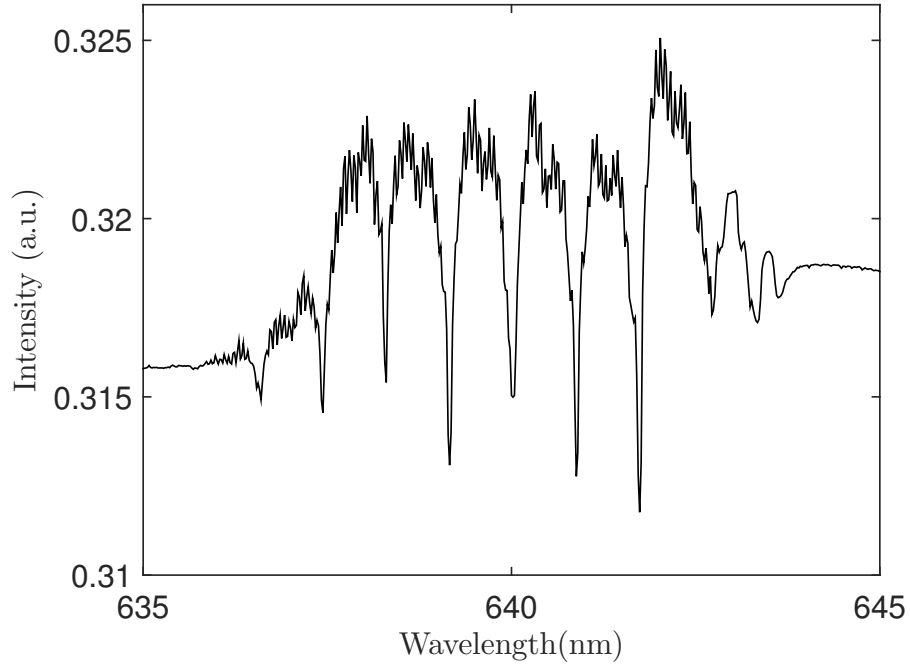
Figure 4.7 Transmission spectrum of a 200 μm-diameter silica microdisk in buffer ($Q \simeq 10^4$). Coupling was achieved using a 2 μm waist diameter taper made of single mode fiber in red.

4.4 Conclusion

In this chapter, the experimental methodology that was used during this Ph.D. project has been provided. Firstly, the detailed microfabrication procedure that was developed within the Microphotonics laboratory is provided. It is then followed by a specific functionalization process optimized to be selective towards the bacteria we were interested to detect. The functionalization process was developed and improved with the collaboration of Pr. Jay L. Nadeau and Hicham Chibli from the Department of Biomedical Engineering of McGill. An overview of the work done with McGill as well as the results generated will be given in Chapter 5. Finally, the optical characterization setup used to detect real-time binding of bacteria was described above. The experimental results along with some theoretical calculations will be provided in the following chapter.

CHAPTER 5   Synthesis of the work and experimental results

This chapter starts by presenting the experiments that led to the use of the functionalization process detailed above in section 3.2, as well as the techniques used to prove that each functionalization layer was well present and had a good adherence to the surface of the microresonator. In order to prove the specificity of the functionalization process, experiments using fluorescence microscopy and a visible camera were performed. This is followed by the results obtained for real-time detection of S. aureus on a microdisk using the optical characterization setup described in section 3.3. It is worth noting that, to our knowledge, no real-time binding experiments using bacteria were carried on optical microdisks before. The last section of this chapter presents the development of a theoretical equation to quantify the wavelength shift due to bacterial binding on the surface of a microdisk. This last part was inspired by the theory of reactive sensing developed by Arnold et al. (2003) for a microsphere.

5.1   Experimental results

5.1.1   Specificity of the functionalization process

The work introduced in this section was presented in an article published in collaboration with professor Jay L. Nadeau's group from the biomedical engineering department of McGill University (Chibli et al., 2014).

As discussed in section 3.2, a proper surface functionalization is crucial in order to obtain a specific biosensor that will allow to eliminate the risks of false positives in complex environments. In the literature, three different proteins or bacteriophages have been used to lyse staphylococci strains; LysK, Phi11 and Lysostaphin. Before introducing the phages used in the experiments, it is important to define what are bacteriophages and the advantages to use them for biosensing.

Bacteriophages are viruses that target and infect bacteria. Their name is derived from a Greek word, meaning "to devour" bacteria. They are composed of three parts : the head that encapsulates a DNA or RNA genome, the collar and the tail (Fig. 5.1). They are amongst the most diverse entities on Earth, and help regulate its microbial balance (Tolba et al., 2010). They are highly specific to their target host cell, the interaction between the phage and the bacterial cell is very strong and they are able to lyse and kill the host cell. All of these characteristics make bacteriophages a valuable tool for biodetection and eventually for rapid diagnostics of bacterial diseases.

However, using whole bacteriophages in biosensing applications can have certain disadvantages. The purification from the host bacteria is difficult. The lytic or enzymatic activity of the phage may cause the signal to become unstable, and since whole phages are large, they decrease the signal strength in biosensors that depend upon distance such as SPR or optical microresonators (Chibli et al., 2014). To overcome these limitations, it is possible to isolate specific proteins from the bacteriophages, called purified phage proteins or endolysins. Endolysins usually consist of a cell-wall binding domain (CBD) which is very specific and shows rapid binding to the target cell and an N-terminal catalytic domain.
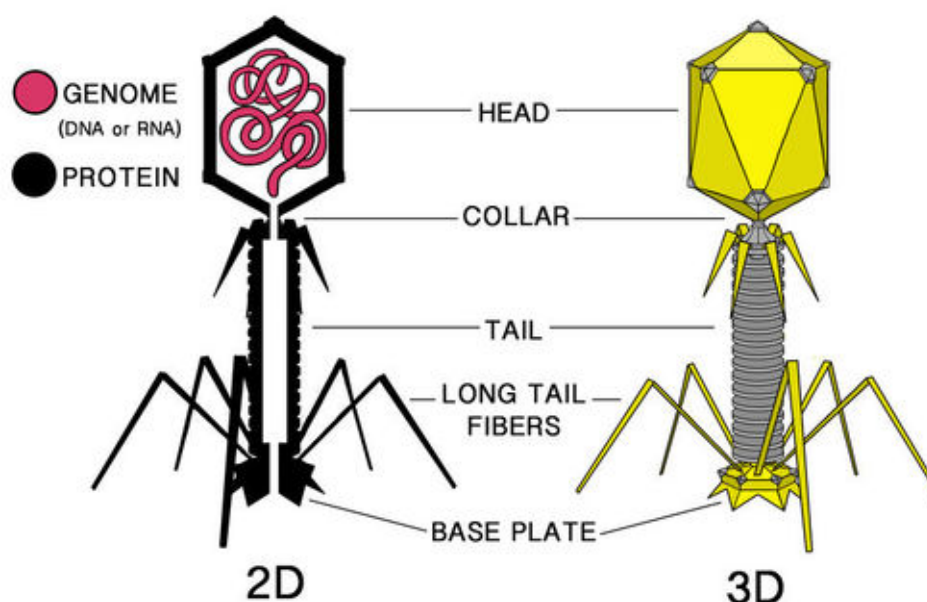
Figure 5.1 Structure of a bacteriophage showing its three parts : the head containing the DNA or RNA genome, the collar and the tail (www.ck12.org)

In the following, a brief description of each of these protein phages is given along with the results that gave rise to the functionalization process used to generate the results for real-time detection of S. aureus bacteria.

The LysK phage protein is an endolysin from the staphylococcal phage K that acts strongly on S. aureus strains. It contains three domains : an N-terminal cystein, a histidine-dependent amidohydrolase/peptidase (CHAP) domain, a midprotein amidase-2 domain, and a C-terminal SH3b cell wall-binding domain (Becker et al., 2008). The CHAP domain alone is sufficient to cause cell lysis of staphylococci. Although LysK is not species specific, it acts very strongly on S. aureus strains, and more weakly on other staphylococci and has no effect on E. coli strains.

Another protein phage thought to act on S. aureus strain is the Phi11. Φ11 produces an endolysin that has similar domains to LysK, but has low sequence similarity. It acts against several living forms of staphylococci, including S. aureus (Sass and Bierbaum, 2007).

Lysostaphin is an endopeptidase that can also lyse staphylococci. It has been shown to eliminate staphylococci in wounds in *in vitro* (Miao et al., 2011) and animal models (Satishkumar et al., 2011), and it specifically binds to the cell wall of S. aureus.

All three bacteriophages were tested against S. aureus bacteria (diameter = 0.6 μm), and E. coli (rodlike shape 2 x 0.5 μm) was used as a negative control. Φ11 and lysostaphin did not show consistent results over different trials. While some Φ11 and lysostaphin-functionalized wafers showed binding of S. aureus bacteria, other wafers prepared identically did not show any attachment. S. aureus bacteria attached to the wafers that were functionalized with LysK protein on every trial. However, none of the proteins acted on the E. coli strain. Since LysK protein was proven the most reliable to bind to S. aureus, it will be used in all the experiments described in this thesis. More details of these trials are given in (Chibli et al., 2014).

In order to verify that the functionalization process was well performed and that each step allowed a good adherence of the PEG-Silane and LysK protein on the surface of the resonator, ellipsometry and X-Ray Photoelectron Spectroscopy (XPS) were performed. Polyethylene glycol (PEG) is used to prevent non-specific binding of staphylococcus aureus on the surface of the microdisk.

Ellipsometry is an optical technique that allows to determine the dielectric properties such as the refractive index of a thin film. It can also be used to characterize the composition, roughness and thickness of the thin film, just to name a few. In the following, we are interested to find the thickness of the Si-PEG layer and the LysK protein deposited on top of a glass microscope slide. Microscope slides were used instead of thermal silica on silicon chips because their surface is smoother and more uniform, generating less error when measuring the surface roughness.

A RC2 ellipsometer with dual rotating compensators (J.A. Woollam Co.) was used to measure the thickness of each functionalization layer. Six different positions on at least two replicates of each sample type were analyzed. Data were taken at four different incident angles (45, 55, 65 and 75°) from 292 to 1690 nm. Using CompleteEase software (J.A. Woollam Co.), the resulting data were fit using a three-term experimental Cauchy fit.

For starters, the thickness of the glass was measured separately on a clean microscope slide and subtracted from the total layer thickness. The measured root mean square (RMS) rough-

ness of the glass was of 10.5 ± 0.03 Å.

Measurements were done on each slide before and after surface modification. Three regions of each sample were scanned. The resulting thickness of Si-PEG was 2.97 ± 0.23 nm, with an average refractive index of 1.42. This result is consistent with what has been presented in the literature (Schlapak et al., 2006). The LysK protein thickness was equal to 5 ± 0.05 nm. These values are summarized in Table 5.1.

Table 5.1 Ellipsometry measurements of Si-PEG and LysK layers thicknesses

Glass slide	Si-PEG	LysK protein
10.5 ± 0.03 Å	2.79 ± 0.23 nm	5 ± 0.05 nm

In order to confirm adequate attachment of Si-PEG and LysK protein to the surface of silica and to identify their elemental composition, X-ray photoelectron spectroscopy was used. Measurements were done using a VG scientific ESCALAB 3 MKII XPS spectrometer with an Mg Kα X-ray source. The electron beam power was of 206 W (12 kV, 18 mA). High-resolution spectra were taken with a 20 eV pass energy and a resolution of 0.05 eV. Six different positions on at least two replicates of each sample were analyzed, and the background noise was subtracted using the Shirley method. The XPS spectra of the silica surface treated with PEGylated-aminosilane only as well as silica with Si-PEG and LysK protein are shown in Fig. 5.2 and Fig. 5.3 respectively.

Both figures show high-resolution regions of C1s, O1s, N1s and Si2p, indicating the presence of Si-PEG and LysK on the surface. The binding of the Si-PEG molecule on the surface of silica is confirmed by the appearance of an oxygen peak, O1s, centered at 532.5 eV (Fig. 5.2). This peak is due to the O-Si link that forms between the PEGylated aminosilane and the glass surface. After the addition of LysK protein, the carbon peak, C, centered at 288.3 eV, becomes more significant, indicating the presence of amine bonds (N-C=O) from the protein (Fig. 5.3). The increase in the nitrogen quantity, N1s centered at 400.2 eV, is also a proof of the presence of LysK protein and is typical of the N-C=O bonds. Fig. 5.4A and C show the XPS measurements of carbon (C) and nitrogen (N) respectively for a PEGylated silica wafer. Fig. 5.4B and D show the XPS measurements of carbon and nitrogen respectively for a PEGylated silica wafer with LysK phage protein. When comparing Fig. 5.4B to A, a C peak appears at 288.3 eV corresponding to the amine bonds N-C=O in LysK. In Fig. 5.4D, the N peak intensity at 400.2 eV increases considerably compared to Fig. 5.4C, indicating the presence of LysK protein.

As discussed earlier, specificity is a very important feature of any biosensor. Before we proceed with the real-time detection of bacteria, the specificity of the functionalization technique
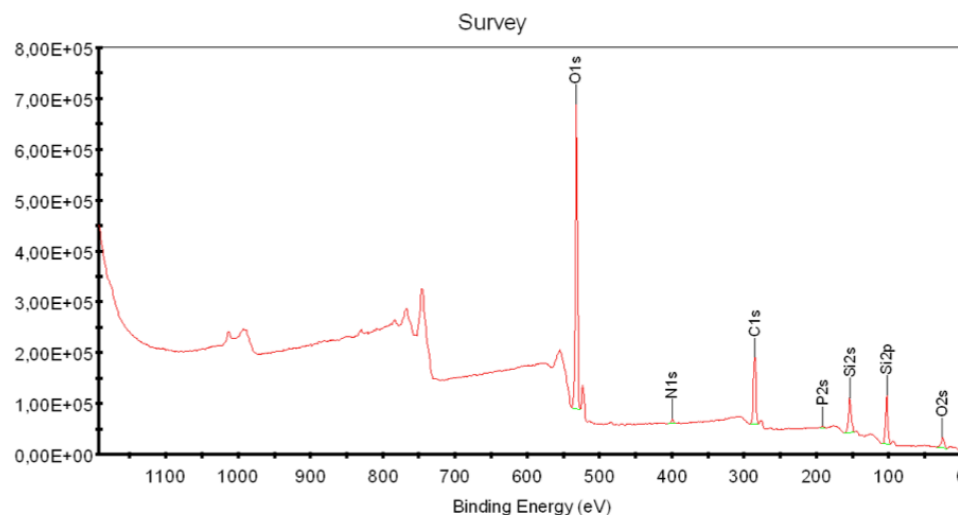
Figure 5.2 XPS measurements of silica functionalized with PEGylated aminosilane
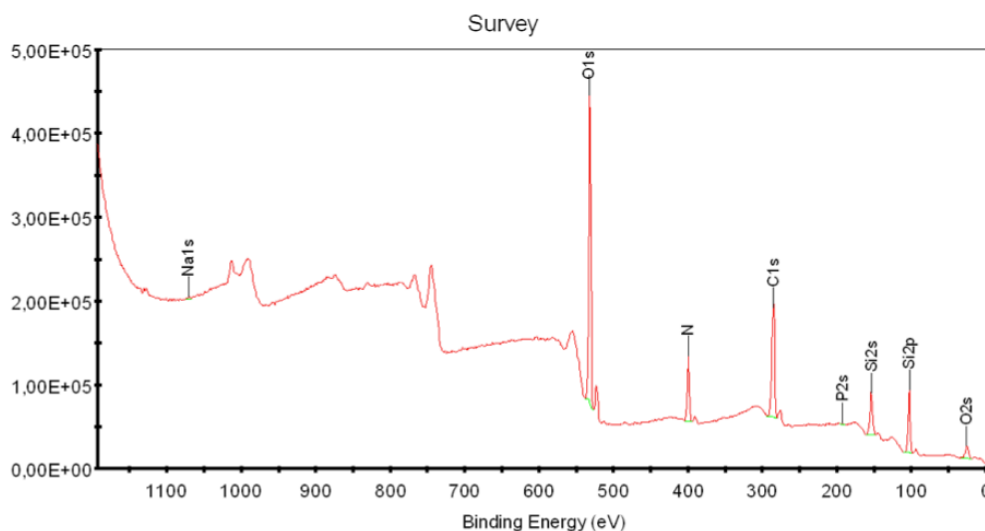
Figure 5.3 XPS measurements of silica functionalized with PEGylated aminosilane and LysK protein

needs to be proven. While the tapered optical fiber coupled the light from a red laser inside a 200 μm-diameter disk, images were taken using a visible camera, as can be seen in Fig. 5.5. Four different combinations of functionalization processes were tried and two different strains of bacteria were used. Fig. 5.5A shows a microdisk without PEGylated aminosilane but with LysK protein attached directly on the surface of silica. S. aureus bacteria was then added. As may be observed, S. aureus (the green dots in the figures) attached nonspecifically to the surface of the resonator, forming small islands. When no LysK functionalization was perfor-
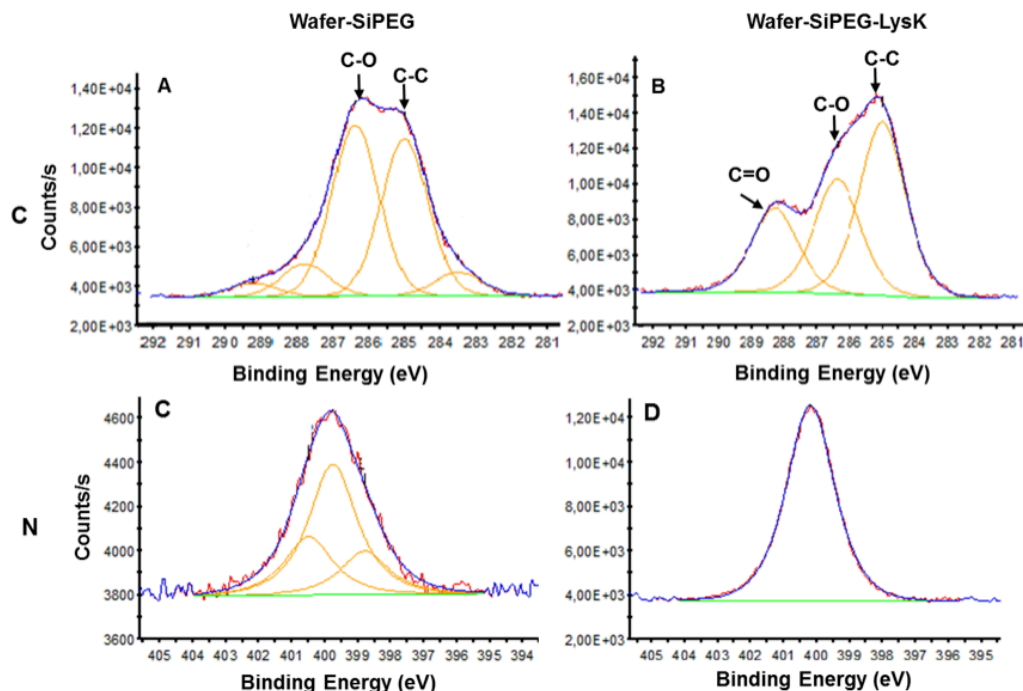
Figure 5.4 Carbon and nitrogen XPS measurements on silica with Si-PEG (A and C) and silica with Si-PEG-LysK (B and D)

med on the microdisk, as in Fig. 5.5B, S. aureus bacteria did not bind to the microresonator. In Fig. 5.5C, the silica microdisk was functionalized with PEGylated aminosilane and LysK protein, and E. coli bacteria were then added to the surface. Again, no specific binding of bacteria to the resonator was observed, since LysK protein is not specific to E. coli strains. Fig. 5.5D confirms the latter affirmation, where S. aureus bacteria (the green dots) attached specifically to the surface of a microdisk that was functionalized with Si-PEG and LysK protein. This proves the functionalization process used is specific to the S. aureus strains of bacteria we are interested in detecting. It is worth noting that some bacteria also bound to the silicon substrate. This is simply due to the presence of a thin film of native oxide that formed on the substrate and that was also functionalized during the process. This binding will however not alter the results of the optical characterization since only the binding that occurs at the edge of the resonator will give rise to the spectral shift.

The specificity of the functionalization process was also confirmed using fluorescence microscopy. Two silica wafers were cleaned using oxygen plasma and then functionalized with Si-PEG and LysK protein. On one substrate, S. aureus bacteria were added (Fig. 5.6A), whereas E. coli bacteria were deposited on the other (Fig. 5.6B). As can be clearly seen, S. aureus attached specifically to the resonator's surface, while E. coli formed random islands
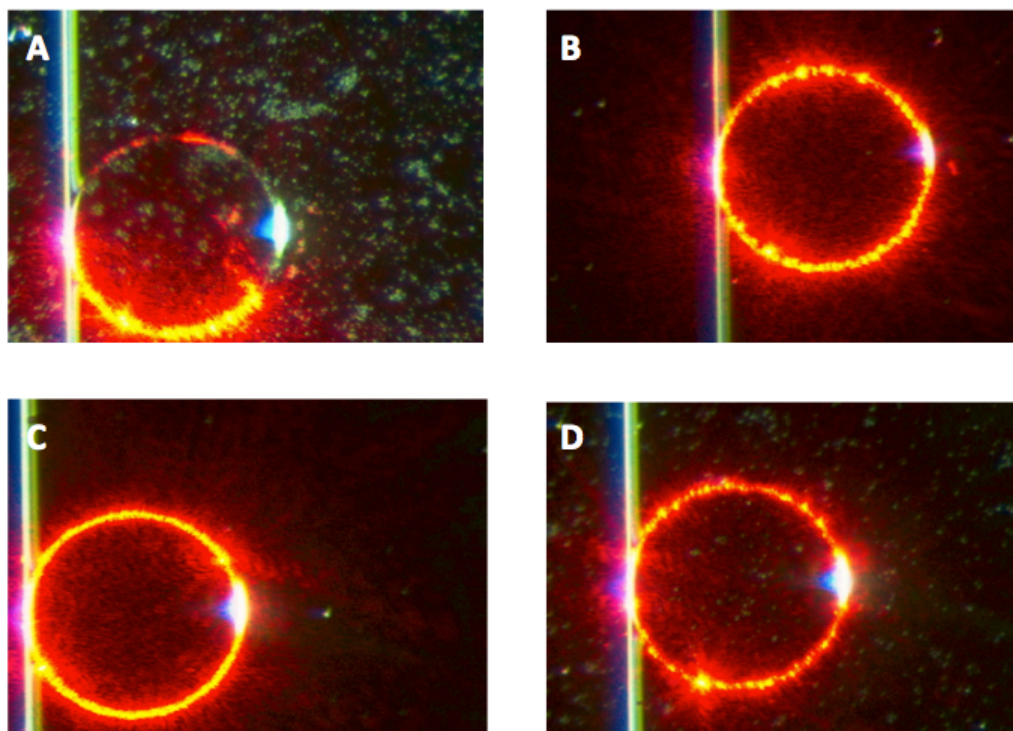
Figure 5.5 Visible camera images of a tapered optical fiber coupled to a 200 μm diameter microdisk. A) Disk-LysK-S. aureus, B) Disk-S. aureus, C) Disk-Si-PEG-LysK-E. coli and D) Disk-Si-PEG-LysK-S. aureus

demonstrating nonspecific binding. A suitable rinsing of the substrate using Tween solution, a non-ionic detergent for use in immunoassay wash buffer, diluted in phosphate buffered saline (0.05% in PBS) can help remove any unspecific binding.
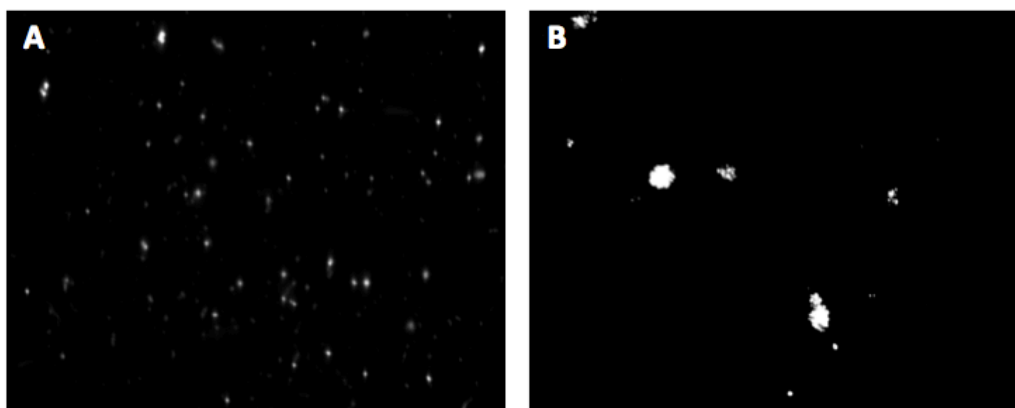
Figure 5.6 Fluorescent microscope images of a silica substrate functionalized with A) Si-PEG-LysK-S. aureus bacteria and B) Si-PEG-LysK-E. coli bacteria

In Figure 5.7, the specific functionalization process was used with five different protein concentrations. The number of bacteria bound was roughly proportional to the LysK concentration, up to a plateau value of ~7.5 μM. This plateau could be due to the steric inhibition at high concentrations. Each atom within a molecule occupies a given space. When these atoms are brought too close together, their electron cloud can overlap, causing some energy loss, which may affect the reactivity of the molecule. Thus, the number of bacteria that bind to the surface will not increase for greater concentrations of LysK protein phage. This demonstrates that the ability of functionalized wafers to attach S. aureus bacteria was dependent on the density of immobilized protein on the surface (Fig. 5.8).

The limit of detection (LOD) was determined using wafers functionalized with 2 μM of LysK and immersed in several concentrations of S. aureus. The concentrations used were 500, 5x10^3, 5x10^4 and 5x10^5 CFU/ml. The control wafer was only covered with Si-PEG and immersed in a solution of 5x10^5 CFU/ml. The number of bacteria that bound to the wafers increased with the solution concentrations. The limit of detection was defined as the lowest concentration tested for which the mean number of S. aureus attached to the functionalized wafer was higher than the standard deviation of the control and it was 5000 cells/ml.
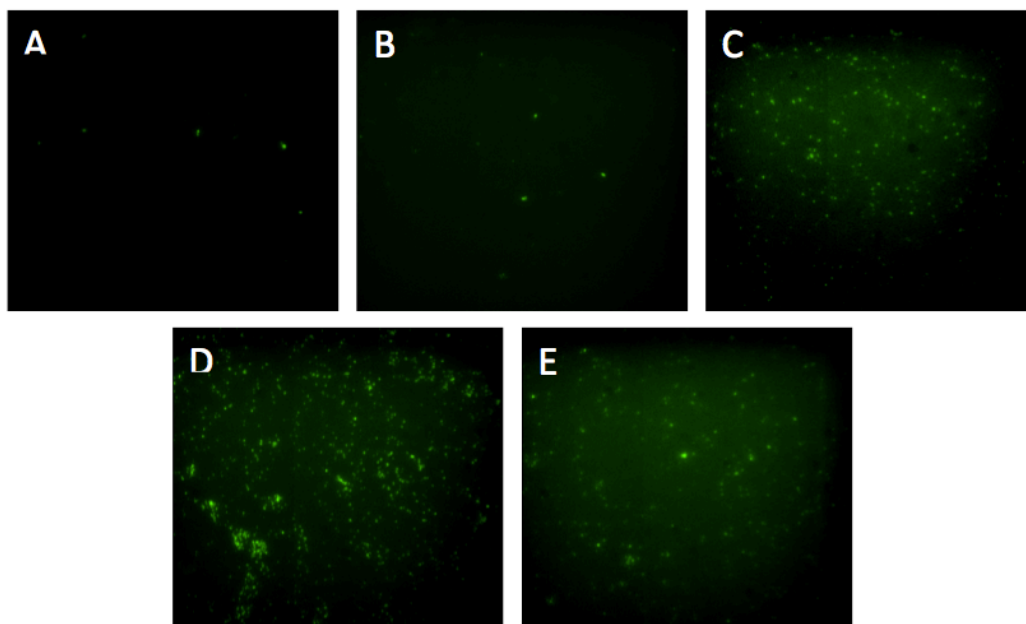
Figure 5.7 Fluorescence microscope images of S. aureus bacteria bound to silica wafers functionalized with different concentrations of LysK. A) 0 μM, B) 0.06 μM, C) 0.3 μM, D) 1.5 μM and E) 7.5 μM
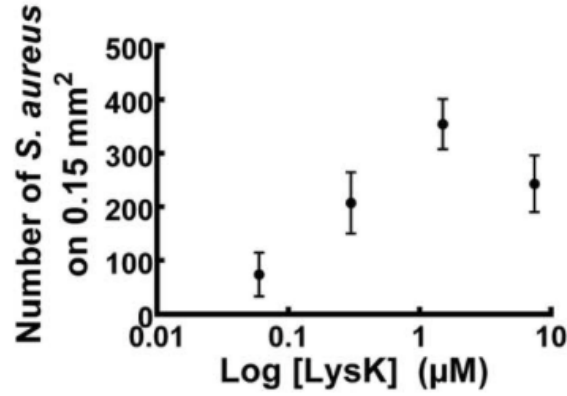
Figure 5.8 Mean number of bacterial cells on a surface area of 0.15 mm^2 versus LysK concentration (Chibli et al., 2014)

5.1.2   Real-time binding of bacteria

In the following, the optical characterization setup described earlier is used to achieve real-time detection of bacteria through the observation of the wavelength shift. Measurements are performed on eight different microdisks for each concentration and results are mean values of the experiments done for each concentration. All microdisks used have the same size of 200 μm diameter and a quality factor of around 10^4 for the sake of comparison. Silica microdisks are functionalized with a 2μM LysK solution and coupled to a tapered optical fiber. The wavelength is scanned between 632.5 and 637.5 nm. 2 μl of elution buffer (10 mM Tris-HCl, pH 8.5) is added to the surface of the resonator using a micropipette and the transmission spectrum is observed on an oscilloscope. Making sure to keep the same coupling mode, another 2 μl of elution buffer containing S. aureus at $OD_{600} = 0.5$ (around 5.10^9 CFU/ml) is added (CFU : colony forming unit). The wavelength shift is observed over a period of 30 minutes.

It can be seen in Fig. 5.9 that the wavelength begins to shift immediately after adding the bacteria, indicating an immediate attachment of the bacteria to the surface of the resonator. It takes around 15 minutes for most of the bacteria to bind to the surface. The resulting wavelength shift is at its highest and is about 0.22 ± 0.002 nm. The error on the shift value is mainly due to the laser drift, which is around ± 1 pm and the error in calculating the wavelength shift from the transmission spectra observed (± 1 pm). After 15 minutes, the wavelength shift starts to decrease. The LysK protein having a high lysing efficiency over S. aureus strain (Becker et al., 2008; Chibli et al., 2014), most of the bacteria bound to the surface will be dead after 30 minutes.

The same experiment was carried out, this time by changing the concentration of the S. aureus solution used. Starting with the $OD_{600} = 0.4$ solution, dilutions of 10, 100 and 1000
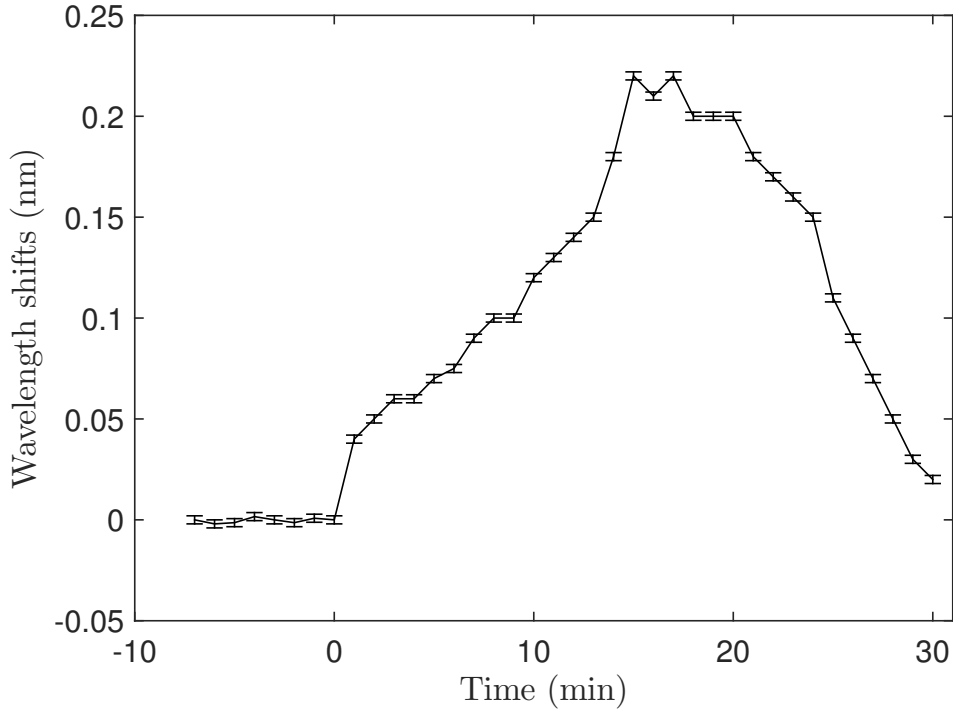
Figure 5.9 Wavelength shift in time after S. aureus binding to the resonator

fold were made. Fig. 5.10 shows the mean values of the wavelength shifts for the four different concentrations, also summarized in Table 5.2. From the reactive sensing mechanism, it can be predicted that the resonance shift will decrease with smaller concentrations (Arnold et al., 2003). However, due to the high concentrations of bacteria used, the relation is not quite linear. Thus, the number of bacteria binding to the surface is significantly high. The 100- and 1000- fold dilutions show almost the same wavelength shift, meaning that almost the same number of bacteria bound to the resonator in both cases. A limit of detection of 5 pg/ml, corresponding to 30 bacteria binding to the surface of the microdisk, is found in section 5.2.2. Experiments with lower concentrations couldn't be carried out because of the limitations due to the relatively small quality factors of the microdisks ($Q \simeq 10^4$) and the instabilities of the optical characterization setup, as discussed in the following chapter. The tunable laser used during the experiments shows a drift of ± 1 pm, thus making it difficult in this case to detect a single bacterium. It is worth noting that the Q-factor did not significantly change before and after the bacterial binding. The dominant sensing mechanism in this case is the reactive principle which sees the resonant frequency shifting towards longer wavelengths, as described in section 3.1.4.

Specificity of the functionalization process was once again demonstrated, this time using
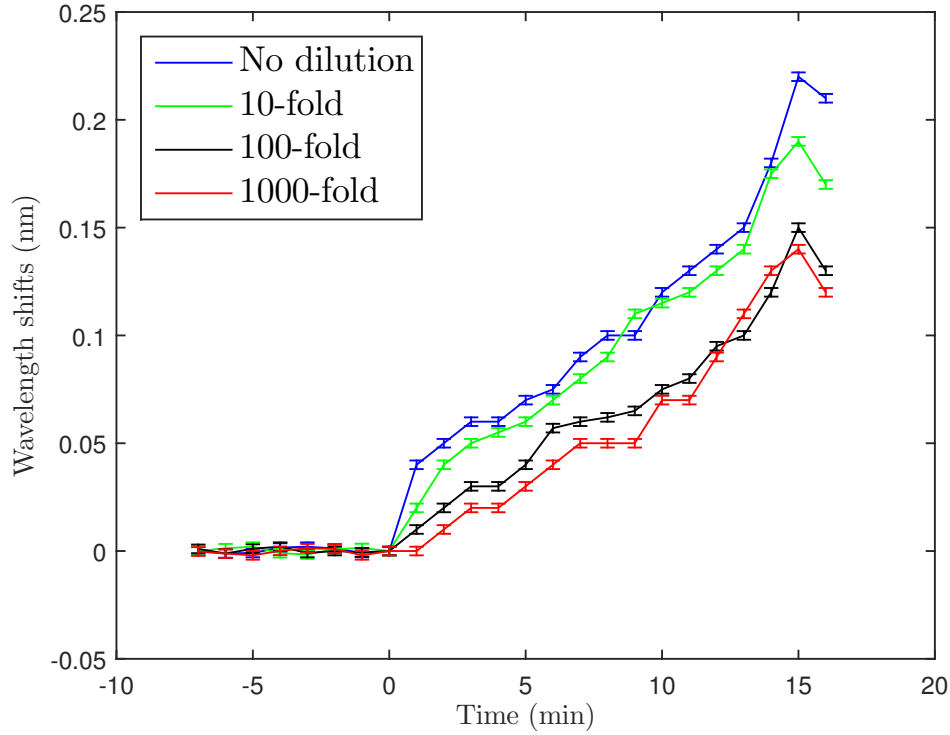
Figure 5.10 Wavelength shifts after S. aureus binding for four different concentrations

Table 5.2 Mean values of the wavelength shifts versus bacterial concentration

No dilution	Diluted 10x	Diluted 100x	Diluted 1000x
0.22 ± 0.01 nm	0.19 ± 0.01 nm	0.15 ± 0.01 nm	0.14 ± 0.01 nm

the real-time binding of bacteria. A 200 μm-diameter microdisk was functionalized with the LysK protein phage. When coupled to the tapered optical fiber, a solution of elution buffer containing E. coli bacteria ($OD_{600} = 0.4$) was added to the resonator. As can be seen in Fig. 5.11, the transmission spectrum between times 0 and 20 minutes did not change. No shift was observed, meaning no E. coli bound to the surface of the microdisk. When both E. coli and S. aureus bacteria were added together to the surface of the resonator, a wavelength shift of 0.22 nm was observed, similar to the one obtained with the S. aureus bacteria alone.
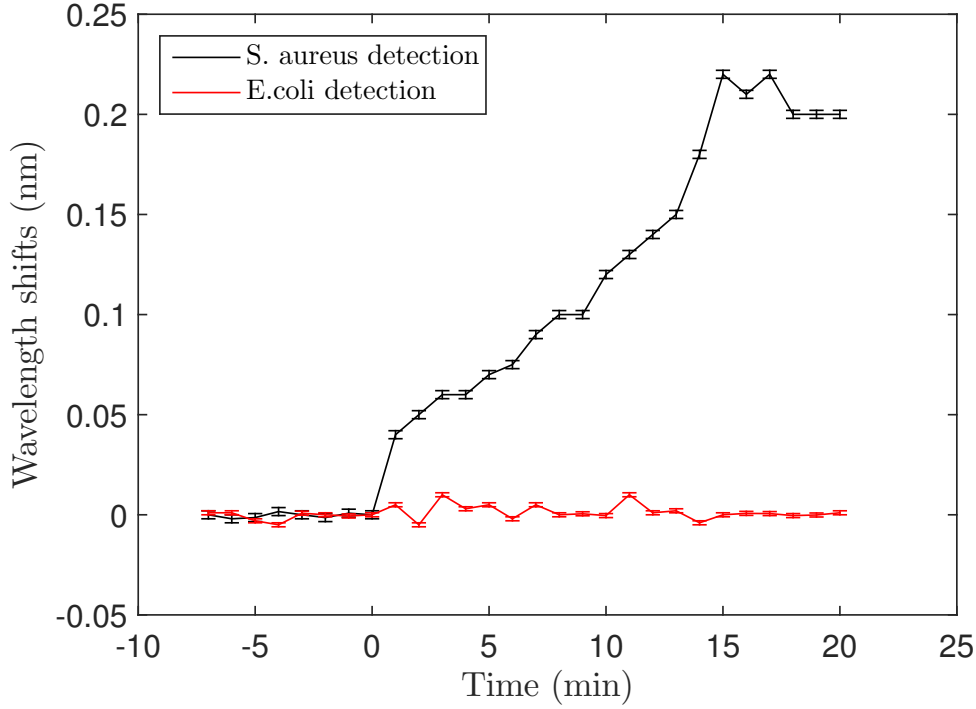
Figure 5.11 Wavelength shifts for S. aureus and E. coli binding to a functionalized silica microdisk

5.2 Theoretical reactive shift for a microdisk

A theoretical equation to determine the resonance shift in a sphere following a binding event was developed by Arnold et al. (2003). This formulation allows to determine the surface area covered by the molecules using the experimental wavelength shift (Vollmer et al., 2002). To our knowledge, similar equations were not developed for microdisks, mainly because it is not possible to obtain exact analytical solution to the spatial distribution $\vec{E}(\vec{r}, \omega_0)$ of a microdisk.

In this section, a theoretical wavelength shift equation for a microdisk is developed, inspired by the one applied to microspheres. An analytical approximation detailed by Borselli et al. (2005) of the spatial distribution of the electric field in the microdisk is used, as shown in Eq. 5.18.

A brief reminding of the Maxwell's equations is given, followed by the expression of the TE mode for a microsphere and an analytical approximation of this mode for a microdisk. Although the wavelength shift for a microsphere can be expressed as a simple equation (Arnold et al., 2010), it is not the case for a microdisk. The expression is more complex for a disk since no exact solutions exist to define its modes. Thus, it becomes less obvious to deduce

some dependencies such as the effect of the microdisk radius or the medium refractive index on the spectral shift.

5.2.1 Maxwell's equations

The propagation of the electric and magnetic fields in dielectric media with no free charges is expressed by Maxwell's equations as follows :

$$\nabla \cdot \vec{D}(\vec{r}, t) = 0 \tag{5.1}$$

$$\nabla \cdot \vec{B}(\vec{r}, t) = 0 \tag{5.2}$$

$$\nabla \times \vec{E}(\vec{r}, t) = -\frac{\partial \vec{B}(\vec{r}, t)}{\partial t} \tag{5.3}$$

$$\nabla \times \vec{H}(\vec{r}, t) = \frac{\partial \vec{D}(\vec{r}, t)}{\partial t} \tag{5.4}$$

$$\vec{D}(\vec{r}, t) = \epsilon(\vec{r})\vec{E}(\vec{r}, t) \tag{5.5}$$

$$\vec{H}(\vec{r}, t) = \frac{1}{\mu_0}\vec{B}(\vec{r}, t) \tag{5.6}$$

with $\vec{D}$ being the electric flux density, $\vec{B}$ the magnetic flux density, $\vec{E}$ the electric field, $\vec{H}$ the magnetic field, ϵ the permittivity of the medium and μ_0 the permeability of the medium. Maxwell's equations can be combined into one second-order wave equation as follows :

$$\nabla^2 \vec{F} - \frac{n^2(\vec{r})}{c^2}\frac{\partial^2 \vec{F}}{\partial t^2} = 0 \tag{5.7}$$

with

$$\vec{F} = \left\{\vec{E}, \vec{H}\right\}, \ c^2 = \frac{1}{\epsilon_0 \mu_0} \ and \ n^2(\vec{r}) = \frac{\epsilon(\vec{r})}{\epsilon_0} \tag{5.8}$$

where n is the medium refractive index, c the speed of light in free space and ϵ_0 the vacuum permittivity.

The solution will have an oscillatory form,

$$\vec{F}(\vec{r}, t) = \vec{F}(\vec{r})\exp(-i\omega t) \tag{5.9}$$

allowing to write the time-independent Maxwell's equation into a cylindrical form as

$$\left(\frac{\partial^2}{\partial \rho^2} + \frac{1}{\rho}\frac{\partial}{\partial \rho} + \frac{1}{\rho^2}\frac{\partial^2}{\partial \phi^2} + \frac{\partial^2}{\partial z^2} + \left(\frac{\omega}{c}\right)^2 n^2(\vec{r})\right)\vec{F}(\vec{r}) = 0 \tag{5.10}$$

The high index contrast in a thin semiconductor microdisk provides large vertical confinement, which will help approximate the problem to a two-dimensional equation. Two polarizations are dominant in this case : transverse electric (TE) where the electric field is parallel to the disk plane, and transverse magnetic (TM) where the electric field is perpendicular to the disk plane. The time-independent equation (Eq. 5.10) becomes thus scalar in the $\hat{z}$ direction, and for ρ smaller than the disk radius R, the separation of variables can be used to write the equation as follows :

$$\frac{1}{W}\left(\frac{\partial^2 W}{\partial \rho^2} + \frac{1}{\rho}\frac{\partial W}{\partial \rho} + \frac{1}{\rho^2}\frac{\partial^2 W}{\partial \phi^2}\right) + \frac{1}{Z}\frac{\partial^2 Z}{\partial z^2} + k_0^2 n^2(\vec{r}) = 0 \tag{5.11}$$

where

$$F_z = W(\rho, \phi)Z(z) \text{ and } k_0 = \frac{\omega}{c} \text{ is the wave number} \tag{5.12}$$

It is worth noting that F_z is continuous across the interfaces for the TE mode and discontinuous for the TM mode. Eq. 5.11 can thus be separated into two differential equations :

$$\left(\frac{\partial^2 W}{\partial \rho^2} + \frac{1}{\rho}\frac{\partial W}{\partial \rho} + \frac{1}{\rho^2}\frac{\partial^2 W}{\partial \phi^2}\right) + k_0^2 n_m^2(\rho)W = 0$$
$$\frac{\partial^2 Z}{\partial z^2} + k_0^2(n^2(z) - n_m^2)Z = 0 \tag{5.13}$$

The second equation can be easily solved and the solution expressed as :

$$Z(z) = A_m \exp(ik_0(\sqrt{n_d^2 - n_m^2})z) \tag{5.14}$$

The separation of variable is once again applied to the first equation in 5.13 with W$(\rho, \phi) = \Psi(\rho)\Omega(\phi)$, leading to equations 5.15 and 5.16.

$$\frac{\partial^2 \Psi}{\partial \rho^2} + \frac{1}{\rho}\frac{\partial \Psi}{\partial \rho} + \left(k_0^2 n_m^2(\rho) - \frac{m^2}{\rho^2}\right)\Psi = 0 \tag{5.15}$$

$$\frac{\partial^2 \Omega}{\partial \phi^2} + m^2 \Omega = 0 \Rightarrow \Omega(\phi) \sim \exp(im\phi) \tag{5.16}$$

Eq. 5.16 is simply an exponential solution $\Omega(\phi) \sim \exp(im\phi)$, and Eq. 5.15 is solved approximately and is expressed as Bessel functions inside the disk and Hankel functions approximated by a decaying exponential outside the disk.

Using the boundary conditions at R $= \rho$ and matching $H_z(E_z)$ and E_ϕ for TE(TM) modes lead to the following transcendental equation :

$$k_0 n_m(k_0) J_{l+1}(k_0 n_m(k_0)R) = \left(\frac{m}{R} + \eta_\alpha\right) J_l(k_0 n_m(k_0)R) \tag{5.17}$$

with

$$\eta = \begin{cases} \frac{n_m^2}{n_0^2} & \text{for TE modes} \\ 1 & \text{for TM modes} \end{cases}$$

The unnormalized radial mode dependence is then expressed as :

$$\Psi(\rho) = \begin{cases} J_l(k_0 n_m \rho) & \text{if } \rho \leq R \\ J_l(k_0 n_m R)\exp(-\alpha(\rho - R)) & \text{if } \rho > R \end{cases}$$

with the decay constant $\alpha = k_0(n_m^2 - n_0^2)^{1/2}$.

The electric field inside a microdisk can thus be approximated by the following expression :

$$E_0 = \Psi(\rho)\Omega(\phi)Z(z) = J_l(k_0 n_m \rho)\,\exp(im\phi)\,\exp\left(ik_0(\sqrt{n_d^2 - n_m^2})z\right) \tag{5.18}$$

5.2.2 Resonant shift for a microdisk

The resonant shift of a microresonator can be written as follows (Arnold et al., 2003) :

$$\left(\frac{\delta\omega}{\omega}\right)_i \cong \frac{-\alpha_{ex}|\vec{E}_0(\vec{r_i})^2|}{2\int \epsilon_s |\vec{E}_0(\vec{r})|^2 dV} \tag{5.19}$$

with

$$\sum_i^N |E_0(\vec{r}_i)|^2 \cong \sigma_s \int |E_0(\vec{r})|^2 dA \tag{5.20}$$

and where A is the surface area of the resonator, V its volume, α_{ex} the excess polarizability of the molecules binding to the resonator's surface, σ_s the surface area covered by the molecules and $\epsilon_s = \epsilon_0 \epsilon_{rs}$ the resonator's permittivity.

The frequency shift caused by the binding of a biomolecule considers the energy of interaction as a first-order perturbation to a single-photon resonant state. The integral in the denominator is taken over the edge of the microdisk which contains the majority of the mode energy. The addition of equal electric and magnetic contributions is accounted for by adding the factor 2 in front of the integral.

The surface coverage can be expressed as the number of bound molecules (N) per surface unit as follows :

$$\sigma_s = \frac{N}{\pi(R_{max}^2 - r_{1/e}^2) + 2\pi R h} \tag{5.21}$$

Eq. 5.21 considers that bacteria only attach on the top surface of the microdisk. Since the majority of the mode energy is contained on the edge of the microdisk, only bacteria that attach in this region will contribute to the spectral shift. The surface area taken into consideration is then the surface of a ring of outer diameter $R_{max} \simeq 90$ μm where the electric field is maximum, and an inner diameter $r \simeq 84$ μm where the intensity of the electric field decays to 1/e of its maximum, in addition to the surface of the edge.

The excess polarizability of the molecules binding to the resonator's surface can be written as follows (Vollmer et al., 2002) :

$$\alpha_{ex} = 4\pi\epsilon_0 \left(\frac{n_m}{2\pi}\right)\left(\frac{dn_m}{dc}\right) m \tag{5.22}$$

with n_m the solvent refractive index, $\frac{dn_m}{dc} = lim_{c\to 0}(\frac{n_m - n_0}{c})$ the differential refractive index of molecules in water, where c is the solvent concentration, and is usually of the order of 0.1 mL/g for polymers in water (Tumolo et al., 2004), and m the mass of a biomolecule, in this case the mass of a bacterium.

The parameters used to determine the spectral shift due to S. aureus binding to a 200 μm-diameter silica microdisk submerged in Tris-buffered saline (TBS) are defined in Table 5.3. Their typical values are also given and are used for the simulations shown at the end of this

section.

Table 5.3 Parameters of the wavelength shift equation for a microdisk

Parameter	Definition	Value
α_{ex}	Excess polarizability	$4\pi\epsilon_0$ x 2.12x10^{-20} (m^3)
σ_s	Surface coverage	$\frac{N}{1.257\text{x}10^5}$ (μm^{-2})
ϵ_0	Vacuum permittivity	8.854x10^{-12} F/m
ϵ_{rs}	Relative permittivity of silica	3.9
k$_0$	Wavenumber $\left(\frac{2\pi}{\lambda}\right)$	9.895x10^{-3} nm^{-1}
n$_d$	Refractive index of the microdisk	1.457
n$_m$	Refractive index of the buffer	1.332
h	Thickness of the microdisk	800 nm
R	Radius of the microdisk	100 μm
m	Mass of one bacterium	10^{-12} g
l	Mode number $\left(\frac{2\pi Rn_{eff}}{\lambda}\right)$	1442

The frequency shift due to the reactive mechanism caused by a binding event to the surface of a WGM optical microresonator can thus be written as :

$$\frac{\delta\omega}{\omega} \cong -\frac{\alpha_{ex}\sigma_s}{2\epsilon_0\epsilon_{rs}} \frac{\int |\vec{E}_0(\vec{r})|^2 dA}{\int |\vec{E}_0(\vec{r})|^2 dV} \tag{5.23}$$

Using Eq. 5.18 and Eq. 5.23, and considering that bacteria attach only on the top surface of the microdisk, the resonant shift for the TE mode of the microdisk can be written as follows :

$$\frac{\delta\lambda}{\lambda} \simeq \frac{\alpha_{ex}\sigma_s}{2\epsilon_0\epsilon_{rs}} \frac{\left[\int_0^R \int_0^{2\pi} |\Psi(\rho)|^2 \; |\Omega(\phi)|^2 \; \left|Z\left(\frac{h}{2}\right)\right|^2 \rho d\phi d\rho + \int_0^h \int_0^{2\pi} |\Psi(R)|^2 \; |\Omega(\phi)|^2 \; |Z(z)|^2 R d\phi dz\right]}{\int_0^h \int_0^R \int_0^{2\pi} |\Psi(\rho)|^2 |\Omega(\phi)|^2 |Z(z)|^2 \rho d\phi d\rho dz} \tag{5.24}$$

The integral of the first-kind Bessel function and the integral of the cosine function can be written according to Eq. 5.25 and Eq. 5.26 respectively.

$$\int_0^R [J_l(k_0 n_m \rho)]^2 \rho d\rho = \frac{1}{2} \; R^2 \; [J_{l+1}^2(k_0 n_m R)] \tag{5.25}$$

$$\int_0^h \exp^2\left[ik_0\left(\sqrt{n_d^2 - n_m^2}\right)z\right] dz = h \tag{5.26}$$

The three integrals of Eq. 5.24 will each be solved separately according to Eq. 5.27, 5.28 and 5.30.

The first double integral in the numerator will be expressed as follows :

$$\int_0^R \int_0^{2\pi} |J_l^2(k_0 n_m \rho)| \; |\exp(im\phi)|^2 \; \exp^2\left[ik_0\left(\sqrt{n_d^2 - n_m^2}\right)\frac{h}{2}\right]\rho d\phi d\rho$$
$$= \frac{2\pi}{2}R^2 \left[J_{l+1}^2(k_0 n_m R)\right] \tag{5.27}$$

The second double integral of the numerator can be written as :

$$\int_0^h \int_0^{2\pi} \left|J_l^2(k_0 n_m R)\right| \; \left|\exp(im\phi)\right|^2 \; \exp^2\left[ik_0\left(\sqrt{n_d^2 - n_m^2}\right)z\right] R \; d\phi dz$$
$$= 2\pi R \left[J_l^2(k_0 n_m R)\right] \; h \tag{5.28}$$

with

$$\int_0^{2\pi} |\exp(im\phi)|^2 d\phi = 2\pi \tag{5.29}$$

The denominator of Eq. 5.24 will be calculated as follows :

$$\int_0^h \int_0^R \int_0^{2\pi} \left|J_l^2(k_0 n_m \rho)\right| \; |\exp(im\phi)|^2 \; \exp^2\left[ik_0\left(\sqrt{n_d^2 - n_m^2}\right)z\right] \rho d\phi d\rho dz$$
$$= \frac{2\pi}{2}R^2 \left[J_{l+1}^2(k_0 n_m R)\right] h \tag{5.30}$$

The integral part (I) of the spectral shift equation (Eq. 5.24) can be grouped and simplified as can be seen in Eq. 5.31.

$$I = \frac{R\left[J_{l+1}^2(k_0 n_m R)\right] + 2h\left[J_l^2(k_0 n_m R)\right]}{Rh\left[J_{l+1}^2(k_0 n_m R)\right]} = \frac{1}{h} + \frac{2\left[J_l^2(k_0 n_m R)\right]}{R\left[J_{l+1}^2(k_0 n_m R)\right]} \tag{5.31}$$

Microdisks are considered as 2D structures. Since there are no exact solutions of the electric field of the microdisks, an approximation of the modes inside the disks was demonstrated in Eq. 5.18. Furthermore, only the bacteria that bind to the top surface of the microresonator are taken into account to calculate the wavelength shift. Based on these approximations, the

resonance shift for a WGM microdisk can then be estimated by the following equation :

$$\frac{\delta\lambda}{\lambda} \simeq \frac{\alpha_{ex}\sigma_s}{2\epsilon_0\epsilon_{rs}} \left\{ \frac{1}{h} + \frac{2\left[J_l^2(k_0 n_m R)\right]}{R\left[J_{l+1}^2(k_0 n_m R)\right]} \right\} \tag{5.32}$$

Figure 5.12 relates the wavelength shift found experimentally for a 200 μm-diameter silica microdisk with a $Q = 10^4$ to the calculated number of bacteria that bind to the surface found from Eq. 5.21 and 5.32.
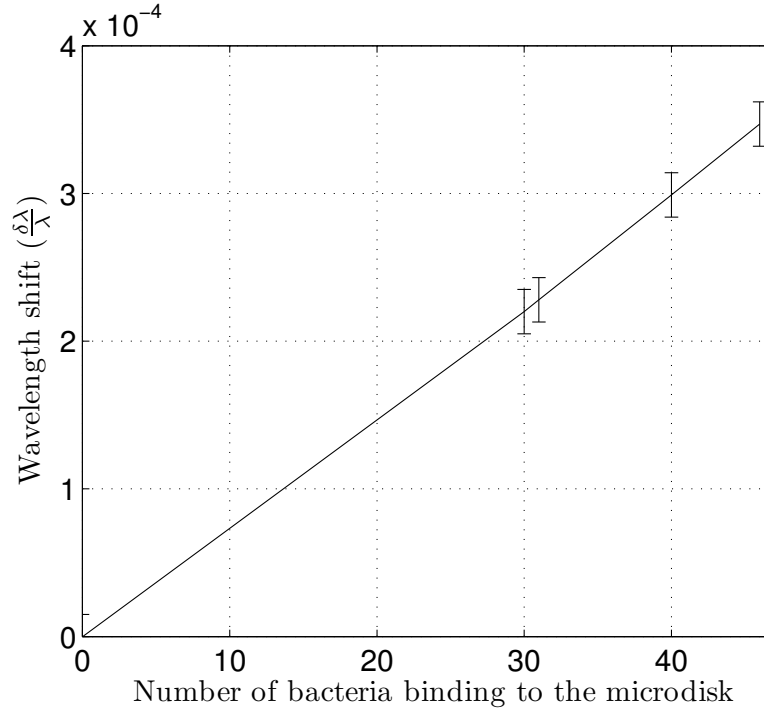
Figure 5.12 Wavelength shifts in terms of number of bacteria contributing to the shift

As can be seen from Eq. 5.32, the wavelength shift is proportional to the excess polarizability, the surface coverage and hence the number of bacteria binding to the surface. For the shifts found above experimentally, it becomes possible to estimate approximately the number of bacteria that binds to the surface and contributes to the reactive shift. These numbers are summarized in Table 5.4 for the four concentrations of bacterial solution used above.

Table 5.4 Surface coverage and number of bacteria binding to the resonator for four different concentrations

Bacterial solution concentration (cfu/ml)	Wavelength shift (nm)	Surface coverage (m^{-2})	Bacteria bound to the surface
5.10^9	0.22	8.21 x 10^9	46
5.10^8	0.19	7.15 x 10^9	40
5.10^7	0.15	5.56 x 10^9	31
5.10^6	0.14	5.3 x 10^9	30

Previously, the values of the wavelength shifts given for the four different bacterial concentrations were the mean values resulting from repeating the real-time binding experiments several times. In Table 5.5, the standard deviation (SD) of the wavelength shifts is given for the different concentrations. It can be seen that the SD increases with lower concentrations. The same functionalization process was done on all the microdisks used for the experiments, meaning that the binding sites for all cases were the same. For greater concentrations of bacteria, the possibility of binding to the surface are limited due to the great number of bacteria present, giving almost the same wavelength shift every time the experiment was repeated. When the concentration decreases, the bacteria will attach more randomly on the surface of the microdisk, having more possible sites to bind to. However, not all these sites are necessarily situated on the sensitive part of the microdisk, hence they won't contribute similarly to the wavelength shift every time. This makes the calculation of the number of bacteria that binds to the surface for lower concentrations less accurate. Considering the four concentrations tested, the limit of detection of the biosensor for a Q-factor of 10^4 was 5×10^6 CFU/ml or 5 pg/ml.

Table 5.5 Standard deviation of the wavelength shift for four different bacterial concentrations

Bacterial solution concentration (cfu/ml)	Wavelength shift (nm)	Standard deviation (nm)
5.10^9	0.22	0.01
5.10^8	0.19	0.02
5.10^7	0.15	0.04
5.10^6	0.14	0.05

As can be observed in Fig. 5.12, the spectral shift varies linearly with the number of bacteria that attach to the surface of a microdisk. Accordingly, an extrapolation shows that the binding of a single bacterium is expected to cause a shift of 5 pm. The smallest shift that

can be detected using the optical characterization setup described in chapter 4 is equivalent to the full width at half maximum (FWHM) of the resonance peak. Considering a FWHM of 5 pm and a cavity resonance wavelength of 635 nm, the corresponding quality factor would be equal to $9.1 \text{x} 10^4$, meaning that optical microdisks can be used to specifically bind a single bacterium. It is thus important to make sure that the single bacterium binds to the edge of the microdisk where the mode energy is at its highest to be able to observe the spectral shift resulting from the attachment. This can be achieved using appropriate microfluidics devices, as described in the following chapter. It is also important to make sure that the optical characterization setup is stable, and environmental changes such as vibrations or temperature variations don't have any effect on the spectral shift. In section 6.1.2, the effect of temperature changes on the spectral shift are discussed. When the temperature variations are controlled to 0.01 °C, the associated thermal spectral shift would be 38.1 fm (section 6.1.2). A well-controlled environment will then allow the detection of a single bacterium using optical microdisks.

5.3   Conclusion

In this chapter, the studies done to find a reliable specific functionalization process to attach S. aureus bacteria on the surface of optical microdisks were presented. Real-time binding of S. aureus bacteria was done for the first time on the surface of an optical microdisk, giving opportunities for wide range of use of these resonators for point-of-care tests. A theoretical expression of the reactive shift in terms of the number of bacteria that bind to the surface of the resonator was also developed, using an analytical approximation of the cavities modes. It was used to estimate the number of bacteria that attached to the whispering gallery micro-cavity experimentally and contributed to the wavelength shift. The challenges faced during the project and some recommendations that could improve the use of optical microdisks as biosensors will be provided in the following chapter.

CHAPTER 6   GENERAL DISCUSSION

Real-time bacterial sensing using high-Q optical microcavities is a very delicate process, in the sense that it can be highly affected by the environmental and experimental parameters. Since one of the main goals is to achieve a sensitive robust biosensor that includes integrated optics and microfluidics for on-site use, some improvements need to be made on the current platform. In this section, a description of the main challenges faced during the project is given, mainly the ones related to the use of a tapered optical fiber, followed by some suggestions and recommendations that can bring the use of optical biosensors from the laboratory to a commercially used device.

6.1   Challenges and recommendations for real-time detection experiments

6.1.1   Tapered optical fiber

The tapered fiber is one of the most efficient ways to achieve evanescent coupling to an optical microdisk with low losses. They are easily fabricated by stretching a single mode fiber and can be easily placed

However, tapered fibers are very fragile and can break easily. They are also unstable in the presence of liquid which can cause fluctuations in the measurements due to the hydrodynamic-induced instabilities in the taper-microdisk coupling (Lu et al., 2011). This phenomenon was reduced by using a micropipette to inject the liquid on the surface of the microdisk, while making sure not to touch neither the disk nor the tapered fiber, instead of a syringe pump that generates more vibrations.

Another issue faced when measuring the real-time binding of bacteria is the evaporation of the buffer during the experiment. Elution buffer originally covered the microdisk, the tapered optical fiber coupled to the disk and the gap between them. While performing the experiments over several minutes, the buffer evaporated, causing a change in the coupling efficiency. This was observed as a change in the intensity of the transmission peaks. Adding more liquid lead to the same problem, even worse sometimes when the coupling was completely lost due to the shifting of the tapered fiber. Also, adding a high volume of buffer can lead to high surface tensions between the liquid and the tapered fiber and eventually break the taper.

In order to overcome this problem, the waveguide can be integrated on chip with the optical microdisk. One proposed process was the integration of a silicon MEMS actuators with silica optical microdisk and waveguide (Grutter et al., 2010), as shown in Fig. 6.1.
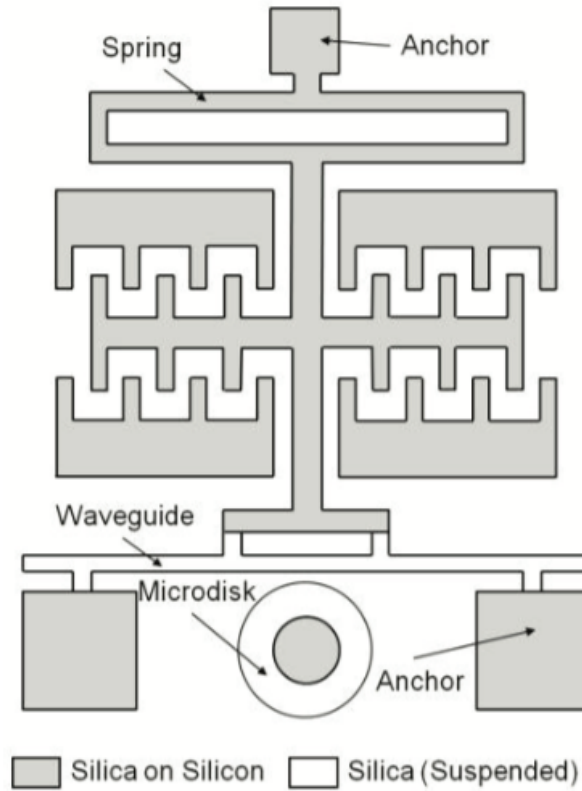
Figure 6.1 Schematic of an integrated silica microdisk and waveguide (Grutter et al., 2010)

The process used to fabricate this device is a modified Single Crystal Reactive Etching and Metallization (SCREAM) fabrication process on a Silicon-on-Insulator (SOI) wafer. A 1 μm-thick layer of phosphosilicate glass (PSG) is deposited on the SOI. Several steps of photolithography and etching are performed, to finally release the structures using a XeF$_2$ etch of the silicon.

Although integrating the waveguide adds several steps to the fabrication process, it can remove many challenges related to the use of tapered fiber mentioned above, and bring the bionsensors based on optical microcavities one step closer to becoming portable and robust sensors.

6.1.2 Temperature variation

It was previously described that the detection of bacteria that attach to the surface of a microcavity is observed through the reactive sensing mechanism, where the binding leads to a change in the optical path length and results in a red shift of the resonance wavelength.

Another mechanism resulting from a binding event can also be responsable of a red shift; the

thermo-optic effect. The high intensities that circulate in the cavity will heat the molecules attached to its surface. The heated molecules will increase the temperature of the whispering gallery microcavity, hence shifting the resonance towards longer wavelength (Armani et al., 2007), since the thermo-optic coefficient (dn/dT) in dielectric materials is positive (Socorro et al., 2015). It has been reported that this mechanism is much smaller than its reactive counterpart, accounting for about one thousandth of the wavelength shift associated with the binding of a single protein (Arnold et al., 2010).

The thermally induced resonance shift is expressed by the following equation (Carmon et al., 2004) :

$$\Delta\lambda/\Delta T = \lambda_0 \left[\epsilon + (dn_0/dT) / n_0\right] \tag{6.1}$$

with λ_0 the cavity resonance wavelength, ϵ the expansion coefficient (m/m °C), dn_0/dT the thermal optic coefficient ($1/°$ C) and n_0 the refractive index of the cavity. Silica has a positive thermo-optic coefficient of $0.55\text{x}10^{-6}$ K (Weber, 2002). This low thermo-optic coefficient confers an improved stability to the devices made of silica, which is an essential feature for a reliable biosensor. For silica, the coefficient $[\epsilon + (dn_0/dT) / n_0]$ is equal to $6\text{x}10^{-6}$ $[1/°C]$ (Carmon et al., 2004). Considering a cavity resonance wavelength of 635 nm, the thermal spectral shift will be equal to 3.81 pm/$°C$. This shift is almost 60 times smaller than the reactive shift caused by bacterial binding to a microdisk with a Q-factor of 10^4. In this case, the temperature changes don't have a major effect on the wavelength shift and can be ignored. However, for a single bacterium detection, the spectral shift would be of the order of 5 pm, as discussed in section 5.2.2 in the previous chapter. Temperature thus needs to be controlled and stabilized so the variations do not exceed 0.01 °C. One method to control the temperature is to use a Peltier heat pump device and thermistor that could control the temperature to 0.01 °C (Barrios et al., 2007). Nonetheless, the use of these systems can add some complexity, size and increase the cost of the device (Xu et al., 2010).

6.1.3   Multiplexing assays

Multiplexed biosensing can have many interesting applications in clinical diagnostics and environmental monitoring. It can help achieve fast simultaneous responses for multiple sample solutions. Optical biosensors intended for multiplexing use can be easily fabricated using a series of microdisks that are close one to another. However, coupling using tapered optical fibers can add some difficulties to the multiplexed devices, making integrated waveguides more appropriate for this purpose.

Multiplexed biosensing assays are a series of optical microdisks coupled to a single waveguide. Each resonator is functionalized with a different antibody or bacteriophage, specific to the target molecule it needs to detect. The resonance wavelength is observed for each microcavity independently, and it shifts according to the strain and concentration of the target molecule that binds to its surface, as shown in Fig. 6.2. Usually, micropipettes or syringe pumps are used to deliver the sample to the microcavity. However, these techniques can cause non-specific binding and cross-reactivity between the capture agents because they deliver relatively large volumes of analytes. The cross-reactivity to non-target proteins is common and ubiquitous to antibodies (Juncker et al., 2014). The use of smaller volumes to deliver the analytes to the specified position can help overcome this problem. The use of inkjet printing is one proposed way to do so. Inkjet printing is a non-impact technology that deposits the liquid drops directly on a pre-specified position through a small aperture (Li et al., 2015). This method can deliver volumes as small as 0.6 picoliter on a surface as small as 5 μm wide (SonoPlot GIX microplotter), reducing sample consumption and automating the assays. A potential complication of this technique, especially when used with protein based analytes, is the spot drying. Proteins should always be kept in aqueous environment to avoid their denaturation.

The potential of inkjet printing in the biosensing field is still largely untapped. The development of automated processes to deposit the samples or even the miniaturization of the printer into a portable machine can lead to highly efficient, portable, high resolution and rapid biosensing tools.
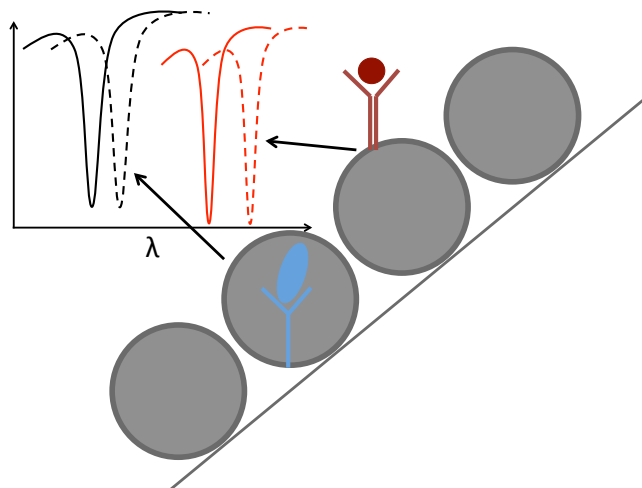
Figure 6.2 Multiplexed biosensing showing a series of optical microdisks coupled to a single waveguide. Two of the disks are functionalized with two different bacteriophages specific to two different strains of bacteria. The spectral shifts are observed for each of these resonators, according to the nature and concentration of bacteria attached to their surface.

6.2 Conclusion

In this chapter, a brief description of the problems and limitations encountered during the project was given. Due to the developments in the optical and microfluidics fields, we could suggest some recommendations that would allow the use of optical microdisks on-site for clinical diagnostics and environmental sampling. This could lead the way towards the commercialization of optical biosensors based on optical microdisks.

CHAPTER 7   CONCLUSION AND RECOMMENDATIONS

The presence of pathogenic bacteria and virus particles in food supplies and contaminated water can cause serious infections and diseases and is responsible for a high percentage of mortality around the world. Over the years, several biosensing techniques have been developed to detect the presence of viruses and bacteria and prevent the spread of infectious diseases. The first biosensors to be studied and used were label-based sensors. However, these sensors can be very expensive, and the labeling process can be time-consuming and can interfere with the immunoreactivity of the antibodies and the biomolecules to be detected. From here came the need to develop label-free biosensors to overcome these problems. Label-free electromechanical and electrical sensors had many limitations, like having a short shelf life or a long detection time as well as complex fabrication processes. This lead researchers to turn towards a new family of biosensors, the optical bioensors, and more specifically whispering gallery mode microcavities.

Numerous studies have emerged in the last decade using whispering gallery mode microcavities as biosensors. Optical microcavities are structures that can efficiently confine light at the microscale, and are thus characterized by their high quality factors. They have a wide range of applications in telecommunications as filters and lasers, optomechanics and sensing. In addition to their high Q factors, they are easy to fabricate and to integrate with microfluidics and multiplexing essays, which make them ideal for biosensing applications.

The aim of this project is to develop a specific label-free biosensor based on whispering gallery mode microdisks. The first step towards achieving this goal is via an appropriate surface preparation. Specificity is a very important feature of a biosensor that makes it suitable for clinical and medical use in complex environments, and we have demonstrated an important step towards it. During this PhD project, a novel functionalization process was developed that used specific protein phages instead of whole phages to avoid unnecessary and additional purification steps. After a series of experiments, LysK protein phage turned out to be the most specific to bind Staphylococcus aureus strains of bacteria. This binding event on the surface of the microdisk was quantified through the reactive sensing mechanism. The attachment of bacteria changes the refractive index of the resonator, hence shifting its resonance wavelength towards longer wavelengths.

The reactive sensing principle was only developed for a microsphere (Arnold et al., 2010), since it is impossible to find an exact expression of the electromagnetic field inside a microdisk. In this thesis, a theoretical expression for the wavelength shift was developed using an

analytical approximation of the electric field inside a microdisk. This expression allowed to approximately determine the concentration of bacteria that bind to the surface of the resonator and contribute to the reactive shift. It has been found that for an initial concentration of 5.10^9 CFU/ml of S. aureus bacteria, the reactive shift was about 0.22 nm, which corresponds to approximately 46 bacteria that attach to the sensitive part of the microdisk.

The observation of the wavelength shift also allowed to learn more about the kinetics of the binding between the LysK protein phage and its host bacteria, S. aureus. The graphics showed that LysK has a high lysing efficiency on S. aureus, and began to act strongly on the bacteria the moment it was added into the sample. It took about 15 minutes for the LysK to attach the maximum number of bacteria. After that time, the shift started to decrease until it reached its initial value. After about 30 minutes, the bacteria were totally destroyed by the protein phage. The limit of detection for a solution of 2 μM of LysK was of 5×10^6 CFU/ml or 5 pg/ml, corresponding to 30 bacteria.

For the first time, label-free detection of bacteria using optical microdisks was achieved. The device obtained was highly specific, easily fabricated and gave fast responses. Despite this success, some improvements are still needed, especially if the use of such biosensors needs to be expanded outside the academic laboratory. It becomes thus important to integrate this biosensor into a lab on a chip in order to have a robust, low cost, easy to use and reproduce portable device that requires low sample volumes and improved multiplexing capabilities.

The developments in optical and microfluidics fields allow the integration of many optical components and microfluidic channels with the microdisk. As mentioned in the previous chapter, optical waveguides have been integrated with a silica microdisk on a chip using standard lithographic techniques (Grutter et al., 2010). This will lead to a more robust biosensor with improved stability and more efficient coupling that won't be affected by the instabilities caused by the use of a tapered optical fiber.

Multiplexing assays are also of a great interest especially when fast sample throughput or multiple simultaneous assays are required (Luchansky and Bailey, 2011). Advancements in microfluidics and the possibility to use inkjet printing to automate and reduce sample consumption can lead the way towards having very efficient, low cost, integrated and rapid biosensing tools.

Many studies have demonstrated the ability of optical microcavities to detect a single molecule thanks to their high sensitivity. However, this kind of experiments is still unlikely to be feasible in complex environments like blood or serum. The high sensitivity of optical microcavities can be put to use by analysing the interactions between the molecules or the kinetics of the binding between the protein and the bacteria, as described earlier in the thesis.

Single molecule detection using whispering gallery optical microcavities can be a very useful tool for biochemists and biotechnologists to study the mechanisms and behaviours of single nanoparticles such as proteins, enzymes and viruses (Foreman et al., 2015). It can help understand the fundamental physical and biological mechanisms of these molecules as well as providing new tools to study nanomachines using label-free techniques, for example, when using optical tweezers.

Single molecule detection can also provide very useful information of the interactions between a molecule and its receptor to be applied in clinical diagnostics.

Integration of whispering gallery mode biosensors on lab-on-chips with microfluidics, photonics and electric devices will enable the use of robust and portable biosensors for environmental and health diagnostics and monitoring. They can be used for early-stage detection of infections and diseases rapidly and accurately, and can eventually become a new family of commercialized label-free biosensors.

Although the studies and research in the biosensors field are developing fast, many bacteria strains are mutating and becoming resistant to antibiotics and other treatments. That's why the biosensing field is in continuous improvement to always have the most sensitive, specific, robust, high resolution and fast response biosensors.

BIBLIOGRAPHY

T. Amrane, "Fabrication et caractérisation de cavités organiques à modes de galerie", Thèse de doctorat, École Polytechnique de Montréal, 2012.

A. M. Armani, "Single molecule detection using optical microcavities", dans *Photonic Microresonator Research and Applications.* Springer, 2010, pp. 253–273.

A. M. Armani, R. P. Kulkarni, S. E. Fraser, R. C. Flagan, et K. J. Vahala, "Label-free, single-molecule detection with optical microcavities", *Science*, vol. 317, no. 5839, pp. 783–787, 2007.

S. Arnold, M. Khoshsima, I. Teraoka, S. Holler, et F. Vollmer, "Shift of whispering-gallery modes in microspheres by protein adsorption", *Optics letters*, vol. 28, no. 4, pp. 272–274, 2003.

S. Arnold, S. Shopova, et S. Holler, "Whispering gallery mode bio-sensor for label-free detection of single molecules : thermo-optic vs. reactive mechanism", *Optics Express*, vol. 18, no. 1, pp. 281–287, 2010.

C. A. Barrios, K. B. Gylfason, B. Sánchez, A. Griol, H. Sohlström, M. Holgado, et R. Casquel, "Slot-waveguide biochemical sensor", *Optics letters*, vol. 32, no. 21, pp. 3080–3082, 2007.

M. Basta, M. Karmali, et C. Lingwood, "Sensitive receptor-specified enzyme-linked immunosorbent assay for escherichia coli verocytotoxin." *Journal of clinical microbiology*, vol. 27, no. 7, pp. 1617–1622, 1989.

S. C. Becker, J. Foster-Frey, et D. M. Donovan, "The phage k lytic enzyme lysk and lysostaphin act synergistically to kill mrsa", *FEMS microbiology letters*, vol. 287, no. 2, pp. 185–191, 2008.

R. Berger, E. Delamarche, H. P. Lang, C. Gerber, J. K. Gimzewski, E. Meyer, et H.-J. Güntherodt, "Surface stress in the self-assembly of alkanethiols on gold", *Science*, vol. 276, no. 5321, pp. 2021–2024, 1997.

S. Bergeron, "Microcavités diélectriques circulaires et applications", Thèse de doctorat, École Polytechnique de Montréal, 2010.

S. Bergeron, F. Vanier, et Y.-A. Peter, "Silica microdisk coupled resonator optical waveguide", *IEEE/LEOS International Conference on Optical MEMS and Nanophotonics*, pp. 73–74, 2009.

M. Borselli, T. Johnson, et O. Painter, "Beyond the rayleigh scattering limit in high-q silicon microdisks : theory and experiment", *Optics Express*, vol. 13, no. 5, pp. 1515–1530, 2005.

R. W. Boyd et J. E. Heebner, "Sensitive disk resonator photonic biosensor", *Applied Optics*, vol. 40, no. 31, pp. 5742–5747, 2001.

J. Bures, *Guided optics.* John Wiley & Sons, 2009.

T. P. Burg, M. Godin, S. M. Knudsen, W. Shen, G. Carlson, J. S. Foster, K. Babcock, et S. R. Manalis, "Weighing of biomolecules, single cells and single nanoparticles in fluid", *Nature*, vol. 446, no. 7139, pp. 1066–1069, 2007.

H. Cai, J. Caswell, et J. Prescott, "Nonculture molecular techniques for diagnosis of bacterial disease in animals a diagnostic laboratory perspective", *Veterinary Pathology Online*, vol. 51, no. 2, pp. 341–350, 2014.

M. Cai, O. Painter, et K. J. Vahala, "Observation of critical coupling in a fiber taper to a silica-microsphere whispering-gallery mode system", *Physical review letters*, vol. 85, no. 1, p. 74, 2000.

T. Carmon, L. Yang, et K. Vahala, "Dynamical thermal behavior and thermal self-stability of microcavities", *Optics Express*, vol. 12, no. 20, pp. 4742–4750, 2004.

C.-y. Chao et L. J. Guo, "Polymer microring resonators fabricated by nanoimprint technique", *Journal of Vacuum Science & Technology B*, vol. 20, no. 6, pp. 2862–2866, 2002.

C.-Y. Chao et L. J. Guo, "Biochemical sensors based on polymer microrings with sharp asymmetrical resonance", *Applied Physics Letters*, vol. 83, no. 8, pp. 1527–1529, 2003.

H. Chibli, H. Ghali, S. Park, Y.-A. Peter, et J. L. Nadeau, "Immobilized phage proteins for specific detection of staphylococci", *Analyst*, vol. 139, no. 1, pp. 179–186, 2014.

T. M. Chinowsky, M. S. Grow, K. S. Johnston, K. Nelson, T. Edwards, E. Fu, et P. Yager, "Compact, high performance surface plasmon resonance imaging system", *Biosensors and Bioelectronics*, vol. 22, no. 9, pp. 2208–2215, 2007.

L. C. Clark et C. Lyons, "Electrode systems for continuous monitoring in cardiovascular surgery", *Annals of the New York Academy of sciences*, vol. 102, no. 1, pp. 29–45, 1962.

M. A. Cooper, "Optical biosensors in drug discovery", *Nature Reviews Drug Discovery*, vol. 1, no. 7, pp. 515–528, 2002.

R. Datar, S. Kim, S. Jeon, P. Hesketh, S. Manalis, A. Boisen, et T. Thundat, "Cantilever sensors : nanomechanical tools for diagnostics", *Mrs Bulletin*, vol. 34, no. 06, pp. 449–454, 2009.

E. Engvall et P. Perlmann, "Enzyme-linked immunosorbent assay (elisa) quantitative assay of immunoglobulin g", *Immunochemistry*, vol. 8, no. 9, pp. 871–874, 1971.

X. Fan, I. M. White, S. I. Shopova, H. Zhu, J. D. Suter, et Y. Sun, "Sensitive optical biosensors for unlabeled targets : A review", *analytica chimica acta*, vol. 620, no. 1, pp. 8–26, 2008.

M. Ferrari, "Cancer nanotechnology : opportunities and challenges", *Nature Reviews Cancer*, vol. 5, no. 3, pp. 161–171, 2005.

M. R. Foreman, J. D. Swaim, et F. Vollmer, "Whispering gallery mode sensors", *Advances in Optics and Photonics*, vol. 7, no. 2, pp. 168–240, 2015.

J. Fritz, M. Baller, H. Lang, H. Rothuizen, P. Vettiger, E. Meyer, H.-J. Güntherodt, C. Gerber, et J. Gimzewski, "Translating biomolecular recognition into nanomechanics", *Science*, vol. 288, no. 5464, pp. 316–318, 2000.

S. D. Gan et K. R. Patel, "Enzyme immunoassay and enzyme-linked immunosorbent assay", *Journal of Investigative Dermatology*, vol. 133, no. 9, p. e12, 2013.

S. Garcia, J. M. Crance, A. Billecocq, A. Peinnequin, A. Jouan, M. Bouloy, et D. Garin, "Quantitative real-time pcr detection of rift valley fever virus and its application to evaluation of antiviral compounds", *Journal of Clinical Microbiology*, vol. 39, no. 12, pp. 4456–4461, 2001.

L. Garibyan et N. Avashia, "Research techniques made simple : Polymerase chain reaction (pcr)", *The Journal of investigative dermatology*, vol. 133, no. 3, p. e6, 2013.

M. L. Gorodetsky, A. A. Savchenkov, et V. S. Ilchenko, "Ultimate q of optical microsphere resonators", *Optics Letters*, vol. 21, no. 7, pp. 453–455, 1996.

K. E. Grutter, A. M. Yeh, S. K. Patra, et M. C. Wu, "A new fabrication technique for integrating silica optical devices and mems", dans *2010 International Conference on Optical MEMS and Nanophotonics*, 2010, pp. 33–34.

K. E. Grutter, A. Grine, M.-K. Kim, N. Quack, T. Rocheleau, C. T. Nguyen, et M. C. Wu, "A platform for on-chip silica optomechanical oscillators with integrated waveguides", dans *CLEO : Science and Innovations.* Optical Society of America, 2012, pp. CW1M–5.

A. Gupta, D. Akin, et R. Bashir, "Detection of bacterial cells and antibodies using surface micromachined thin silicon cantilever resonators", *Journal of Vacuum Science & Technology B*, vol. 22, no. 6, pp. 2785–2791, 2004.

G. M. Hale et M. R. Querry, "Optical constants of water in the 200-nm to 200-μm wavelength region", *Applied optics*, vol. 12, no. 3, pp. 555–563, 1973.

J. Heebner, R. Grover, T. Ibrahim, et T. A. Ibrahim, *Optical microresonators : theory, fabrication, and applications.* Springer Science & Business Media, 2008.

X. Hoa, A. Kirk, et M. Tabrizian, "Towards integrated and sensitive surface plasmon resonance biosensors : a review of recent progress", *Biosensors and Bioelectronics*, vol. 23, no. 2, pp. 151–160, 2007.

F. Huber, M. Hegner, C. Gerber, H.-J. Güntherodt, et H. P. Lang, "Label free analysis of transcription factors using microcantilever arrays", *Biosensors and Bioelectronics*, vol. 21, no. 8, pp. 1599–1605, 2006.

H. K. Hunt et A. M. Armani, "Label-free biological and chemical sensors", *Nanoscale*, vol. 2, no. 9, pp. 1544–1559, 2010.

R. v. d. Hurk et S. Evoy, "A review of membrane-based biosensors for pathogen detection", *Sensors*, vol. 15, no. 6, pp. 14 045–14 078, 2015.

V. S. Ilchenko et L. Maleki, "Novel whispering-gallery resonators for lasers, modulators, and sensors", dans *Photonics West 2001-LASE.* International Society for Optics and Photonics, 2001, pp. 120–130.

F. N. Ishikawa, H.-K. Chang, M. Curreli, H.-I. Liao, C. A. Olson, P.-C. Chen, R. Zhang, R. W. Roberts, R. Sun, R. J. Cote *et al.*, "Label-free, electrical detection of the sars virus n-protein with nanowire biosensors utilizing antibody mimics as capture probes", *Acs Nano*, vol. 3, no. 5, pp. 1219–1224, 2009.

K. Janyapoon, S. Korbsrisate, H. Thamapa, S. Thongmin, S. Kanjanahareutai, N. Wong-predee, et S. Sarasombath, "Rapid detection of salmonella enterica serovar choleraesuis in blood cultures by a dot blot enzyme-linked immunosorbent assay", *Clinical and diagnostic laboratory immunology*, vol. 7, no. 6, pp. 977–979, 2000.

D. Juncker, S. Bergeron, V. Laforte, et H. Li, "Cross-reactivity in antibody microarrays and multiplexed sandwich assays : shedding light on the dark side of multiplexing", *Current opinion in chemical biology*, vol. 18, pp. 29–37, 2014.

T. Kippenberg, S. Spillane, D. Armani, et K. Vahala, "Fabrication and coupling to planar high-q silica disk microcavities", *Applied Physics Letters*, vol. 83, no. 4, pp. 797–799, 2003.

A. Koyun, E. Ahlatcolu, Y. Koca, et S. Kara, "Biosensors and their principles", *A Roadmap of Biomedical Engineers and Milestones*, 2012.

O. Krupin, H. Asiri, C. Wang, R. N. Tait, et P. Berini, "Biosensing using straight long-range surface plasmon waveguides", *Optics express*, vol. 21, no. 1, pp. 698–709, 2013.

W.-C. Kuo, C. Chou, et H.-T. Wu, "Optical heterodyne surface-plasmon resonance biosensor", *Optics letters*, vol. 28, no. 15, pp. 1329–1331, 2003.

P. Lee, T. Plavina, A. Castro, M. Berman, D. Jaiswal, S. Rivas, B. Schlain, et M. Subramanyam, "A second-generation elisa (stratify jcv™ dxselect™) for detection of jc virus antibodies in human serum and plasma to support progressive multifocal leukoencephalopathy risk stratification", *Journal of Clinical Virology*, vol. 57, no. 2, pp. 141–146, 2013.

S. X. Leng, J. E. McElhaney, J. D. Walston, D. Xie, N. S. Fedarko, et G. A. Kuchel, "Elisa and multiplex technologies for cytokine measurement in inflammation and aging research", *The Journals of Gerontology Series A : Biological Sciences and Medical Sciences*, vol. 63, no. 8, pp. 879–884, 2008.

J. Li, F. Rossignol, et J. Macdonald, "Inkjet printing for biosensor fabrication : combining chemistry and technology for advanced manufacturing", *Lab on a chip*, vol. 15, no. 12, pp. 2538–2558, 2015.

Q. Li, F. Liu, Z. Zhang, M. Qiu, et Y. Su, "High-rate data buffering in silicon nanophotonic devices", *SPIE Newsroom*, 2008.

B. Liedberg, C. Nylander, et I. Lunström, "Surface plasmon resonance for gas detection and biosensing", *Sensors and actuators*, vol. 4, pp. 299–304, 1983.

B. E. Little, J.-P. Laine, et S. T. Chu, "Surface-roughness-induced contradirectional coupling in ring and disk resonators", *Optics letters*, vol. 22, no. 1, pp. 4–6, 1997.

T. Lu, H. Lee, T. Chen, S. Herchak, J.-H. Kim, S. E. Fraser, R. C. Flagan, et K. Vahala, "High sensitivity nanoparticle detection using optical microcavities", *Proceedings of the National Academy of Sciences*, vol. 108, no. 15, pp. 5976–5979, 2011.

M. S. Luchansky et R. C. Bailey, "High-q optical sensors for chemical and biological analysis", *Analytical chemistry*, vol. 84, no. 2, pp. 793–821, 2011.

M. J. Madou, *Fundamentals of microfabrication : the science of miniaturization.* CRC press, 2002.

S. Mehrabani, A. J. Maker, et A. M. Armani, "Hybrid integrated label-free chemical and biological sensors", *Sensors*, vol. 14, no. 4, pp. 5890–5928, 2014.

J. Miao, R. C. Pangule, E. E. Paskaleva, E. E. Hwang, R. S. Kane, R. J. Linhardt, et J. S. Dordick, "Lysostaphin-functionalized cellulose fibers with antistaphylococcal activity for wound healing applications", *Biomaterials*, vol. 32, no. 36, pp. 9557–9567, 2011.

W. Moerner, "New directions in single-molecule imaging and analysis", *Proceedings of the National Academy of Sciences*, vol. 104, no. 31, pp. 12 596–12 602, 2007.

M. Nordström, S. Keller, M. Lillemose, A. Johansson, S. Dohn, D. Haefliger, G. Blagoi, M. Havsteen-Jakobsen, et A. Boisen, "Su-8 cantilevers for bio/chemical sensing ; fabrication, characterisation and development of novel read-out methods", *Sensors*, vol. 8, no. 3, pp. 1595–1612, 2008.

O. Olerup et H. Zetterquist, "Hla-dr typing by pcr amplification with sequence-specific primers (pcr-ssp) in 2 hours : an alternative to serological dr typing in clinical practice including donor-recipient matching in cadaveric transplantation", *Tissue antigens*, vol. 39, no. 5, pp. 225–235, 1992.

F. Patolsky, G. Zheng, et C. M. Lieber, "Fabrication of silicon nanowire devices for ultrasensitive, label-free, real-time detection of biological and chemical species", *Nature protocols*, vol. 1, no. 4, pp. 1711–1724, 2006.

N. M. M. Pires, T. Dong, U. Hanke, et N. Hoivik, "Recent developments in optical detection technologies in lab-on-a-chip devices for biosensing applications", *Sensors*, vol. 14, no. 8, pp. 15 458–15 479, 2014.

N. M. Pires, T. Dong, Z. Yang, N. Høivik, et X. Zhao, "A mediator embedded micro-immunosensing unit for electrochemical detection on viruses within physiological saline media", *Journal of Micromechanics and Microengineering*, vol. 21, no. 11, p. 115031, 2011.

S. M. Radke et E. C. Alocilja, "A high density microelectrode array biosensor for detection of e. coli o157 : H7", *Biosensors and Bioelectronics*, vol. 20, no. 8, pp. 1662–1667, 2005.

A. Ramachandran, S. Wang, J. Clarke, S. Ja, D. Goad, L. Wald, E. Flood, E. Knobbe, J. Hryniewicz, S. Chu *et al.*, "A universal biosensing platform based on optical micro-ring resonators", *Biosensors and Bioelectronics*, vol. 23, no. 7, pp. 939–944, 2008.

R. K. Saiki, S. Scharf, F. Faloona, K. B. Mullis, G. T. Horn, H. A. Erlich, et N. Arnheim, "Enzymatic amplification of beta-globin genomic sequences and restriction site analysis for diagnosis of sickle cell anemia", *Science*, vol. 230, no. 4732, pp. 1350–1354, 1985.

P. Sass et G. Bierbaum, "Lytic activity of recombinant bacteriophage φ11 and φ12 endolysins on whole cells and biofilms of staphylococcus aureus", *Applied and environmental microbiology*, vol. 73, no. 1, pp. 347–352, 2007.

F. Sassa, K. Morimoto, W. Satoh, et H. Suzuki, "Electrochemical techniques for microfluidic applications", *Electrophoresis*, vol. 29, no. 9, pp. 1787–1800, 2008.

R. Satishkumar, S. Sankar, Y. Yurko, A. Lincourt, J. Shipp, B. T. Heniford, et A. Vertegel, "Evaluation of the antimicrobial activity of lysostaphin-coated hernia repair meshes", *Antimicrobial agents and chemotherapy*, vol. 55, no. 9, pp. 4379–4385, 2011.

R. Schlapak, P. Pammer, D. Armitage, R. Zhu, P. Hinterdorfer, M. Vaupel, T. Frühwirth, et S. Howorka, "Glass surfaces grafted with high-density poly (ethylene glycol) as substrates for dna oligonucleotide microarrays", *Langmuir*, vol. 22, no. 1, pp. 277–285, 2006.

K. Senda, Y. Arakawa, S. Ichiyama, K. Nakashima, H. Ito, S. Ohsuka, K. Shimokata, N. Kato, et M. Ohta, "Pcr detection of metallo-beta-lactamase gene (blaimp) in gram-negative rods resistant to broad-spectrum beta-lactams." *Journal of Clinical Microbiology*, vol. 34, no. 12, pp. 2909–2913, 1996.

L. Shao, X.-F. Jiang, X.-C. Yu, B.-B. Li, W. R. Clements, F. Vollmer, W. Wang, Y.-F. Xiao, et Q. Gong, "Detection of single nanoparticles and lentiviruses using microcavity resonance broadening", *Advanced Materials*, vol. 25, no. 39, pp. 5616–5620, 2013.

A. B. Socorro, S. Soltani, I. Del Villar, J. M. Corres, et A. M. Armani, "Temperature sensor

based on a hybrid ito-silica resonant cavity", *Optics express*, vol. 23, no. 3, pp. 1930–1937, 2015.

K. Suzuki, T. Sawada, A. Murakami, T. Matsui, S. Tohma, K. Nakazono, M. Takemura, Y. Takasaki, T. Mimori, et K. Yamamoto, "High diagnostic performance of elisa detection of antibodies to citrullinated antigens in rheumatoid arthritis", *Scandinavian journal of rheumatology*, vol. 32, no. 4, pp. 197–204, 2003.

A. D. Taylor, Q. Yu, S. Chen, J. Homola, et S. Jiang, "Comparison of e. coli o157 : H7 preparation methods used for detection with surface plasmon resonance sensor", *Sensors and Actuators B : Chemical*, vol. 107, no. 1, pp. 202–208, 2005.

M. Tolba, O. Minikh, L. Brovko, S. Evoy, et M. Griffiths, "Oriented immobilization of bacteriophages for biosensor applications", *Applied and environmental microbiology*, vol. 76, no. 2, pp. 528–535, 2010.

S. Tombelli, M. Minunni, E. Luzi, et M. Mascini, "Aptamer-based biosensors for the detection of hiv-1 tat protein", *Bioelectrochemistry*, vol. 67, no. 2, pp. 135–141, 2005.

T. Tumolo, L. Angnes, et M. S. Baptista, "Determination of the refractive index increment (dn/dc) of molecule and macromolecule solutions by surface plasmon resonance", *Analytical biochemistry*, vol. 333, no. 2, pp. 273–279, 2004.

K. Vahala, *Optical microcavities.* World Scientific, 2004.

B. Van Weemen et A. Schuurs, "Immunoassay using antigen—enzyme conjugates", *FEBS letters*, vol. 15, no. 3, pp. 232–236, 1971.

F. Vollmer, D. Braun, A. Libchaber, M. Khoshsima, I. Teraoka, et S. Arnold, "Protein detection by optical shift of a resonant microcavity", *Applied Physics Letters*, vol. 80, no. 21, pp. 4057–4059, 2002.

F. Vollmer, S. Arnold, et D. Keng, "Single virus detection from the reactive shift of a whispering-gallery mode", *Proceedings of the National Academy of Sciences*, vol. 105, no. 52, pp. 20 701–20 704, 2008.

F. Vollmer et L. Yang, "Review label-free detection with high-q microcavities : a review of biosensing mechanisms for integrated devices", *Nanophotonics*, vol. 1, pp. 181–291, 2012.

F. Vollmer, S. Arnold, D. Braun, I. Teraoka, et A. Libchaber, "Multiplexed dna quantification by spectroscopic shift of two microsphere cavities", *Biophysical journal*, vol. 85, no. 3,

pp. 1974–1979, 2003.

R.-F. Wang, W.-W. Cao, et C. E. Cerniglia, "Pcr detection and quantitation of predominant anaerobic bacteria in human and animal fecal samples." *Applied and Environmental Microbiology*, vol. 62, no. 4, pp. 1242–1247, 1996.

A. L. Washburn, L. C. Gunn, et R. C. Bailey, "Label-free quantitation of a cancer biomarker in complex media using silicon photonic microring resonators", *Analytical chemistry*, vol. 81, no. 22, pp. 9499–9506, 2009.

M. J. Weber, *Handbook of optical materials.* CRC press, 2002, vol. 19.

B. Weeks, J. Camarero, A. Noy, A. Miller, L. Stanker, et J. De Yoreo, "Development of a microcantilever-based pathogen detector", *Scanning*, vol. 25, no. 6, pp. 297–299, 2003.

N. Wongkaew, P. He, V. Kurth, W. Surareungchai, et A. J. Baeumner, "Multi-channel pmma microfluidic biosensor with integrated iduas for electrochemical detection", *Analytical and bioanalytical chemistry*, vol. 405, no. 18, pp. 5965–5974, 2013.

G. Wu, R. H. Datar, K. M. Hansen, T. Thundat, R. J. Cote, et A. Majumdar, "Bioassay of prostate-specific antigen (psa) using microcantilevers", *Nature biotechnology*, vol. 19, no. 9, pp. 856–860, 2001.

G. Wu, H. Ji, K. Hansen, T. Thundat, R. Datar, R. Cote, M. F. Hagan, A. K. Chakraborty, et A. Majumdar, "Origin of nanomechanical cantilever motion generated from biomolecular interactions", *Proceedings of the National Academy of Sciences*, vol. 98, no. 4, pp. 1560–1564, 2001.

Y. Wu et F. Vollmer, "Whispering gallery mode biomolecular sensors", dans *Cavity-Enhanced Spectroscopy and Sensing.* Springer, 2014, pp. 323–349.

D.-X. Xu, M. Vachon, A. Densmore, R. Ma, S. Janz, A. Delâge, J. Lapointe, P. Cheben, J. Schmid, E. Post *et al.*, "Real-time cancellation of temperature induced resonance shifts in soi wire waveguide ring resonator label-free biosensor arrays", *Optics express*, vol. 18, no. 22, pp. 22 867–22 879, 2010.

X. Yao, X. Li, F. Toledo, C. Zurita-Lopez, M. Gutova, J. Momand, et F. Zhou, "Subattomole oligonucleotide and p53 cdna determinations via a high-resolution spr combined with oligonucleotide-capped gold nanoparticle signal amplification", *Anal Biochem*, vol. 354, pp. 220–8, 2006.

X. Zhang et A. M. Armani, "Silica microtoroid resonator sensor with monolithically integrated waveguides", *Optics express*, vol. 21, no. 20, pp. 23 592–23 603, 2013.

X. Zhang, H. S. Choi, et A. M. Armani, "Ultimate quality factor of silica microtoroid resonant cavities", *Applied physics letters*, vol. 96, no. 15, p. 153304, 2010.

APPENDIX A   ARTICLE 1 : Wavelength Shift in a Whispering Gallery Microdisk due to Bacterial Sensing : A Theoretical Approach

Wavelength Shift in a Whispering Gallery Microdisk due to Bacterial Sensing : A Theoretical Approach

Wavelength Shift in a Whispering Gallery Microdisk due to Bacterial Sensing: A Theoretical Approach

Hala Ghali[a,*], Pablo Bianucci[b], Yves-Alain Peter[a]

[a]*Department of Engineering Physics, Polytechnique Montréal, H3T 1J4, Canada*
[b]*Physics Department, Concordia University, Montréal, H4B 1R6, Canada*

Abstract

Whispering gallery mode microcavities have recently been studied as a means to achieve real-time label-free detection of biological targets such as virus particles, specific DNA sequences, or proteins. Binding of a biomolecule to the surface of a microresonator will increase its path length, leading to a shift in the resonance frequency according to the reactive sensing principle. In this paper, we develop a theoretical expression that will link the reactive shift to the bacteria and microdisk parameters and help quantify the number of bacteria that bind to the surface of a 200 μm-diameter silica microdisk.

Keywords: optical microdisk; wavelength shift; bacterial sensing

1. Introduction

Whispering gallery microcavities (WGM) have attracted increased attention in the last decade as tools for label-free biosensing [1, 2, 3, 4]. They are structures that can efficiently confine light at the microscale due to total internal reflection of light at the interface between the cavity and its surrounding medium. WGM have a high sensitivity potential due to their high quality factors, as well as being selective when their surface is properly functionalized with the appropriate recognition element, relatively low cost and yield fast response. While the bulk of the research in this field is oriented towards the detection of viruses and small molecules, whispering gallery modes microcavities have a great potential

---

*Corresponding author

for the detection of bacteria. For instance, *Staphylococcus aureus (S. aureus)* is a gram-positive bacterium, which is a common cause of skin and respiratory infections and presents antibiotic-resistant strains such as methicillin-resistant *S. aureus* (MRSA). MRSA is responsible for over 60% of staphylococcal infections in hospitals. It becomes thus crucial to find tools to achieve fast diagnosis and early detection of staphylococcal infections. There exist several techniques that are widely used for this purpose. Bacterial culture is used in most hospitals to identify the presence of Staphylococcus aureus. However this kind of tests can take several days to identify the pathogenic bacteria [5]. Real-time PCR is the most widespread FDA-approved test for MRSA [6, 7]. However, this technique is time-consuming (about 2 hours), require prior isolation of bacterial DNA, can be very expensive and is impractical for use on-site or in developing countries. Another study shows the detection of Staphylococcus aureus using aptamer-conjugated gold nanoparticles [8]. Although this technique is very sensitive, it can take up to 1.5 hours to detect the presence of the bacteria, making it unsuitable for real-time detection. Recently, we have shown the detection of *S. aureus* bacteria in Tris-buffered saline (TBS) (10 mM Tris-HCL, 150 mM NaCl, pH 7.5) by measuring the resonance shifts in silica microdisks which were specifically functionalized to react only to *S. aureus* [9].

2. Materials and Methods

2.1. Microdisks fabrication

Optical microdisks are fabricated using standard silicon micromachining techniques [10]. The substrates used are silicon topped with an 800 nm thermal silicon dioxide layer. The first step performed is UV photolithography to generate photoresist patterns of 200 μm-diameter microdisks with AZ5214 photoresist. Patterns are then transferred to silica using buffered oxide etch (B.O.E.) of silicon dioxide. The last step is isotropic dry etching of silicon with SF_6 gas to obtain microdisks on pedestals. A scanning electron micrograph of

40 a fabricated 200 μm-diameter silica microdisk is shown in Fig. 1.

2.2. Surface functionalization

The functionalization process, needed for the response to be specific to *S. Aureus* [11] and shown in Fig. 2 starts by cleaning the microdisks using

45 oxygen plasma to remove organic residues. The samples are then immersed in an ethanol:water (95:5) solution containing 2.5% triethoxysilane-PEG-NH$_2$ (Nanocs, MW = 3400) for 2 h, then thoroughly washed with ethanol and dionized water. The PEGylated wafers were then immersed in a 2 μM LysK : 2000 μM EDC (1-Ethyl-3-(3-dimethylaminopropyl)carbodiimide) (1:1000) solution in

50 buffer (10 mM Tris.HCl pH 7.5, 150 mM NaCl, 1 % glycerol) at 4 °C overnight, then thoroughly washed with PBS and water.

After the functionalization process, the microdisk surface exposes a layer of LysK, an endolysin from the staphylococcal phage K that binds strongly to staphylococci. It contains three domains: an N-terminal cysteine, a histidine-

55 dependent amidohydrolase / peptidase (CHAP) domain, a midprotein amidase-2 domain, and a C-terminal SH3b cell wall-binding domain [12]. This layer causes approaching bacteria to stick to the surface of the microdisk and then starts lysing their cell membranes. Lysing starts immediately after the addition of Staphylococcus aureus to LysK.

60 2.3. Optical characterization setup

The resonance shifts caused by the binding of bacteria were measured with the experimental setup represented in Fig. 3. Light from a tunable laser source was coupled into a tapered optical fiber next to the 200 μm-diameter silica microdisk, and the transmitted light intensity was measured as the laser wave-

65 length was scanned. The resonances appeared as dips in the transmission spectrum. A typical transmission spectrum of a 200 μm-diameter silica microdisk coupled to a 1.2 μm waist diameter tapered optical fiber is shown in Fig. 4. Quantitative sensing of the bacterial concentration is important, as a simple

presence/absence detection scheme might not be efficient enough in a clinical setting. In this article, we develop a detailed model of the silica microdisks as biosensors in order to quantify the number of detected bacteria based on the measured resonance shifts.

3. Biosensing principle

The biodetection principle has been demonstrated and described in several studies [13, 14]. When particles bind to the surface of the microresonator, they interact with its evanescent field, hence increasing the optical path length, leading to a shift towards lower frequencies, i.e. longer wavelengths. This is known as the reactive mechanism for biosensing[15]. The wavelength shift is given by:

$$\frac{\Delta\lambda}{\lambda} = \frac{\Delta R}{R} + \frac{\Delta n}{n},\tag{1}$$

where R is the radius of the microresonator and n its refractive index. For more complex cases where the protein or biomolecules are not uniformly distributed across the resonator surface, the analysis becomes less straightforward. The polarizability of the particles as well as the surface density will have an effect on the resonant wavelength shift [13].

3.1. Theoretical wavelength shift

In order to convert the resonance shifts to more useful information we need a theoretical wavelength shift equation for a microdisk. This formulation allows to determine the surface area covered by the analytes using the experimental wavelength shift, and hence estimate the number or concentration of bacteria that bind to the surface of the disk and contribute to the reactive shift.

The frequency shift caused by the binding of a biomolecule considers the energy of interaction as a first-order perturbation to a single-photon resonant state. When a particle binds at a position $\vec{r_i}$, the resonant shift can be expressed as

follows [16]:

$$\left(\frac{\delta\lambda}{\lambda}\right)_i \cong \frac{-\alpha_{ex}|\vec{E}_0(\vec{r_i})^2|}{2\displaystyle\int_V \epsilon_s|\vec{E}_0(\vec{r})|^2 \, dV}. \tag{2}$$

The integral in the denominator of Eq. (2) is taken over the microdisk's volume (V). The excess polarizability of the particles binding to the resonator's surface is α_{ex}, while the resonator's dielectric constant is $\epsilon_s = \epsilon_0\epsilon_{rs}$. The addition of equal electric and magnetic contributions is accounted for by adding the factor 2 in front of the integral.

If there is a relatively large number of binding sites with a reasonably uniform distribution, we can approximate the sum in the numerator of Eq. (2) by:

$$\sum_i^N |E_0(\vec{r_i})|^2 \cong \sigma_s \int |E_0(\vec{r})|^2 dA, \tag{3}$$

with A being the surface area of the resonator and σ_s is the surface area density of the particle covering.

The surface coverage density can be expressed as the number of bound molecules (N) per surface unit as follows:

$$\sigma_s = \frac{N}{\pi(R^2 - r_{1/e}^2) + 2\pi Rh}, \tag{4}$$

where R is the radius of the microcavity. Equation (4) considers that bacteria only attach on the top surface of the microdisk. Since the majority of the mode energy is contained on the edge of the microdisk, only bacteria that attach in this region will contribute to the spectral shift. The surface area taken into consideration is then the surface of a ring of outer diameter R where the electric field is maximum, and an inner diameter $r_{1/e}$ where the intensity of the electric field decays to 1/e of its maximum, in addition to the surface of the edge.

The excess polarizability of the molecules binding to the resonator's surface

can be expressed as follows [13]:

$$\alpha_{ex} = 4\pi\epsilon_0 \left(\frac{n_m}{2\pi}\right) \left(\frac{dn_m}{dc}\right) m_{bact}, \tag{5}$$

where n_m is the medium (TBS) refractive index, $\frac{dn_m}{dc} = lim_{c\to0}(\frac{n_m-n_0}{c})$, the differential refractive index of molecules in water, where c, is the solvent concentration, and is usually of the order of 0.1 mL/g for polymers in water [17], and m_{bact}, the mass of a single particle.

The only missing piece of information is the spatial distribution of the amplitude of the electric field in the resonator, $|\vec{E}(\vec{r})|$. We use an analytical approximation to the electric field in a microdisk[18], where the amplitude of the field is separated as follows:

$$E_0 = \Psi(\rho)\Omega(\phi)Z(z) = J_l(k_0 n_m \rho) \, \exp(im\phi) \, \exp(ik_0(\sqrt{n_d^2 - n_m^2})z), \tag{6}$$

where ρ is the microdisk's radius, ϕ represents the angle on the top surface of the disk, k_0 the wavelength number, n_d and n_m the refractive indices of the disk and the medium, respectively, and z the thickness of the resonator, as shown in Fig. 5.

The parameters used to determine the spectral shift due to S. aureus binding to a 200 μm-diameter silica microdisk submerged in Tris buffer are defined in Table 1. These values are used for the calculations shown below.

Using Eq. (2), (3) and (6), the resonant shift for the TE mode of the microdisk can be written as follows:

$$\frac{\delta\lambda}{\lambda} \simeq \frac{\alpha_{ex}\sigma_s}{2\epsilon_0\epsilon_{rs}} \frac{\left[\int_0^R \int_0^{2\pi} |\Psi(\rho)|^2 \, |\Omega(\phi)|^2 \, \left|Z\left(\frac{h}{2}\right)\right|^2 \rho d\phi d\rho + \int_0^h \int_0^{2\pi} |\Psi(R)|^2 \, |\Omega(\phi)|^2 \, |Z(z)|^2 R d\phi dz\right]}{\int_0^h \int_0^R \int_0^{2\pi} |\Psi(\rho)|^2 |\Omega(\phi)|^2 |Z(z)|^2 \rho d\phi d\rho dz}. \tag{7}$$

The integrals in the numerator of Eq. (7) are taken over the top surface of the microdisk and its edge surface respectively. The denominator is the volume integral of the electric field inside the microcavity. The integral of the first-kind

125 Bessel function can be written according to Eq. (8).

$$\int_0^R [J_l(k_0 n_m \rho)]^2 \rho d\rho = \frac{1}{2} R^2 [J_{l+1}^2(k_0 n_m R)].$$ (8)

The three integrals of Eq. (7) are each solved separately. The first double integral in the numerator is expressed as follows:

$$\int_0^R \int_0^{2\pi} |J_l^2(k_0 n_m \rho)| \ |\exp(im\phi)|^2 \ \exp^2\left[ik_0\left(\sqrt{n_d^2 - n_m^2}\right)\frac{h}{2}\right]\rho d\phi d\rho$$
$$= \frac{2\pi}{2}R^2 \ \left[J_{l+1}^2(k_0 n_m R)\right]$$ (9)

The second double integral of the numerator can be expressed as:

$$\int_0^h \int_0^{2\pi} |J_l^2(k_0 n_m R)| \ |\exp(im\phi)|^2 \ \exp^2\left[ik_0\left(\sqrt{n_d^2 - n_m^2}\right)z\right] R \ d\phi dz$$
$$= 2\pi R \left[J_l^2(k_0 n_m R)\right] \ h$$ (10)

with

$$\int_0^h \exp^2\left[ik_0\left(\sqrt{n_d^2 - n_m^2}\right)z\right] dz = h$$ (11)

and

$$\int_0^{2\pi} |\exp(im\phi)|^2 \, d\phi = 2\pi$$ (12)

The denominator of Eq. (7) is calculated as follows:

$$\int_0^h \int_0^R \int_0^{2\pi} |J_l^2(k_0 n_m \rho)| \ |\exp(im\phi)|^2 \ \exp^2\left[ik_0\left(\sqrt{n_d^2 - n_m^2}\right)z\right]\rho d\phi d\rho dz$$
$$= \frac{1}{2}R^2 \ \left[J_{l+1}^2(k_0 n_m R)\right] h \int_0^{2\pi} |\exp(im\phi)|^2 \, d\phi$$ (13)

130 The integral part (I) of the spectral shift equation (Eq. 7) can be grouped and

simplified as follows:

$$I = \frac{R\ \left[J_{l+1}^2(k_0 n_m R)\right] + 2h\left[J_l^2(k_0 n_m R)\right]}{Rh\ \left[J_{l+1}^2(k_0 n_m R)\right]} = \frac{1}{h} + \frac{2\left[J_l^2(k_0 n_m R)\right]}{R\left[J_{l+1}^2(k_0 n_m R)\right]} \qquad (14)$$

With an explicit expression for the integral in Eq. (7) in hand, we can then use Eq. (2) to find out an expression for the spectral shift. This expression is an approximation rather than an exact solution because there is no exact solution to the modes of a microdisk. Furthermore, microdisks are considered as 2D structures, and only the bacteria that bind to the edge of the microresonator are taken into account to calculate the wavelength shift. The resonance shift for a WGM microdisk can then be estimated by the following equation:

$$\frac{\delta\lambda}{\lambda} \simeq \frac{\alpha_{ex}\sigma_s}{2\epsilon_0\epsilon_{rs}}\left\{\frac{1}{h} + \frac{2\left[J_l^2(k_0 n_m R)\right]}{R\left[J_{l+1}^2(k_0 n_m R)\right]}\right\} \qquad (15)$$

As can be seen in Eq. (15), the wavelength shift depends on the radius of the microdisk and is not affected by its Q-factor. This relationship can hence be applied to all optical microdisks of different sizes and Q-factors.

3.2. Experimental results

Bacteria were added to the surface of a functionalized silica microdisk using a micropipette. As soon as the bacteria stick to the surface of the microdisk, LysK phage starts immediately lysing the Staphylococcus aureus. It takes about 30 minutes for most of the bacteria to be lysed. A graph showing the variation of the wavelength shift in time after the binding of S. aureus to the surface of an optical microdisk is shown in Fig. 6.

Four different concentrations of bacteria were used experimentally, leading to four different wavelength shifts [9]. Fig. 7 shows the maximum wavelength shifts obtained experimentally for the four different concentrations. From these wavelength shifts, the corresponding number of bacteria that bind to the surface of the resonator in each case was calculated using Eq. (15). The results are summarized in Table 2 and plotted on Figure 8.

155　　The minimum shift that could be observed was of 0.14 nm, corresponding to 20 bacteria binding to the surface of the microresonator and contributing to the spectral shift. The bacterial concentration used in this case was 5.10^6 CFU/ml.

　　Figure 8 is a graphical representation of the theoretical wavelength shift relationship of Eq. (15). It shows the variation of the theoretical wavelength

160　shift versus the number of bacteria that bind to the surface of a 200 μm-diameter silica microdisk with a $Q = 10^4$, found from Eq. (4) and (15). As can be observed in Fig. 8, the spectral shift varies linearly with the number of bacteria that attach to the surface of a microdisk. Accordingly, an extrapolation shows that the binding of a single bacterium is expected to cause a shift of 7 pm. Since

165　the shift caused by the attachment of a single bacterium is relatively small, it becomes crucial to have a stabilized optical characterization setup to avoid the effects of laser instabilities or temperature changes on the spectral shift. The thermal spectral shift for a cavity resonance wavelength of 635 nm is equal to 3.81pm/°C. A method to control the temperature could be to use a Peltier heat

170　pump device and thermistor that could control the temperature to 0.01 °C [19]. Another method could be the use of thermal-stabilized reference interferometer with a high-Q optical microcavity[20]. This could enhance the signal to noise ratio and allow to have a highly sensitive biosensor. The use of appropriate microfluidic channels could also ensure that the bacterium binds to the edge of

175　the microdisk that contains most of the mode energy so it could be accurately detected.

4. Conclusion

　　In this work, we have developed an equation to estimate the number of bacteria that bind to a 200 μm-diameter silica microdisk from the wavelength

180　shift observed experimentally. This expression has allowed us to find a limit of detection for Staphylococcus aureus of 5 pg/ml for a microdisk with $Q = 10^4$, correponding to 20 cells [9]. The theoretical expression of the wavelength shift developed in this work can be applied more generally to find the spectral shift

that results from the binding of any biological particle on the surface of an optical microdisk. It is important however to use the appropriate parameters corresponding to these particles while calculating their excess polarizability in order to obtain an accurate result. It is believed that using microdisks with higher quality factors combined with an adequate and stabilized optical characterization setup so that environmental changes don't affect the biosensing process, would allow real-time single bacterium detection using optical microdisks.

5. Acknowledgments

References

[1] K. J. Vahala, Optical microcavities, Nature 424 (6950) (2003) 839–846.

[2] N. Massad-Ivanir, G. Shtenberg, A. Tzur, M. A. Krepker, E. Segal, Engineering nanostructured porous sio2 surfaces for bacteria detection via direct cell capture, Analytical chemistry 83 (9) (2011) 3282–3289.

[3] X. Lopez-Yglesias, J. M. Gamba, R. C. Flagan, The physics of extreme sensitivity in whispering gallery mode optical biosensors, Journal of Applied Physics 111 (8) (2012) 084701–084701.

[4] M. R. Foreman, J. D. Swaim, F. Vollmer, Whispering gallery mode sensors, Advances in Optics and Photonics 7 (2) (2015) 168–240.

[5] D. Ivnitski, I. Abdel-Hamid, P. Atanasov, E. Wilkins, Biosensors for detection of pathogenic bacteria, Biosensors and Bioelectronics 14 (7) (1999) 599–624.

[6] J.-C. Cheng, C.-L. Huang, C.-C. Lin, C.-C. Chen, Y.-C. Chang, S.-S. Chang, C.-P. Tseng, Rapid detection and identification of clinically important bacteria by high-resolution melting analysis after broad-range ribosomal rna real-time pcr, Clinical chemistry 52 (11) (2006) 1997–2004.

[7] S. Van Hal, D. Stark, B. Lockwood, D. Marriott, J. Harkness, Methicillin-resistant staphylococcus aureus (mrsa) detection: comparison of two molecular methods (idi-mrsa pcr assay and genotype mrsa direct pcr assay) with three selective mrsa agars (mrsa id, mrsaselect, and chromagar mrsa) for use with infection-control swabs, Journal of clinical microbiology 45 (8) (2007) 2486–2490.

[8] Y.-C. Chang, C.-Y. Yang, R.-L. Sun, Y.-F. Cheng, W.-C. Kao, P.-C. Yang, Rapid single cell detection of staphylococcus aureus by aptamer-conjugated gold nanoparticles, Scientific reports 3.

[9] H. Ghali, H. Chibli, J. L. Nadeau, P. Bianucci, Y.-A. Peter, Real-time detection of staphylococcus aureus using whispering gallery mode optical microdisks, Biosensors 6 (2) (2016) 20.

[10] S. Bergeron, F. Vanier, Y.-A. Peter, Silica microdisk coupled resonator optical waveguide, in: Optical MEMS and Nanophotonics, 2009 IEEE/LEOS International Conference on, IEEE, 2009, pp. 73–74.

[11] H. Chibli, H. Ghali, S. Park, Y.-A. Peter, J. L. Nadeau, Immobilized phage proteins for specific detection of staphylococci, Analyst 139 (1) (2014) 179–186.

[12] S. C. Becker, J. Foster-Frey, D. M. Donovan, The phage k lytic enzyme lysk and lysostaphin act synergistically to kill mrsa, FEMS microbiology letters 287 (2) (2008) 185–191.

[13] F. Vollmer, D. Braun, A. Libchaber, M. Khoshsima, I. Teraoka, S. Arnold, Protein detection by optical shift of a resonant microcavity, Applied Physics Letters 80 (21) (2002) 4057–4059.

[14] S. Arnold, S. Shopova, S. Holler, Whispering gallery mode bio-sensor for label-free detection of single molecules: thermo-optic vs. reactive mechanism, Optics Express 18 (1) (2010) 281–287.

[15] F. Vollmer, S. Arnold, D. Keng, Single virus detection from the reactive shift of a whispering-gallery mode, Proceedings of the National Academy of Sciences 105 (52) (2008) 20701–20704.

[16] S. Arnold, M. Khoshsima, I. Teraoka, S. Holler, F. Vollmer, Shift of whispering-gallery modes in microspheres by protein adsorption, Optics letters 28 (4) (2003) 272–274.

[17] T. Tumolo, L. Angnes, M. S. Baptista, Determination of the refractive index increment (dn/dc) of molecule and macromolecule solutions by surface plasmon resonance, Analytical biochemistry 333 (2) (2004) 273–279.

[18] M. Borselli, T. Johnson, O. Painter, Beyond the rayleigh scattering limit in high-q silicon microdisks: theory and experiment, Optics Express 13 (5) (2005) 1515–1530.

[19] C. A. Barrios, K. B. Gylfason, B. Sánchez, A. Griol, H. Sohlström, M. Holgado, R. Casquel, Slot-waveguide biochemical sensor, Optics letters 32 (21) (2007) 3080–3082.

[20] T. Lu, H. Lee, T. Chen, S. Herchak, J.-H. Kim, S. E. Fraser, R. C. Flagan, K. Vahala, High sensitivity nanoparticle detection using optical microcavities, Proceedings of the National Academy of Sciences 108 (15) (2011) 5976–5979.
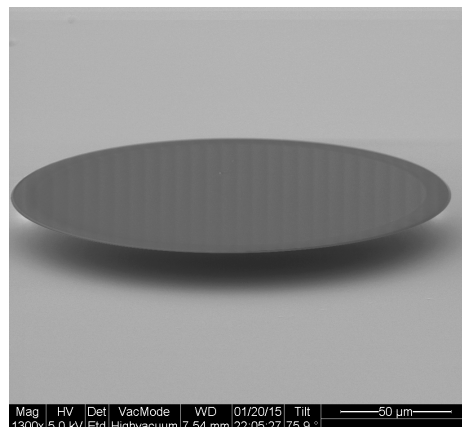
Figure 1: Scanning electron micrograph of an optical microdisk.
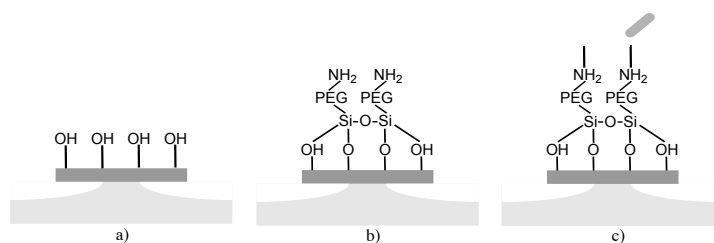
Figure 2: Functionalization of silica microdisks. (a) The silicon dioxide surface is hydroxylated with oxygen plasma. (b) The disk is immersed in triethoxysilane-PEG-NH$_2$. (c) The free amines of the PEG-silane are covalently coupled to LysK using carbodiimide coupling.
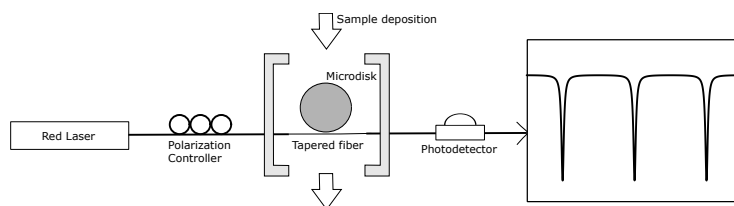
Figure 3: Optical characterization setup. The light from a tunable laser at 630 nm propagates through a polarization controller and is coupled inside the microdisk using a tapered fiber. The signal conveyed from the photodetector to the oscilloscope yields the transmission spectrum. Resonant modes are observed as a series of dips.
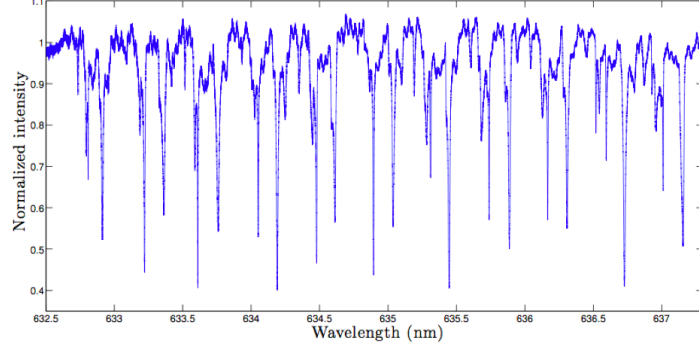
Figure 4: Transmission spectrum of a 200μm-diameter silica microdisk coupled to a 1.2 μm waist diameter tapered optical fiber.
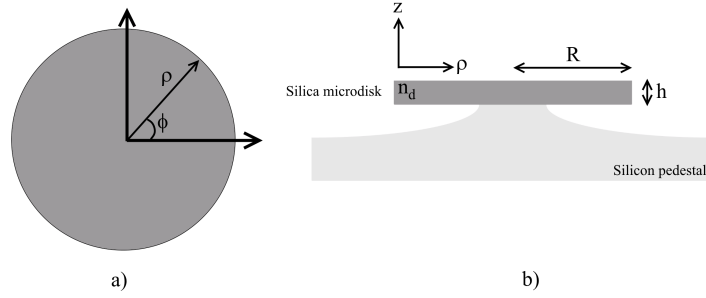
Figure 5: Schematic representation of a fabricated microdisk a) Top view and b) vertical cut view

Table 1: Parameters of the wavelength shift equation for a microdisk

| Parameter	Definition	Value
α_{ex}	Excess polarizability	$4\pi\epsilon_0$ x $2.12\text{x}10^{-20}$ (m^3)
σ_s	Surface coverage	$\frac{N}{3.78\text{x}10^{-9}}$ (m^{-2})
ϵ_0	Vacuum permittivity	$8.854\text{x}10^{-12}$ F/m
ϵ_{rs}	Relative permittivity of silica	3.9
k$_0$	Wavenumber $\left(\frac{2\pi}{\lambda}\right)$	$9.895\text{x}10^{6}$ m^{-1}
n$_d$	Microdisk refractive index	1.457
n$_m$	TBS refractive index	1.332
h	Microdisk thickness	800 nm
R	Microdisk radius	100 μm
m$_{bact}$	Mass of one bacterium	10^{-12} g
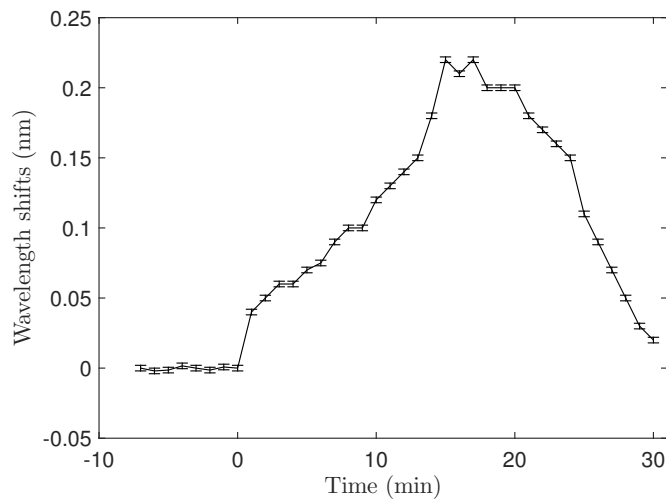
Figure 6: Wavelength shift in time after S. aureus binding to the resonator. A buffer solution is added to the surface of the microdisk using a micropipette. At time T = 0, the same buffer containing S. aureus bacteria is added. Error bars are due to uncertainties in the values resulting from laser drift and error in calculating the shift from the transmission spectra (±2pm).
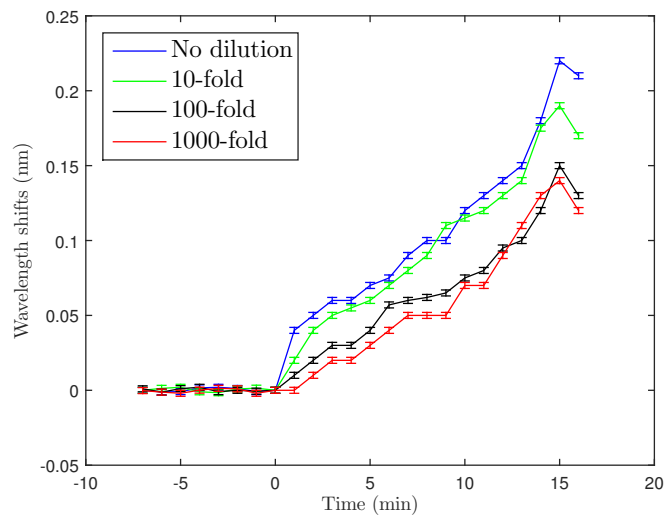
Figure 7: Wavelength shifts after *S. aureus* binding for four different concentrations. A buffer solution is added to the surface of the microdisks using a micropipette. At time T = 0, the same buffer containing four different concentrations of S. aureus bacteria is added to the microdisks. Error bars are due to uncertainties in the values resulting from laser drift and error in calculating the shift from the transmission spectra (±2pm).

Table 2: Number of bacteria binding to the resonator for four different concentrations

Bacterial Solution Concentration (CFU/mL)	Wavelength Shift ($\delta\lambda$ in nm)	Bacteria Bound to the Surface
5×10^9	0.22	31
5×10^8	0.19	27
5×10^7	0.15	21
5×10^6	0.14	20
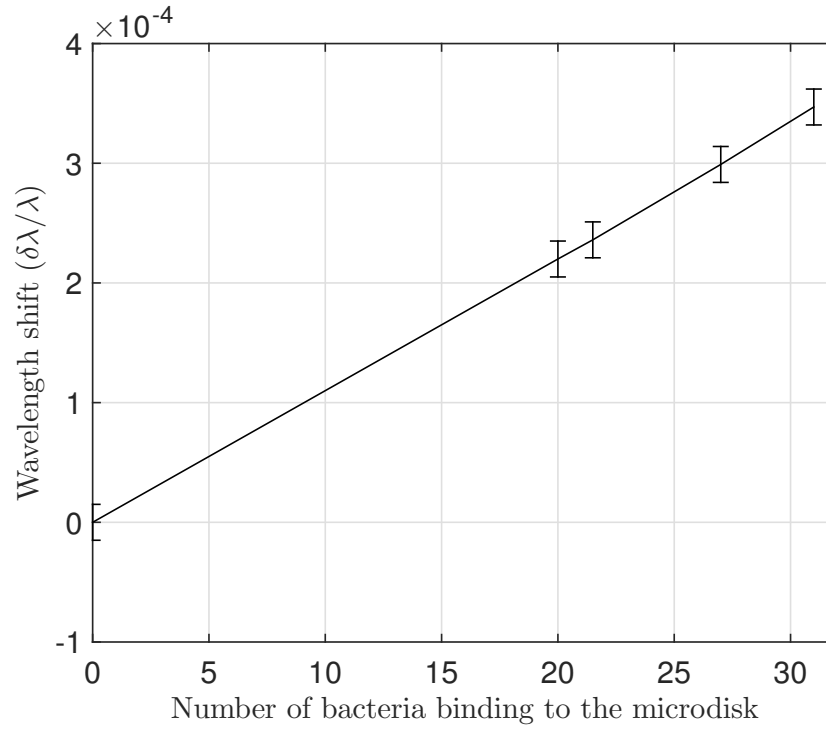
Figure 8: A graphical representation of the theoretical wavelength shift relationship of Eq. (15) in terms of number of bacteria contributing to the shift. The graph shows the variation of the wavelength shift versus the number of bacteria that bind to the surface of a 200 μm-diameter silica microdisk with a Q = 10^4, found from Eq. (4) and (15).

APPENDIX B   ARTICLE 2 : Real-Time Detection of *Staphylococcus Aureus* Using Whispering Gallery Mode Optical Microdisks

Real-Time Detection of *Staphylococcus Aureus* Using Whispering Gallery Mode Optical Microdisks

biosensors

MDPI

Real-Time Detection of *Staphylococcus Aureus* Using Whispering Gallery Mode Optical Microdisks

Hala Ghali [1],*, Hicham Chibli [2], Jay L. Nadeau [2], Pablo Bianucci [3] and Yves-Alain Peter [1]

[1] Department of Engineering Physics, Polytechnique Montreal, Montreal, QC, H3T 1J4, Canada; yves-alain.peter@polymtl.ca

[2] Department of Biomedical Engineering, McGill University, Montreal, QC, H3A 2B4, Canada; hicham.chibli@mcgill.ca (H.C.); jay.nadeau@mcgill.ca (J.L.N.)

[3] Physics Department, Concordia University, Montreal, QC, H4B 1R6, Canada; pablo.bianucci@concordia.ca

* Correspondence: hala.ghali@polymtl.ca; Tel.: +1-514-340-4711

Abstract: Whispering Gallery Mode (WGM) microresonators have recently been studied as a means to achieve real-time label-free detection of biological targets such as virus particles, specific DNA sequences, or proteins. Due to their high quality (Q) factors, WGM resonators can be highly sensitive. A biosensor also needs to be selective, requiring proper functionalization of its surface with the appropriate ligand that will attach the biomolecule of interest. In this paper, WGM microdisks are used as biosensors for detection of *Staphylococcus aureus*. The microdisks are functionalized with LysK, a phage protein specific for staphylococci at the genus level. A binding event on the surface shifts the resonance peak of the microdisk resonator towards longer wavelengths. This reactive shift can be used to estimate the surface density of bacteria that bind to the surface of the resonator. The limit of detection of a microdisk with a Q-factor around 10^4 is on the order of 5 pg/mL, corresponding to 20 cells. No binding of *Escherichia coli* to the resonators is seen, supporting the specificity of the functionalization scheme.

---

1. Introduction

Viruses and bacteria are a major cause of human disease [1]. *Staphylococcus aureus* causes serious skin and respiratory infections and food poisoning. Overuse of antibiotics has given rise to antibiotic-resistant strains such as methicillin-resistant *Staphylococcus aureus* (MRSA), which is responsible for over 60% of staphylococcal infections in hospitals [2,3]. It is crucial to find new approaches to fast diagnosis and early detection of staphylococcal infections. Real-time PCR is the fastest (about 2 h) [4] and most widespread (FDA) (United States Food and Drug Administration)-approved test for MRSA. However, this technique can be very expensive and is impractical for use on-site or in developing countries.

Other biosensing techniques such as fluorescent immunoassays require labeling of the target molecule, adding an extra step to the functionalization process. Although these methods can be very specific, especially in complex environments such as blood, they require a prior knowledge of the target molecule [5].

Therefore, it is useful to develop label-free sensors to detect the bacterium itself, rather than a fluorescent label. Whispering gallery mode microresonators have been recently studied for this purpose, considering their high quality factors that yield high sensitivity, as well as their selectivity, fast response, low cost and reproductibility [6–9]. In order to obtain good selectivity, the biosensor needs to be properly functionalized with a ligand that is specific to the biomolecule to be detected.

This ligand may be an antibody, aptamer, complementary sequence, or other molecule that binds specifically to the target of interest while ideally protecting the resonator from non-specific binding.

Non-specific bacterial detection has been demonstrated in previous studies [10,11]. However, non-specific biosensors are not suited for clinical uses in complex environments such as blood or serum. In this study, we demonstrate real-time specific detection of *Staphylococcus aureus* using whispering gallery mode microdisks. Specific functionalization was achieved using LysK phage protein. LysK is an endolysin from the staphylococcal phage K that binds strongly to staphylococci. It contains three domains: an *N*-terminal cysteine, a histidine-dependent amidohydrolase/peptidase (CHAP) domain, a midprotein amidase-2 domain, and a *C*-terminal SH3b cell wall-binding domain [12]. It has previously been studied as a potential antimicrobial [13] and a biosensor [14]. The LysK-functionalized microdisks showed a concentration-dependent wavelength shift in the presence of *S. aureus*. No shift was seen with a control strain (*E. coli*), indicating specificity at least at the genus level.

2. Materials and Methods

2.1. Microdisk Fabrication

Optical microdisks were fabricated using silicon micromachining techniques [15]. The substrates used were silicon topped with an 800 nm thermal silicon dioxide layer. The first step performed was UV photolithography to generate photoresist patterns of 200 μm-diameter microdisks with AZ5214 photoresist. Patterns were then transferred to silica using buffered oxide etch (B.O.E.) of silicon dioxide. The last step was isotropic dry etching of silicon with SF_6 gas to obtain microdisks on pedestals. Microdisks were characterized by scanning electron microscopy (Hitachi S-4700, Tokyo, Japan).

2.2. Plasmids and LysK Purification

Phage proteins expressed in the pET21 plasmid vector were kindly provided by David M. Donovan. The plasmid constructs [16,17] and LysK purification procedure were previously described [14]. In summary, 0.5 mg of plasmid DNA was transformed into *E. coli* BL21 (DE3) and grown overnight in modified lysogeny broth (LB) (15 g tryptone, 8 g yeast extract, 5 g NaCl per liter, pH 7.8). Colonies were picked and grown in modified LB until they reached an optical density at 600 nm (OD_{600}) of 0.4–0.5. Then, protein expression was induced with 1 mM IPTG (Isopropyl *β*-D-1-thiogalactopyranoside) at 10 °C for 20 h. The bacteria were pelleted by centrifugation (5000 rpm, 4 °C) and the pellet was resuspended in lysis buffer (50 mM NaH_2PO_4, 300 mM NaCl, 10 mM imidazole, pH 8.0 and 30% glycerol) and sonicated to lyse the cells. His-tagged proteins were purified through nickel chromatography using Ni-NTA (NitriloTriacetic Acid) Superflow (Qiagen, Hilden, Germany). Supernatant was incubated with Ni-NTA matrix at 4 °C for 1 h. Then, the column was washed once with lysis buffer and twice with wash buffer (50 mM NaH_2PO_4, 300 mM NaCl, 20 mM imidazole, pH 8.0 + 30% glycerol). Protein was eluted with elution buffer (50 mM NaH_2PO_4, 300 mM NaCl, 250 mM imidazole, pH 8.0 + 30% glycerol). The purified protein was analyzed at 10% SDS-PAGE (Sodium Dodecyl Sulfate-PolyAcrylamide Gel Electrophoresis) and visualized with Coomassie blue staining. Lytic activity of the proteins against bacterial strains was tested with a zymogram assay as follows: the mid-log growth phase cell pellet from 75 mL of bacterial culture was mixed with SDS-PAGE resolving gel. The gel was run as usual (1 h), then rinsed with dH_2O and incubated in Tris-Buffered Saline (TBS) (10 mM Tris, 150 mM NaCl, pH 7.5) for up to 24 h until clearing in the turbid gel appeared, indicating lytic activity.

2.3. Surface Functionalization

The samples were cleaned using oxygen plasma or piranha etch to remove organic residues. The wafers were then immersed in an ethanol:water (95:5) solution containing 2.5% triethoxysilane-Polyethylene Glycol (PEG)-Amine (NH_2) (Nanocs, MW = 3400) for 2 h. Samples were then thoroughly

washed with ethanol and deionized water and then annealed at 110 °C for 2 h. The PEGylated wafers were then immersed in a 2 μM LysK:2000 μM EDC (1-Ethyl-3-(3-dimethylaminopropyl)carbodiimide) (1:1000) solution in buffer (10 mM Tris.HCl pH 7.5, 150 mM NaCl, 1% glycerol) at 4 °C overnight, and then thoroughly washed with PBS and water.

2.4. Optical Characterization Setup

The light from an external cavity tunable diode laser (New focus TLB-6300-LN, Newport, VA, USA) emitting at 630 nm was evanescently coupled inside the microdisk through a tapered optical fiber. Tapered fibers were fabricated by gently stretching a single mode fiber while it was heated over a flame until the tapered region reached a 2 μm diameter. A red laser was used to limit the absorption losses in aqueous media. A function generator (Agilent 33220A) fed a trigger signal to the piezo input of the laser. The signal was set to pulse with a 10 ms width, 3.5 V amplitude and 1.75 V offset. A photodetector (Newport 818-SL/CM, Newport, VA, USA) conveyed the output signal to an oscilloscope (Agilent DSO6302A) where the transmission spectrum of the resonator was observed as the laser wavelength was scanned.

2.5. Bacterial Strains and Maintenance

S. aureus strain ATCC (American Type Culture Collection) 29213 and *E. coli* strain 10798 were purchased from ATCC. *S. aureus* and *E. coli* were maintained by serial passages in LB media. For binding studies, cells were pelleted and resuspended in Tris-buffered saline (TBS) (10 mM Tris-HCl, 150 mM NaCl, pH 7.5).

3. Results and Discussion

3.1. Fabrication and Characterization

An SEM image of a typical microfabricated WGM optical microdisk is shown in Figure 1. Functionalization was confirmed by ellipsometry and X-Ray Photoelectron Spectroscopy (XPS). Measurements were taken on the same silica wafers used to fabricate the microdisks and the results are detailed in [14]. The functionalized microdisks were coated with polyethylene glycol (PEG) to block any non-specific binding of bacteria to the surface of the resonator. Microdisks with 2 μM of LysK incubated in a solution of 10^7 CFU/mL are expected to have around 60 ± 5 recognition elements per 3.3×10^3 μm^2 region [14]. A schematic of the functionalization scheme is shown in Figure 2.
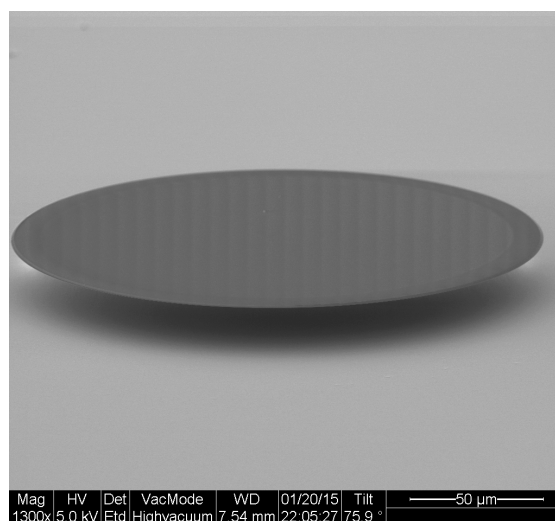

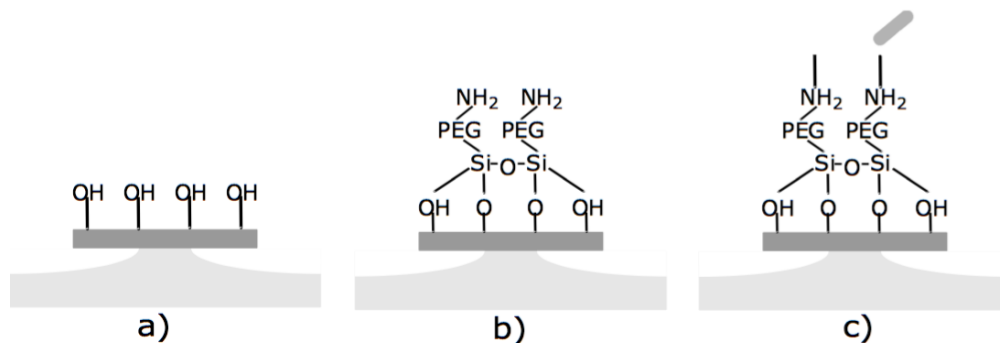**Figure 1.** Scanning electron micrograph of an optical microdisk.

Figure 2. Functionalization of silica microdisks. (**a**) the silicon dioxide surface is hydroxylated with oxygen plasma; (**b**) the disk is immersed in triethoxysilane-PEG-NH$_2$; (**c**) the free amines of the PEG-silane are covalently coupled to LysK using carbodiimide coupling.

3.2. Bacterial Binding

Binding experiments were performed on a functionalized 200 μm-diameter microdisk coupled to a tapered optical fiber, and the wavelength was scanned from 635.2 to 637.5 nm as shown in Figure 3. When the signal was stable, 2 μL of TBS was added to the surface of the disk using a micropipette and the transmission spectrum was observed on an oscilloscope. Addition of TBS did not lead to any wavelength shift. Keeping the same coupling position, another 2 μL of TBS containing *S. aureus* at OD$_{600}$ = 0.4 (approximately 5 × 10^9 CFU/mL) was added. The wavelength shift of a selected mode was observed over 30 min.
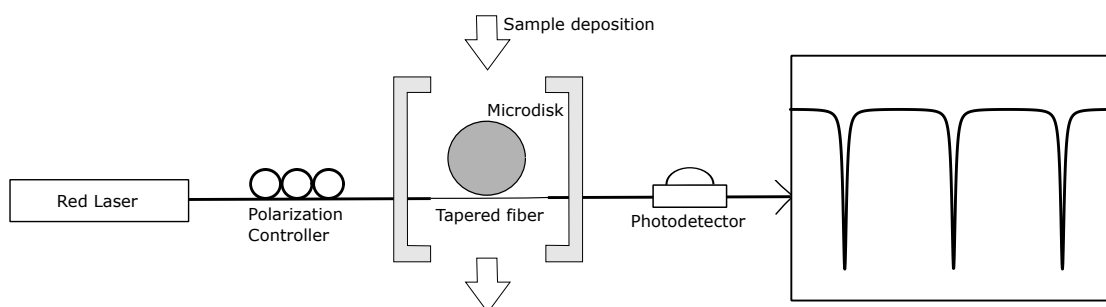
Figure 3. Optical characterization setup. The light from a tunable laser at 630 nm propagates through a polarization controller and is coupled inside the microdisk using a tapered fiber. The signal conveyed from the photodetector to the oscilloscope yields the transmission spectrum. Resonant modes are observed as a series of dips.

The wavelength began to shift almost immediately after adding the bacteria, indicating rapid binding of the bacteria to the surface. The maximum wavelength shift of 0.22 ± 0.002 nm was seen after approximately 15 min (Figure 4). Uncertainties in the values resulted from laser drift (±1 pm) and the error in calculating the wavelength shift from the transmission spectra (±1 pm) . After reaching its maximum, the wavelength shift began to decrease. This is most likely because the LysK protein has strong lytic activity [12,14], so that at 30 min, a majority of the bound cells were lysed.
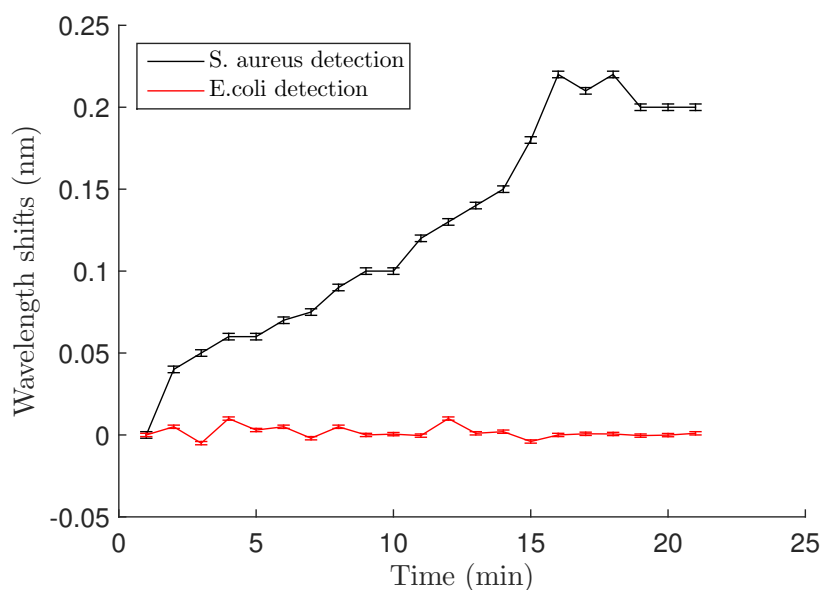
Figure 4. Wavelength shift *vs.* time after *S. aureus* and *E. coli* binding at a cell concentration of OD_{600} = 0.4 (5×10^9 CFU/mL). After 15 min, a maximum shift is obtained and is about 0.22 nm for the Staph., whereas no shift is observed for *E. coli* detection. Error bars are standard deviations as discussed in Section 3.2 of the text.

3.3. Specificity of LysK

Specificity of the PEG-LysK functionalization at the genus level was demonstrated using in a previous study fluorescent labeling [14]. Here, we confirmed this by using *E. coli* as a control with the microdisk system. *E. coli* at OD_{600} = 0.4 was applied to the resonator, and as can be seen in Figure 4, the transmission spectrum at time 0 and after 20 minutes did not change. No shifts were observed, suggesting that *E. coli* did not bind to the surface of the resonator.

When both *S. aureus* (OD_{600} = 0.4) and *E. coli* (OD_{600} = 0.4) were added to the surface of the resonator, a shift of 0.22 nm was observed, similar to the one obtained with the *S. aureus* alone. Thus, no *E. coli* attached to the resonator and only the presence of *S. aureus* contributed to the reactive shift.

3.4. Concentration-Dependent Shift

Concentration-dependence of the shift was examined by varying the concentration of the *S. aureus* solution used for biodetection. The OD_{600} = 0.4 solution was diluted 10, 100 and 1000 fold, and Figure 5 shows the maximum wavelength shifts for the four different concentrations (also summarized in Table 1). The 100- and 1000-fold dilutions showed almost the same wavelength shift, meaning that approximately the same number of bacteria attached to the resonator in both cases. Experiments with lower concentrations could not be carried out because of the limitations due to the relatively small quality factors of the microdisks ($Q \simeq 10^4$). Quality factors of the microdisks were measured after each functionalization step (addition of Si-PEG and LysK) and after biodetection. It is worth noting that the quality factor did not significantly change during the process and a value around 10,000 was found each time.
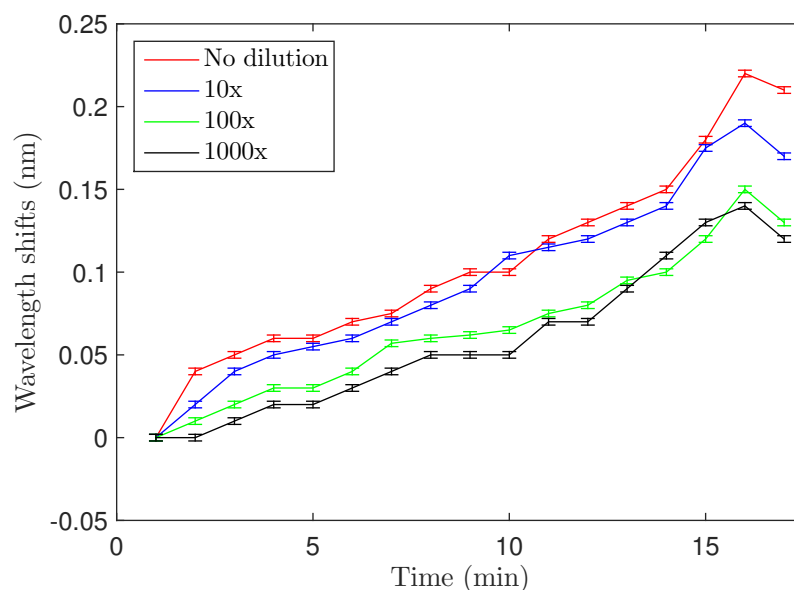
Figure 5. Wavelength shifts after *S. aureus* binding for four different concentrations. Error bars are standard deviations as discussed in Section 3.2 of the text.

Table 1. Resonance shifts in terms of bacterial concentration.

No Dilution	Diluted 10×	Diluted 100×	Diluted 1000×
0.22 ± 0.002 nm	0.19 ± 0.002 nm	0.15 ± 0.002 nm	0.14 ± 0.002 nm

3.5. Bacterial Surface Density

In the previous sections, an experimental wavelength shift was found for several bacterial concentrations. A theoretical expression that links the wavelength shift to the number of bacteria that bind to the surface of the microdisk was developed in [18] and shown in Equation (1). Using this expression, it was possible to obtain an approximate number of bacteria that bound to the surface of the microdisks and contributed to the reactive shift. For example, for the solution with OD = 0.4, the shift was 0.22 nm. With a resonance wavelength of 635 nm, the surface density can be estimated to be around 8.21×10^9 m^{-2}:

$$\frac{\delta\lambda}{\lambda} \simeq \frac{\alpha_{ex}\sigma_s}{2\epsilon_0\epsilon_{rs}} \left\{ \frac{\left(4k_0\left(\sqrt{n_d^2 - n_m^2}\right)\right)\cos^2\left(k_0\left(\sqrt{n_d^2 - n_m^2}\right)\frac{h}{2}\right)}{\left[2k_0\left(\sqrt{n_d^2 - n_m^2}\right)h + \sin\left(2k_0\left(\sqrt{n_d^2 - n_m^2}\right)h\right)\right]} + \frac{2[J_l^2\left(k_0 n_m R\right)]}{R\left[J_{l+1}^2(k_0 n_m R)\right]} \right\} \quad (1)$$

with α_{ex} being the excess polarizability of the molecules binding to the resonator's surface, σ_s the surface area covered by the molecules, ϵ_0 and ϵ_{rs} the vacuum and resonator's relative permittivity, respectively, k_0 the wave number, n_d and n_m the microdisk and the solvent refractive index, respectively, h the thickness of the microdisk, R its radius and $J_l(k_0 n_m R)$ the first kind Bessel function.

The parameters used to determine the spectral shift due to *S. aureus* binding to a 200 μm diameter silica microdisk submerged in TBS are defined in Table 2.

Table 2. Parameters of the wavelength shift equation for a microdisk.

Parameter	Definition	Value	Unit
α_{ex}	Excess polarizability	$4\pi\epsilon_0 \times 2.12 \times 10^{-20}$	m^3
σ_s	Surface coverage	$\frac{N}{1.257 \times 10^5}$ (µ)	m^{-2}
ϵ_0	Vacuum permittivity	8.854×10^{-12}	F/m
ϵ_{rs}	Relative permittivity of silica	3.9	
k_0	Wavenumber ($\frac{2\pi}{\lambda}$)	9.895×10^{-3}	nm^{-1}
n_d	Refractive index of the microdisk	1.457	-
n_m	Refractive index of the buffer	1.332	-
h	Thickness of the microdisk	800	nm
R	Radius of the microdisk	100 µ	m
m	Mass of one bacterium	10^{-12}	g
l	Mode number ($\frac{2\pi R n_{eff}}{\lambda}$)	1442	-

The surface density can be written as:

$$\sigma_s = \frac{N}{\pi(R_{max}^2 - r_e^2) + 2\pi Rh} \qquad (2)$$

where N is the number of bacteria that attach to the surface, R_{max} the radius of the ring where the electric field is maximum, r_e the radius of the ring where the electric field decays to $1/e$ of its maximum value, R the radius of the microdisk and h its height. This suggested that 31 bacteria bound to the surface and contribute to the wavelength shift for the undiluted culture. The estimated surface coverage and the number of bacteria that bound to the surface of the microdisk for the four different concentrations used are given in Table 3.

Table 3. Surface coverage and number of bacteria binding to the resonator for four different concentrations.

Bacterial Solution Concentration (CFU/mL)	Wavelength Shift (nm)	Surface Coverage (m^{-2})	Bacteria Bound to the Surface
5×10^9	0.22	8.21×10^9	31
5×10^8	0.19	7.15×10^9	27
5×10^7	0.15	5.56×10^9	21
5×10^6	0.14	5.3×10^9	20

3.6. Variability in Binding

Measurements were done on eight different microdisks for each concentration, and results were mean values of the experiments done for each concentration. All microdisks used had the same size of 200 µm diameter and a quality factor of around 10^4 for the sake of comparison. In Table 4, the standard deviation (SD) of the wavelength shifts is given for the different concentrations. It can be seen that the SD increased with lower bacterial concentrations. Assuming that the microdisks used were functionalized identically, a saturation of all of the available binding sites by bacterial cells should lead to the same maximum value of the wavelength shift. This is what was seen for the highest bacterial concentration, where the wavelength shift was highly reproducible from experiment to experiment. For more dilute solutions, the bacteria will be depleted before all of the binding sites are saturated. Because some of the active protein sites will not be located on the sensitive part of the microdisk, there will be variability in the number of bound cells that contribute to the wavelength shift. Considering the four concentrations tested, the limit of detection of the biosensor for a Q-factor around 10^4 was 5×10^6 CFU/mL or 5 pg/mL.

Table 4. Standard deviation of the wavelength shift for four different bacterial concentrations.

Bacterial Solution Concentration (CFU/mL)	Wavelength Shift (nm)	Standard Deviation (nm)
5×10^9	0.22	0.01
5×10^8	0.19	0.02
5×10^7	0.15	0.04
5×10^6	0.14	0.05

4. Conclusions

In this work, we achieved real-time specific detection of *S. aureus* using whispering gallery mode microdisks functionalized with the staphylococcal-specific LysK endolysin. We showed that the resonance peak shifted towards longer wavelengths almost immediately after *S. aureus* addition, and the shift continued to increase for 15 minutes as the number of bacteria that bound to the surface of the resonator increased. Different concentrations of bacteria gave rise to different wavelength shifts, showing the dependence of the reactive shift on surface density. The limit of detection of a microdisk with a Q-factor of 10^4 was found to be 5 pg/mL. The selectivity of the functionalization process at the genus level was also demonstrated using *E. coli*, which did not lead to any significant change of the resonance. Specificity is a very important feature of a biosensor that makes it suitable for clinical and medical use in complex environments, and we have demonstrated an important step towards it. Further studies using very low concentrations of bacteria need to be performed in order to achieve single-bacterium detection and exploit the high sensitivity of WGM resonators. The lytic effect of the LysK may be exploited by downstream sensors which could identify the lysed cells at the species or strain level, and thereby differentiate antibiotic-resistant and -sensitive strains of *S. aureus* [19].

Author Contributions: H.G. performed the experiments and wrote the paper. H.C. and J.L.N. developed the surface functionalization process. P.B., J.L.N. and Y.-A.P. reviewed and edited the manuscript. All authors read and approved the manuscript.

Conflicts of Interest: The authors declare no conflict of interest.

References

1. Thapa, B. Antimicrobial resistance: A global threat. *Int. J. Infect. Microbiol.* **2013**, *1*, 41–42.
2. Wisplinghoff, H.; Bischoff, T.; Tallent, S.M.; Seifert, H.; Wenzel, R.P.; Edmond, M.B. Nosocomial bloodstream infections in US hospitals: Analysis of 24,179 cases from a prospective nationwide surveillance study. *Clin. Infect. Dis.* **2004**, *39*, 309–317.
3. Klevens, R.M.; Morrison, M.A.; Nadle, J.; Petit, S.; Gershman, K.; Ray, S.; Harrison, L.H.; Lynfield, R.; Dumyati, G.; Townes, J.M.; *et al.* Invasive methicillin-resistant Staphylococcus aureus infections in the United States. *J. Am. Med. Assoc.* **2007**, *298*, 1763–1771.
4. Van Hal, S.; Stark, D.; Lockwood, B.; Marriott, D.; Harkness, J. Methicillin-resistant Staphylococcus aureus (MRSA) detection: Comparison of two molecular methods (IDI-MRSA PCR assay and GenoType MRSA Direct PCR assay) with three selective MRSA agars (MRSA ID, MRSASelect, and CHROMagar MRSA) for use with infection-control swabs. *J. Clin. Microbiol.* **2007**, *45*, 2486–2490.
5. Luchansky, M.S.; Bailey, R.C. High-Q optical sensors for chemical and biological analysis. *Anal. Chem.* **2011**, *84*, 793–821.
6. Vahala, K.J. Optical microcavities. *Nature* **2003**, *424*, 839–846.
7. Massad-Ivanir, N.; Shtenberg, G.; Tzur, A.; Krepker, M.A.; Segal, E. Engineering nanostructured porous SiO_2 surfaces for bacteria detection via "direct cell capture". *Anal. Chem.* **2011**, *83*, 3282–3289.
8. Lopez-Yglesias, X.; Gamba, J.M.; Flagan, R.C. The physics of extreme sensitivity in whispering gallery mode optical biosensors. *J. Appl. Phys.* **2012**, *111*, doi:10.1063/1.3698319.

9. Foreman, M.R.; Swaim, J.D.; Vollmer, F. Whispering gallery mode sensors. *Adv. Opt. Photonics* **2015**, *7*, 168–240.

10. Arnold, S.; Keng, D.; Shopova, S.; Holler, S.; Zurawsky, W.; Vollmer, F. Whispering gallery mode carousel—A photonic mechanism for enhanced nanoparticle detection in biosensing. *Opt. Express* **2009**, *17*, 6230–6238.

11. Anderson, M.E.; O'Brien, E.C.; Grayek, E.N.; Hermansen, J.K.; Hunt, H.K. The Detection of Helicobacter hepaticus Using Whispering-Gallery Mode Microcavity Optical Sensors. *Biosensors* **2015**, *5*, 562–576.

12. Becker, S.C.; Foster-Frey, J.; Donovan, D.M. The phage K lytic enzyme LysK and lysostaphin act synergistically to kill MRSA. *FEMS Microbiol. Lett.* **2008**, *287*, 185–191.

13. Nelson, D.; Loomis, L.; Fischetti, V.A. Prevention and elimination of upper respiratory colonization of mice by group A streptococci by using a bacteriophage lytic enzyme. *Proc. Natl. Acad. Sci. USA* **2001**, *98*, 4107–4112.

14. Chibli, H.; Ghali, H.; Park, S.; Peter, Y.A.; Nadeau, J.L. Immobilized phage proteins for specific detection of staphylococci. *Analyst* **2014**, *139*, 179–186.

15. Bergeron, S.; Vanier, F.; Peter, Y.A. Silica Microdisk Coupled Resonator Optical Waveguide. In Proceedings of the 2009 IEEE/LEOS International Conference on Optical MEMS and Nanophotonics, Clearwater, FL, USA, 17–20 August 2009; pp. 73–74.

16. Becker, S.C.; Foster-Frey, J.; Stodola, A.J.; Anacker, D.; Donovan, D.M. Differentially conserved staphylococcal SH3b_5 cell wall binding domains confer increased staphylolytic and streptolytic activity to a streptococcal prophage endolysin domain. *Gene* **2009**, *443*, 32–41.

17. Donovan, D.M.; Lardeo, M.; Foster-Frey, J. Lysis of staphylococcal mastitis pathogens by bacteriophage phi11 endolysin. *FEMS Microbiol. Lett.* **2006**, *265*, 133–139.

18. Ghali, H.; Bianucci, P.; Peter, Y.A. Wavelength Shift in a Whispering Gallery Microdisk due to Bacterial Sensing: A Theoretical Approach. *J. Biomed. Optics* **2016**, submitted for publication.

19. Guntupalli, R.; Sorokulova, I.; Olsen, E.; Globa, L.; Pustovyy, O.; Vodyanoy, V. Biosensor for detection of antibiotic resistant Staphylococcus bacteria. *J. Vis. Exp.* **2013**, doi:10.3791/50474.

APPENDIX C   ARTICLE 3 : CONFERENCE PAPER : Bacterial Sensing Using Phage-Functionalized Whispering Gallery Microcavities

Bacterial Sensing Using Phage-Functionalized Whispering Gallery Microcavities

Hala Ghali, Pablo Bianucci, Hicham Chibli, Jay L. Nadeau, and Yves-Alain Peter, "Real-Time Detection of Staphylococcus Aureus Using Whispering Gallery Mode Optical Microdisks", *16th International Conference on Miniaturized Systems for Chemistry and Life Sciences in Okinawa, Japan*, pp.749-751, 2012.

BACTERIAL SENSING USING PHAGE-FUNCTIONALIZED WHISPERING GALLERY MICROCAVITIES

Hala Ghali[1], Pablo Bianucci[1], Hicham Chibli[2], Jay L. Nadeau[2], and Yves-Alain Peter[1]

[1]École Polytechnique de Montréal, Canada, [2]McGill University, Canada

ABSTRACT

In this work, we demonstrate the specificity of functionalized optical microcavities as bacteria sensors. We used endolysin LysK as a specific binding molecule to *Staphylococcus aureus (S. aureus)*. Wavelength resonance shifts are observed after each functionalization step and biodetection, confirming the label-free detection of bacteria on the surface of the microresonator. Further experiments conducted using *Escherichia coli* (*E. coli)* bacteria with the same endolysin validate the specificity of our biosensor.

KEYWORDS

Optical microdisk, label-free bacteria detection, resonance shifts, specificity

INTRODUCTION

Whispering gallery optical microcavities are structures which can efficiently confine light at the micro scale [1]. This confinement is based on total internal reflection of light at the interface between the cavity and the surrounding medium. Since the field evanescently extends into the medium, the optical properties of the microcavity are extremely sensitive to changes in its surroundings. In this work, we describe a biosensing application of these optical microcavities for the label-free detection of bacteria.

EXPERIMENT

Silica microdisks were fabricated using conventional microfabrication techniques [2]. The initial substrate was a silicon wafer with an 800 nm layer of thermal silicon dioxide. First we used UV photolithography to define the pattern of disks on the wafer, which is then transferred to the oxide using hydrofluoric acid. This is followed by an isotropic reactive ion etching of the silicon to form a silica disk on a pedestal. A scanning electron micrograph of a microfabricated optical microcavity is shown on Fig.1.
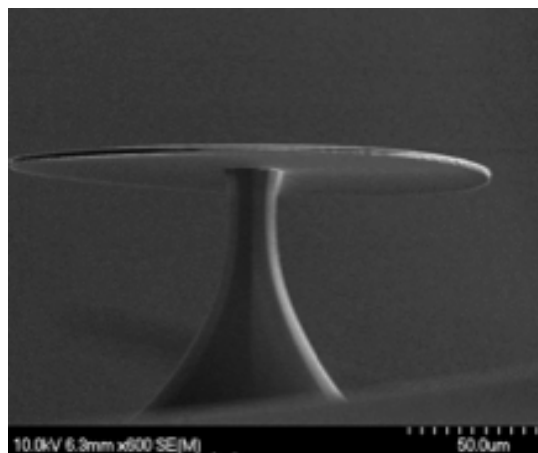

Figure 1: Scanning electron micrograph of an optical microcavity

An as-fabricated microcavity sensor will show a change in its optical response under any alteration of its environment. In order for the sensor to be specific to a particular species of bacteria, we need to properly functionalize its surface so that only that kind of bacteria will result in detectable changes. In our work, we are interested to detect the presence of *Staphylococcus aureus* (*S. aureus*). The microcavity surface was first functionalized using PEGylated aminosilane (PEG-Si). We then introduced phage-derived proteins (the *endolysin LysK*) specific to *S. aureus*. The binding between the bacteria and the phage proteins creates a perturbation in the electromagnetic environment of the microresonator which is observed as a shift in the resonance wavelengths present in the transmission spectrum [3].

We used a tapered optical fiber to couple the light from a tunable red laser (635 nm) into the resonator, and measured the transmission spectra. Resonances appear as dips in the transmission. The microdisk was functionalized using PEG-Si and LysK protein. S. aureus cells were then introduced. Figure 2 represents a resonant mode of this microresonator (shown on Fig. 3 (c)) after microfabrication and each functionalization step, up to biodetection. It can be seen that the mode wavelength (i.e. the wavelength at the center of the dip) changes after each step. The as-fabricated microcavity shows a resonant mode at 635.4 nm. After adding the PEG-Si, the mode shifts to 636.3 nm. We would expect a shift towards longer wavelength after each functionalization step, but the microdisk covered with PEG-Si and LysK protein resonates at 635.1 nm. This blue shift is most likely due to the difficulty of coupling to the same resonant mode when using off-line functionalization (where the microdisk is removed from the setup for each step of the process). When the bacteria attach to the surface of the microdisk, the resonant mode is observed at 637 nm. It should be noted that the quality factor did not undergo a drastic change. It decreased from 2.54×10^4 for a clean microdisk, to 1.59×10^4 after biodetection.
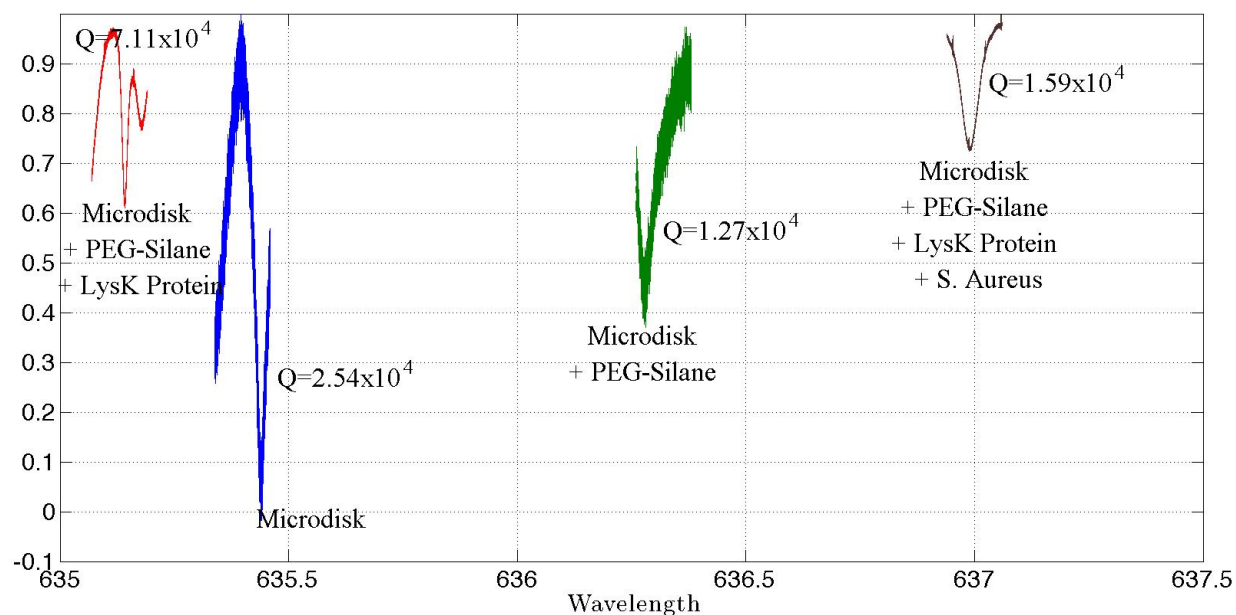

Figure 2: Resonances of the microcavity after each functionalization step and biodetection

To prove the specificity of our microresonator, we tested its surface functionalization. In the absence of PEG-Si and LysK protein, *S. aureus* did not attach on the surface of the microresonator as can be seen on Fig. 3 (a). In microdisks treated only with LysK (Fig. 3 (b)), *S. aureus* cells attached randomly on the surface. When the full treatment with PEG-Si and LysK was performed on the microdisk, a lower density of *S. aureus* attachment was noted, as can be seen on Fig. 3 (c), with a somewhat larger density of attachment on the resonator. Finally, Fig. 3 (d) shows a microdisk treated with PEG-Si, LysK protein and *E. coli* bacteria where no bacteria attached, demonstrating the specificity of the functionalization.

In conclusion, we proved that, with the proper functionalization, we obtained a specific microresonator able to capture *S. aureus* cells on its surface. Optical characterization using a tapered optical fiber showed the response of the sensor after biodetection. We observed a shift of the resonant mode after each functionalization step and biodetection due to a perturbation of the electromagnetic environment. Work is in progress to achieve on-line functionalization and real-time detection of bacteria in order to couple the same resonant mode into the biosensor.
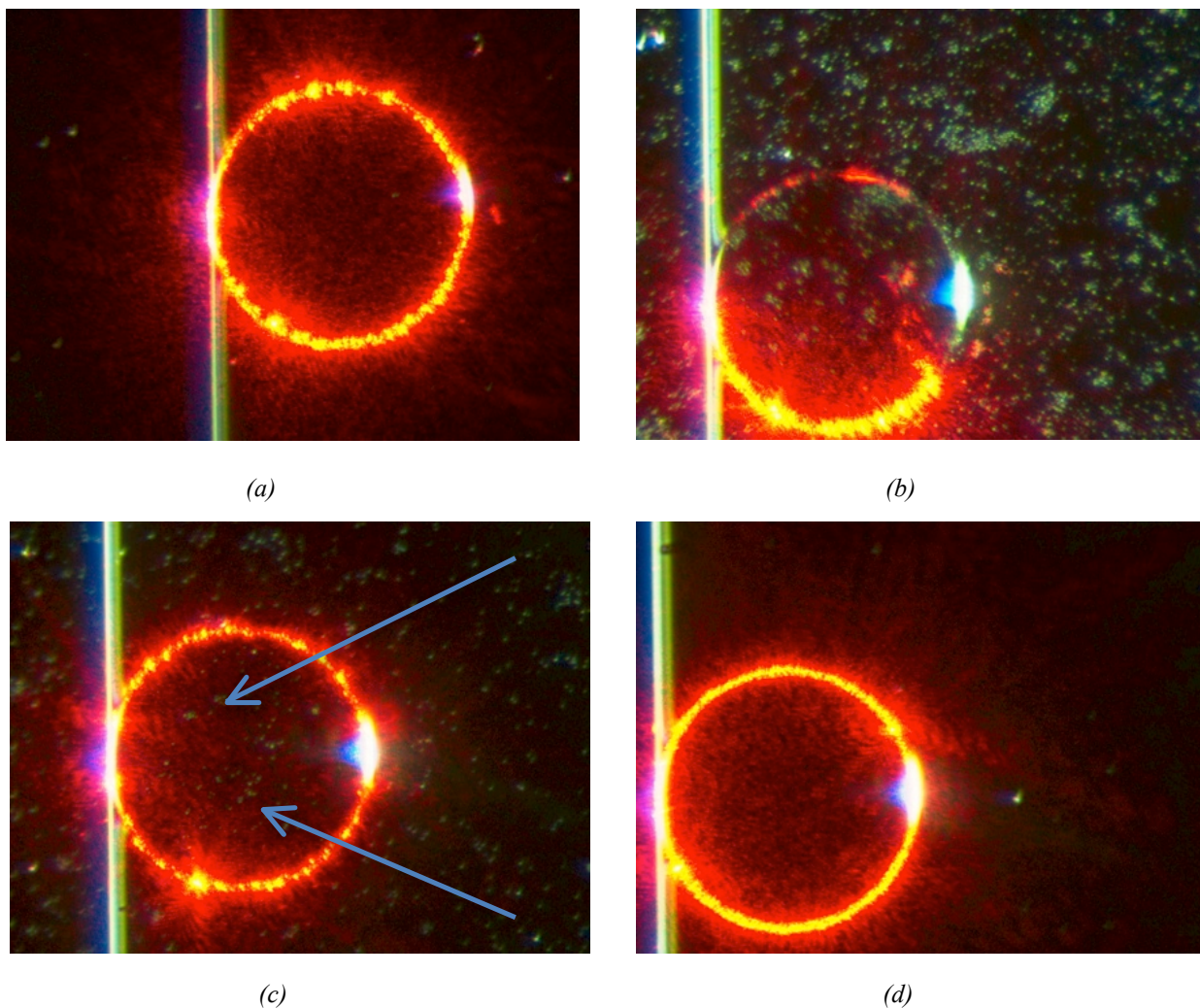
Figure 3 : Microdisk with (a) S. aureus (b) LysK protein and S. aureus (c) PEG-Si, LysK and S. aureus (d) PEG-Si, LysK protein and E. coli

REFERENCES

[1] F. Vollmer and S. Arnold, *Whispering-gallery-mode biosensing: label-free detection down to single molecules*, Nature Methods, **5**, 591 (2008).

[2] S. Bergeron, S. Saïdi, and Y.-A. Peter, *Periodic and non-periodic frequency selection in an erbium doped fiber laser by silica microdisk optical cavity filters*, Optics Express, **18**, 16797 (2010).

[3] S. Arnold, S.I. Shopova, and S. Holler, *Whispering Gallery Mode Bio-sensor for label-free detection of single molecules: thermo-optic vs. reactive mechanism*, Optics Express, **18**, 281-287 (2010).

CONTACT
Hala Ghali   hala.ghali@polymtl.ca

APPENDIX D   PROTEIN INDUCTION AND PURIFICATION PROCESS

The following details the protein expression and purification process that allows obtaining LysK protein phage used in the experiments described in the thesis. This procedure was developed by professor Jay L. Nadeau's group of the biomedical engineering department of McGill University, and adapted to the needs of the project by Soohyang Park and Hicham Chibli.

The first step of the process is the protein induction, followed by its purification. At the end of the appendix, the details of some useful processes are also detailed.

Protein Induction

Everything in this procedure has to be sterile except for IPTG and Ampicillin antibiotic that are made in sterile water. IPTG, Isopropyl β-D-1-thiogalactopyranoside, is a molecular biology reagent, an effective inducer of protein expression.

1. Appropriate DNA plasmid is transformed into BL21(DE3) *E. coli* competent cells and plated on Lysogeny Broth (LB) + 100 μg/ml Ampicillin agar. It is then incubated overnight at 37°C.

2. 5 to 50 colonies are picked from the agar plate the next morning [1], and a starter culture is grown in "modified LB" (15g Tryptone, 8g Yeast Extract, 5g NaCl per litre, pH 7.8) + 150 μg/ml Ampicillin with shaking at 37 °C.

   (a) The starter culture is usually grown in 5 ml mLB+amp in a tube for 1 hour then in 50 ml mLB+Amp in the same 2 L (for 1 hour) flask. The entire 1L culture will be eventually grown.

3. When starter culture shows turbidity (about 2 hours later), 1 L modified LB + Amp is added to the same 2L flask and is incubated at 37 °C with shaking. 1 ml of sterile mLB + Amp is saved to use as a blank for spectrophotometer.

4. The optical density at $\lambda = 600$ nm (OD_{600}) of culture is monitored, and when it reaches 0.4 to 0.5 value, the flask is moved to an ice bath and is incubated on ice for 20-30 minutes.

5. Fresh IPTG is added to a final concentration of 1 mM (1 ml of 1M IPTG per 1L of culture) and the culture is incubated with shaking at 10 °C for 20 hours.

---

1. The plates cannot be stored at 4°C and then colonies picked later as regular transformation. The day after the transformation, the colonies have to be picked and start growing.

6. The last step of protein induction is to pellet cells. First, the culture is spun down at 6000 rpm for 15 minutes at 4 °C. If more than a litre is being spun down, then the supernatant from first spin is poured off and then more is added to the same bottle and spun down again. The supernatant is poured off again and stored at -80 °C until ready to purify protein. The 1L is usually split into 8 x 50 ml tube, depending on the size of the pellet, and is spun down again for 15 minutes at full speed on tabletop centrifuge.

Protein Purification

1. Frozen cell pellets are thawed on benchtop and resuspended in 10 ml Lysis buffer (50 mM NaH$_2$$PO_4$, 300 mM NaCl, 10 mM imidazole, pH 8.0) + 30% glycerol.

2. Resuspended cells are sonicated in ice bath for 5 to 8 minutes.

3. Sonicated cells are centrifuged at $\geq$ 9000 x g for 30 minutes at T= 4°C. Supernatant is then moved to a new 15 ml tube.

4. 1 ml of Ni-NTA Superflow is added to 15 ml tube and rotated at 4°C for one hour.

5. 1 ml of polypropylene column (Qiagen cat. # 34924) is prepared before adding lysate. To do this, the bottom and top cap from column are removed and 6 ml of Lysis buffer is added. Lysis buffer is pulled from bottom outlet with a 10 ml syringe to begin flow. 6 ml of Lysis buffer is then added from syringe back onto column to check flow rate (it should be very fast). If flow rate is still slow (1 drop per second or slower) then Lysis buffer is pulled through with syringe again.

6. Cleared lysate with Ni-NTA matrix is added to column and allowed to drip through.

7. The column is then washed as follows : 10-20 ml Lysis buffer (10 mM imidazole, pH 8.0) + 30% glycerol, then 20-40 ml Wash buffer (50 mM NaH$_2$$PO_4$, 300 mM NaCl, 20 mM imidazole, pH 8.0) + 30% glycerol.

8. All excess wash buffer is pushed or spun out from column. The bottom of the column is then capped and 1.0-1.5 ml Elution buffer (50 mM NaH$_2$PO$_4$, 300 mM NaCl, 250 mM imidazole, pH 8.0) + 30% glycerol is added. The column is vortexed until all Ni-NTA is in solution in the column, followed by 5 minutes of waiting.

   (a) All eluate is collected by pushing it all out, or spinning it out gently for 5 minutes at low speed on the tabletop centrifuge into a 15 ml conical tube.

9. If desalting is necessary for downstream experiments, a Zeba desalting column (Pierce) is used according to the manufacturer's instructions. The proteins are commonly desalted into 10 mM Tris, pH 7.5, 150 mM NaCl, 1% glycerol.

Bacterial Transformation and Culture

1. *E. coli* BL21 (DE3) is thawed on ice. 100 μl is gently pipetted into a tube and 0.4 μg DNA is added and mixed gently.

2. It is then incubated for 15-30 minutes on ice.

3. The solution is heat shocked at 42°C for 45 sec.

4. It is then incubated on ice for 5 minutes.

5. 500 μl of warm SOC (at 42°C) is added into the *E. coli* + DNA. SOC is microbial growth medium composed of 20 g/L Tryptone, 5 g/L Yeast Extract, 4.8 g/L MgSO$_4$, 3.603 g/L dextrose, 0.5g/L NaCl and 0.186 g/L KCl.

6. The culture is incubated at 37°C while shaking for 1 hour.

7. 20-100 μl of *E.coli* is placed in prewarmed plate of LB agar + Ampicillin antibiotic at 37°C overnight.

8. A brain-heart infusion broth (BHI), a highly nutritious growth medium, is prepared and autoclaved to sterilize.

9. A colony is picked and grown in 5 ml BHI overnight.

10. On the day of the experiment, the overnight culture is diluted into more BHI at the desired concentration.

11. *Staph.* and *E. coli* on LB plate are kept at 4 °C. For long term storage, overnight culture is combined with 25 % glycerol and stored in a cryogenic vial at -80°C.

Growth of *E. Coli* and *Staphylococcus Aureus*

1. 2g of Lysogeny Broth (LB) are diluted in 100 ml of water.

2. The solution is then autoclaved for 25 minutes and left to cool until it reaches 37°C.

3. A fine spatula is heated using a Bunsen burner, left to cool and used to scrape off few colonies of bacteria that are put in the LB medium.

4. The bacteria solution is incubated at 37°C at 250 rpm.

5. Optical density is verified after two hours.

6. Solution is incubated until OD reaches 0.4.

Adding Dye to Bacteria Solution

1. 1 ml of bacteria solution is put in LB and centrifuged at 7000g for 12 minutes.

2. The pellet is then suspended in 1ml Buffer solution.

3. 1 μl of DAPI is added, vortexed and centrifuged.

4. The solution is washed then suspended in Buffer.